Accelerated Historical and Future Warming over the Middle East and North Africa in Response to the Global Temperature Change

Abdul Malik[1], Georgiy Stenchikov[1], Suleiman Mostamandi[1], Sagar Parajuli[2], Jos Lelieveld[3,4], George Zittis[4], Muhammad Sheraz Ahsan[5], Luqman Atique[6,7], Muhammad Usman[8]

[1]Physical Science and Engineering Division, King Abdullah University of Science and Technology, 23955 Thuwal, Jeddah, Saudi Arabia, [2]Scripps Institution of Oceanography, University of California, San Diego, CA, USA California, [3]Max Planck Institute for Chemistry, Mainz, Germany, [4]Climate and Atmospheric Research Center (CARE-C), The Cyprus Institute, Nicosia, Cyprus, [5]Institute of Geographical Information Systems, School of Civil and Environmental Engineering, National University of Sciences and Technology, Islamabad, Pakistan, [6]School of Earth Sciences, Zhejiang University, Hangzhou, China, [7]Department of Meteorology, COMSATS University, Islamabad, Pakistan, [8]Department of Life and Environmental Sciences, Zayed University, Abu Dhabi, United Arab Emirates

Corresponding author: Abdul Malik (abdul.malik@kaust.edu.sa) and Georgiy L. Stenchikov (georgiy.stenchikov@kaust.edu.sa)

Key Points:

- Downscaled climate models show world would surpass 1.5, 2, 3, and 4 ℃ warming by years 2028, 2041, 2062, and 2081, respectively
- Global warming is associated with accelerated and spatially incoherent regional warming over the Middle East and North Africa
- Coupled Model Intercomparison Project Phases 5 and 6 show consistent warming patterns over the region compared with observations

Abstract

The global average temperature has increased significantly since the preindustrial era. Translating global warming into regional scales is crucial to formulate effective environmental and climate policies. A realistic assessment of regional climate change requires high-resolution datasets. We present a new high-resolution (9 km) analysis of historical and future regional warming over the Middle East and North Africa (MENA) using observations, reanalysis products, and statistically downscaled global climate models from the Coupled Model Intercomparison Project (CMIP) Phase 5 and 6. The observed regional temperature change over the MENA subregions appears to be up to three times faster than the global average. Regional warming has already surpassed the 1.5 ℃ and is at the brink of exceeding 2 ℃. By the end of the 21st century, the Arabian Peninsula will warm from 2.66 ± 0.57 to 7.61 ± 1.53 ℃ under the low (SSP1–2.6) and high-end (SSP5–8.5) emission scenarios, respectively. We identify spatially distinct summer and winter warming hotspots. The most prominent spots in summer are the Arabian Peninsula Hotspot Region (APHR) and Algerian Hotspot Region. Major winter hotspots appear over Mauritania in West Arica and the Elburz Mountains. Moreover, APHR has already exceeded 2 °C of warming and will warm by about 9 °C under the high-end emission scenario by the end of the century. The 1.5, 2, 3, and 4 ℃ global warming levels are associated with substantial regional warming of 2.1 ± 0.2, 2.76 ± 0.2, 4.19 ± 0.25, and 5.49 ± 0.38 ℃, respectively, over the Arabian Peninsula.

Plain Language Summary

Climate studies consistently conclude that Earth is warming alarmingly in the foreseeable future. This study presents the high-resolution (9 km) analysis of surface air temperature changes over the Middle East and North Africa (MENA) from 1850 until the end of the twenty-first century. It employs the best available observational datasets and climate models, providing the basis for regional-scale studies. The results reveal that the Arabian Peninsula and the entire MENA region's historical and future warming is higher than the globe's average. The warming rate in the central Arabian Peninsula is comparable with that of the Arctic region, as both are warming two to three times faster than the global average, except the Arabian Peninsula is already one of the hottest regions on Earth. It vividly reinforces that the enhanced warming over the region will adversely impact the local to regional socioeconomic and energy consumption patterns, besides jeopardizing human livability.

1 Introduction

The global average temperature has increased since the preindustrial era, primarily due to anthropogenic greenhouse gas (GHG) emissions (Bindoff et al., 2013; Intergovernmental Panel on Climate Change [IPCC], 2021). The rising temperatures affect global and regional climates (Arnell et al., 2019; Olonscheck et al., 2021), causing more frequent and intense heat waves (Im et al., 2017; Power & Delage, 2019; Raymond et al., 2020; Wouters et al., 2022), extreme precipitation events (Fowler & Ali, 2022; Seneviratne et al., 2021; Tabari, 2020), droughts (Dai, 2013; Naumann et al., 2018; Seneviratne et al., 2021), and sea level rise (Mengel et al., 2016; Tebaldi et al., 2021). These extremes result in significant socioeconomic challenges (Gao et al., 2019; Handmer et al., 2012; Kjellstrom et al., 2010) and threats to biodiversity on terrestrial (Botkin et al., 2007; Malcolm et al., 2006) and marine ecosystems (Doney et al., 2012). Recent studies have shown that the Arctic is warming at a rate two to three times faster than the global

68 average (Cohen et al., 2020), and the Antarctic Peninsula has warmed by more than 3 °C in the
69 last 50 years (British Antarctic Survey, 2022). Desert regions have also exhibited significantly
70 stronger temperature trends than the global average warming rates (Zittis et al., 2022). The
71 global warming patterns appear particularly prominent in the tropics and subtropics (Bathiany et
72 al., 2018; Battisti & Naylor, 2009; Fischer & Knutti, 2013; Mora et al., 2017; Willett &
73 Sherwood, 2012; Vargas Zeppetello et al., 2022) where the Middle East and North Africa
74 (MENA) are located.

75 In addition, MENA has a harsh climate (Fonseca et al., 2022) and is considered a global hotspot
76 warming region (Diffenbaugh & Giorgi, 2012; Giorgi, 2006; Waha et al., 2017). This region is
77 under severe threat of climatic changes, as various studies (Dasari et al., 2021; Freychet et al.,
78 2022; Lelieveld et al., 2012; Majdi et al., 2022; Pal & Eltahir, 2016; Safieddine et al., 2022) have
79 predicted the influence of high GHG emissions. People in this region are already vulnerable
80 (Majdi et al., 2022) due to very high summer temperatures (Ntoumos et al., 2022; De Pauw,
81 2002), water scarcity (Waha et al., 2017; World Bank, 2018), persistent droughts (Baza et al.,
82 2018), warm-humid conditions near the coasts (Odnoletkova & Patzek, 2021), and the prevailing
83 hot-dry summer climate away from the sea. Moreover, summers in these regions warm faster
84 than winters (Lelieveld et al., 2016).

85 Due to strong warming in the region (Almazroui et al., 2022; Ntoumos et al., 2022; Suarez-
86 Gutierrez et al., 2020; Zhao et al., 2021; Zittis et al., 2021), there are concerns about future
87 human habitability in the MENA region, especially for areas closer to coastal zones (e.g., the
88 Persian Gulf and Red Sea; Andrews et al., 2018; Pal & Eltahir, 2016; Raymond et al., 2020;
89 Safieddine et al., 2022). Most of the population in the Arabian Peninsula resides in coastal zones
90 away from the inland arid areas (except Riyadh Province) due to milder temperatures and the
91 availability of rain (De Pauw, 2002) or desalinated water. Precise estimates of future warming
92 over the coastal zones of the Arabian Peninsula could help policymakers better plan and address
93 the habitability issues in the region.

94 The global average temperature increase has surpassed 1.1 °C compared to the preindustrial
95 climate (1850–1900) (IPCC, 2021; Tollefson, 2021). Under the 2015 Paris Agreement, several
96 countries have agreed to reduce GHG emissions to limit the global average temperature rise to
97 1.5 °C relative to preindustrial levels (IPCC, 2018). However, the intended nationally determined
98 contributions for GHG emissions indicate that the current efforts are insufficient and global
99 temperature could rise between 2.6 and 3.1 °C by 2100 (Rogelj et al., 2016). According to the
100 Sixth Assessment Report by the IPCC, the global average temperature is expected to rise
101 between 2.1 and 3.5 °C under an intermediate emission scenario (IPCC, 2021). Further, carbon
102 dioxide (CO_2) emissions should not exceed 110 Gt with a 66% probability of keeping warming
103 below 1.5 °C (Lamboll et al., 2022). This study investigates regional warming over MENA and
104 its subregions when the global temperature reaches 1.5, 2, 3, and 4 °C warming thresholds.
105 Understanding and predicting temperature variability over the Arabian Peninsula requires high-
106 resolution reanalyses and climate model outputs. Low-resolution datasets cannot adequately
107 resolve local and regional processes (Pal & Eltahir, 2016). Previous studies (see Almazroui et al.,
108 2022; Majdi et al., 2022; Ntoumos et al., 2022; Safieddine et al., 2022; Zittis et al., 2021) have
109 provided relatively low-resolution climate projections for the region; which may underestimate
110 temperature changes over the coastal zones among other problems. To avoid this drawback, we
111 use the following multiple and high-resolution climate datasets:

i) eight state-of-the-art observational datasets (1° to 5° latitude/longitude) with 200 ensemble members provided by the Met Office Hadley Center/Climatic Research Unit for uncertainty estimates;

ii) three high-resolution reanalysis products (0.1° to 0.5° latitude/longitude) with 10 ensemble members; and

iii) 26 high-resolution statistically downscaled (0.1° to 0.25° latitude/longitude) Atmosphere-Ocean General Circulation Climate Model (AOGCM)s outputs from the Coupled Model Intercomparison Project (CMIP) Phases 5 and 6 with low (shared socioeconomic pathways [SSP] 1–2.6), intermediate (representative concentration pathways [RCP] 4.5), and high (RCP8.5 and SSP5–8.5) GHG emission scenarios.

The recent CMIP6 AOGCMs have improved physics, including aerosol-climate interactions, compared to CMIP5 (IPCC, 2021). We consider models with different climate sensitivity and structural differences to provide robust and updated estimates of historical and future warming in the MENA region and quantify subregional warming in the Arabian Peninsula, addressing the following three critical questions:

i) How much warming has occurred over MENA and its subregions relative to the preindustrial climate (1850–1900), and how well do the CMIP5 and CMIP6 models simulate the observed regional temperature changes?

ii) What is the regional and subregional temperature response to global warming, particularly when the average global temperature surpasses 1.5, 2, 3, and 4 °C warming thresholds?

iii) How consistent are CMIP5 and CMIP6 ensembles in simulating future warming patterns over the region, and what uncertainty is associated with internal climate and inter-model variability?

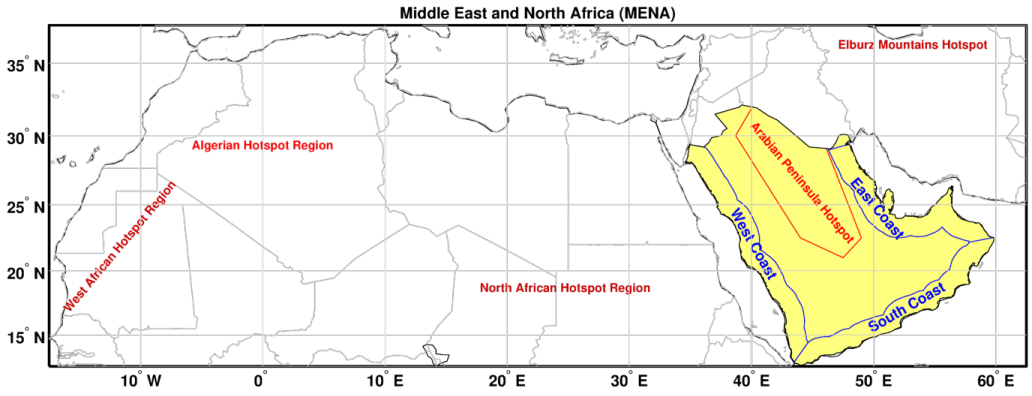

Figure 1. Middle East and North Africa with significant warming hotspots and selected coastal zones. Coastal zones (blue) are 160 km inland from the coastal boundary, where the land-sea breeze predominates. The red polygon marks the Arabian Peninsula Hotspot Region (APHR). See Table S1 for the geographic coordinates of APHR.

Further, we estimate the current and future warming in the coastal zones (Fig. 1) of the Arabian Peninsula. The analysis reveals that the statistically downscaled CMIP5 and CMIP6 models can simulate the observed warming patterns well. The reanalyses and model outputs simulate the observed seasonal warming hotspots. We refer to these warming hotspots as the summer Arabian Peninsula Hotspot Region (APHR), summer Algerian Hotspot Region (AHR), winter North African Hotspot Region (NAHR), winter West African Hotspot Region (WAHR), and winter Elburz Mountain hotspot (Fig. 1).

2. Materials and Methods

2.1. Observational Data

To estimate the historical warming between 1850 and 2020 over MENA and its subregions, we employed monthly means of eight observational datasets with varying latitude/longitude resolutions of 1° to 5° (Table S2). These datasets include the HadCRUT5 analysis (Morice et al., 2021), Berkeley Earth (Rohde & Hausfather, 2020), GISTEMP v4 (Lenssen et al., 2019), NOAAGlobalTemp v5 (Zhang et al., 2019, 2021), CMST-Interim (Sun et al., 2021; Yun et al., 2019), and Cowtan and Way v2 (Cowtan and Way, 2014) with three variants. Combining several datasets can help estimate uncertainty due to missing values and provide the best possible temperature change assessment. These datasets are briefly described in Text S1 in Supporting Information.

2.2. Reanalysis Products

We employed three high-resolution reanalysis products (Table S3) produced at the European Center for Medium-Range Weather Forecasts and provided by the Copernicus Climate Change Service (C3S) through the Climate Data Store. These reanalysis products are i) European reAnalysis (ERA5; 0.25°×0.25° latitude/longitude) with 10 ensemble members (0.5°×0.5° latitude/longitude; Copernicus Climate Change Service, 2023; Hersbach et al., 2019a, 2019b, 2020) and ii) ERA5-Land (0.1°×0.1° latitude/longitude; Copernicus Climate Change Service, 2022a; Muñoz-Sabater et al., 2021) and Watch Forcing Data Methodology (Weedon et al., 2011) applied on ERA5 (WFDE5; 0.5°×0.5° latitude/longitude; Copernicus Climate Change Service, 2022b; Cucchi et al., 2020, 2021) for bias correction using CRUTSv4.06 (Harris et al., 2020). The ERA5 reanalysis products with high spatial resolution and complete spatial coverage are constrained by observational datasets from various sources using advanced data assimilation techniques (Hersbach et al., 2020). These reanalysis products share similar characteristics at different spatial resolutions and provide bias-corrected temperature estimates (e.g., WFDE5). Please refer to Text S2 in Supporting Information for more details.

2.3. Climate Model Outputs

To estimate the historical and future warming over MENA and its subregions, we employed high-resolution statistically downscaled and bias-corrected CMIP5 and CMIP6 outputs provided by Noël et al. (2021, 2022). The statistical downscaling and bias correction make the model climatology comparable to the observational reference dataset (Noël et al., 2021) with high spatial resolution. However, bias-adjusted data inherit errors in the reference data used for bias removal (Coeffel et al., 2018). Further, bias correction assumes that historical bias remains constant in future simulations (Im et al., 2017; Kang, 2019).

2.4. Greenhouse Gas Emission and Shared Socioeconomic Pathways

To assess the regional and subregional temperature change, we considered two representative concentration pathways, RCP4.5 and RCP8.5 (Moss et al., 2010; Riahi et al., 2011; Thomson et al., 2011) from CMIP5 (Taylor et al., 2012), and two shared socioeconomic pathways, SSP1–2.6 and SSP5–8.5 (Riahi et al., 2017) from CMIP6 (Eyring et al., 2016). These scenarios allow calculating future warming under various emission projections. For instance, SSP1–2.6 assumes a sustainable world with the best warming estimate of 1.8 °C by the end of the century (as agreed under the Paris Climate Agreement) and a most-likely range of 1.3 to 2.4 °C (IPCC, 2021). The intermediate mitigation scenario RCP4.5 causes a warming of 2.25 °C (Im et al., 2017). The RCP8.5 and SSP5–8.5 scenarios are the worst-case or high-end emission scenarios with no mitigation policy and high fossil fuel-based development in the future with high mitigation challenges, respectively (Im et al., 2017; Kang, 2019).

2.5. C3S-CMIP5-Adjusted 2 m Air Temperature

We used monthly means of the 2 m surface air temperature (T2m) from 21 CMIP5 models statistically downscaled at 0.25°x0.25° (31 km) by Noël et al. (2021) using the ERA5 reanalysis (Table S4). Downscaling was performed using the trend-preserving cumulative distribution function transform method called quantile mapping. The 1981–2010 period was taken as the calibration period from ERA5. Downscaling and bias correction were performed for the historical (1951–2005) and future (2006–2100) periods for two GHG emission scenarios (RCP4.5 and RCP8.5) over land and the ocean using only the first ensemble member (r1i1p1). The original spatial resolutions for the CMIP5 models vary between 0.75° and 3° (Noël et al., 2021). We present the results using the multimodel mean (MMM) of all chosen CMIP5 models, calculating the inter-model variability at the 99% confidence interval (CI).

2.6. C3S-CMIP6-Adjusted 2 m Air Temperature

We also used monthly means of T2m from five CMIP6 models statistically downscaled at 0.1°x0.1° (9 km) by Noël et al. (2022) with the ERA5-Land reanalysis (Table S5). Only five models were chosen because it was computationally expensive to downscale an extensive range of CMIP6 climate models to a high resolution. The five selected models represent the full range of climate sensitivity of CMIP6 models, as three models (GFDL-ESM4, MPI-ESM1-2-HR, and MRI-ESM2-0) have low climate sensitivity. The other two (IPSL-CM6A-LR and UKESM1-0-LL) have high climate sensitivity (Noël et al., 2022). Further, these models' ocean and atmospheric components are structurally independent, and their process representation is fair to good (Lange, 2021). Downscaling was performed using the same method and calibration period as the C3S-CMIP5-Adjusted dataset. Downscaling and bias correction was performed for the historical (1951–2014) and future (2015–2100) periods for three GHG emission scenarios (SSP1–2.6, SSP2–4.5, and SSP5–8.5) over land only using only the first ensemble member. We analyzed only two (SSP1–2.6 and SSP5–8.5) emission scenarios. The original spatial resolutions of the CMIP6 models chosen for downscaling vary from 0.9° to 2.5° (Noël et al., 2022). For the CMIP6 models, we also present the MMM results, calculating the inter-model variability.

Noël et al. (2022) provided high-resolution statistically downscaled output from five CMIP6 models only over land. We require data over the land and ocean to calculate the years that will surpass the global warming threshold. Thus, we regridded (at 0.25°x0.25°) the same five CMIP6

models and scenarios using ERA5 as reference data from 1981–2010. We applied the simple bias-correction method that adjusts the model output mean bias and temporal variability to the reference data (see Hawkins et al., 2013).

We also used the actual output from the same 21 (5) CMIP5 (CMIP6) models, referred to as CMIP5-unadjusted (CMIP6-unadjusted) models. We compared these unadjusted climate model outputs with their reference reanalysis datasets to determine how much better statistically downscaled data perform than the original model output.

2.7. Definition of Seasons, Coastal Zones, and Climate Anomalies

Based on the synoptic conditions, the climate of the Arabian Peninsula can be divided into two predominant seasons: dry (May–October: MJJASO) and wet (November–April: NDJFMA) (Almazroui, 2006, 2011). This study classifies summer and winter as MJJASO and NDJFMA for MENA and its subregions. We defined coastal zones as regions within 160 km of the coastal boundaries. Land and sea breezes are predominant in these zones, influencing the coastal climate by reducing the temperature and increasing humidity (Yan, 2005). We considered the west, south, and east coasts of the Arabian Peninsula (Fig. 1).

We calculated the global annual mean warming relative to the preindustrial climate (1850–2020) from historical to future periods (1850–2099) and compared it with that of MENA (17.5° W–62.5° E and 12.5° N–37°.5 E; Fig. 1), the Arabian Peninsula, and its coastal zones. We compared warming for the year 2020 and the years when global warming surpasses thresholds of 1.5, 2, 3, and 4 °C. We analyzed the mean climatological spatial warming patterns for the historical (1987–2016), near (2021–2050), and far future (2069–2098) periods.

For all datasets, we calculated the temperature anomalies with respect to the preindustrial climate (1850–1900), where the basic observational datasets are available as anomalies referencing different periods (Table S2). We adjusted these datasets to a standard preindustrial reference period (1850–1900), as done by Morice et al. (2021). To calculate the anomalies for observational datasets (GISTEMPv4, NOAAGlobalTemp, and CMST-Interim) that do not wholly cover the preindustrial reference period (1850–1900), we used the preindustrial climatological mean from the relatively high-resolution and complete spatial Berkeley Earth data. For this purpose, we first aligned these observational datasets to the anomalies of Berkeley Earth (1951–1980) data and then subtracted its climatological reference mean (1850–1900). All observational datasets have been regridded at 0.5°x0.5° (unless otherwise stated) for comparison with relatively high-resolution WFDE5 and further analyses.

For datasets (model and reanalysis products) not extending far enough back to cover the preindustrial reference period (1850–1900), we first calculated the climate anomalies relative to the 20 years from 1986–2005. Then, we added an offset value for global and regional warming estimates from 1986 to 2005 (Table S6–S7). Based on the published global datasets, compared to the preindustrial climate, the world has warmed by 0.63 °C in the 20 years from 1986 to 2005 (Allen et al., 2018); thus, we added this offset value to calculate global warming with respect to the preindustrial period. We found the same global (land and ocean) mean offset value based on eight observational datasets (Table S6), confirming the appropriateness of the proposed method. Based on the eight observational datasets, we found an offset of 0.94 for global land. Thus, using the same concept, we calculated the spatial and temporal offsets for MENA and its subregions

(Table S7). We refer to the observed global average temperature as the global mean average temperature (GMAT) and the simulated temperature as the global surface air temperature (GSAT).

2.8. Time Series Smoothing

Internal climate variability may affect the warming rates temporarily (Allen et al., 2018), resulting in an inaccurate assessment of long-term human-induced warming. Thus, IPCC recommends smoothing the temperature time series on a multidecadal timescale to exclude or minimize the effect of natural fluctuations (Allen et al., 2018; Rogelj et al., 2017). We used an adaptive smoothing approach introduced by Mann (2008) to reduce the influence of natural and internal variability. Climate time series are often nonstationary, particularly those with trends owing to external forcing. The conventional smoothing methods have certain limitations, such as suppressing the amplitude and slope and over-smoothing the trends near the boundaries of a time series. The adaptive smoothing approach overcomes these limitations and produces the best and most realistic trend estimate (Mann, 2008). We used a low-pass filter and smoothed the temperature time series with a cutoff frequency of 0.025 (40 years), as Mann (2008) did. This method resembles the multidecadal smoothing of a time series based on moving averages (e.g., Park et al., 2022).

2.9. Observed and Model-based Uncertainty

We used 200 ensemble members of the HadCRUT5 analysis to calculate the observed uncertainty from 1850 to 2020 at the 99% CI. We used the observed uncertainty in the HadCRUT5 analysis to ensure that all observational datasets employed are within the uncertainty range arising from methods for measuring sea surface temperatures, homogenization, measurement errors, and the presence of data-sparse regions and statistical data reconstruction methods for filling the gaps (Morice et al., 2021).

We calculated the 30-year mean warming over 1987–2016, 2021–2050, and 2069–2098. We estimated the variability in the mean warming as a ±1 standard deviation (SD) calculated from 10,000 statistical realizations of the original datasets. Using the bootstrap resampling with replacement, we generated 10,000 samples of each observational temperature time series and the corresponding years (e.g., 1850–2020). We calculated temperature anomalies for each realization relative to the preindustrial period (1850–1900). Then, for the selected period (1987–2020), we calculated the 30-year mean for each sample. The SD of the means from 10,000 realizations provides the mean warming uncertainty. We assumed this method accounts for the observational uncertainty in temperature anomalies arising from sparse data regions over the preindustrial period. We calculated temperature anomalies for all model-generated datasets relative to the preindustrial period before generating 10,000 realizations, from which we calculated the 30-year mean warming and uncertainty for a selected period (e.g., 2021–2050 and 2069–2098).

We estimated the inter-model variability over the historical and future periods using 21 available climate models from the C3S-CMIP5-Adjusted and five from the C3S-CMIP6-Adjusted datasets. The years crossing the global warming threshold of 1.5, 2, 3, and 4 °C are calculated from the smoothed MMM. Using the smoothed time series for each climate model, we found the year after which the temperature anomaly never falls below a warming threshold (e.g., 1.5 °C). The

SD of all these model years crossing the temperature threshold provides the model-based uncertainty for crossing the temperature threshold.

2.10. Estimates of Uncertainty Due to Internal Climate Variability

The uncertainty in the year of crossing a certain global warming threshold caused by internal variability is estimated using an improved method described by Joshi et al. (2011). Instead of applying a smooth polynomial fit, we smoothed the temperature time series of each model using Mann's (2008) adaptive smoothing approach (Fig. S1). The smoothed time series represents the forced trend. Then, we generated a residual time series by subtracting the trend from the original time series. Instead of simply applying an autoregressive model for sample generation, we generated 10,000 samples of a residual time series using the corrected amplitude-adjusted Fourier transform (Kugiumtzis, 2000) algorithm. We added the calculated trend back to all 10,000 samples. For all 10,000 samples with the added trend, we found the year for crossing a given global warming threshold (e.g., 1.5 °C). One SD of the years crossing a given global warming threshold was measured for each model with 10,000 samples. The mean of the SD from all models provides uncertainty in a year due to the internal variability for crossing the global warming threshold.

We used the same method to calculate the uncertainty due to internal climate variability in the 30-year mean warming (e.g., 1987–2016). We calculated the 30-year mean warming from all 10,000 samples with the added trend. The 99% CI from these 10,000 means provides an uncertainty range due to internal climate variability.

The corrected amplitude-adjusted Fourier transform algorithm preserves the autocorrelation and amplitude distribution of the original time series in the generated samples. This method fits the first-order autoregressive model on the residual time series, from which 10,000 samples are developed and transformed to match the amplitude distribution, cumulative density function, and linear correlations of the residual time series (see Kugiumtzis, 2000; Malik et al., 2018).

2.11. Model Agreement in Spatial Maps

The MMM is an averaged response to external forcing. However, it does not explain its robustness across the models, as if the forced signal's magnitude is greater than the unforced signal (i.e., the internal climate variability; Collins et al., 2013). We tested the statistical significance or robustness of the climate change signal using a method described in the Fifth Assessment Report by IPCC (Collins et al., 2013). However, we defined the internal variability as interannual variability over 30 years, for which we measured the robustness of the forced signal. We assumed that the MMM warming over a grid cell is statistically significant if it is greater than 2 SDs of the internal climate variability, and all models agree on the sign of the change.

3 Results

3.1. Climate Model Evaluation

Figure 2 presents the mean bias (1987–2016) of the CMIP-Unadjusted and C3S-CMIP-Adjusted datasets with reanalyses (ERA5 and ERA5-Land). Significant local mean biases from -7 to 13 °C

exist between the unadjusted CMIP MMMs and reanalysis datasets (Fig. 2a–d). However, the mean bias spatially averaged over the entire MENA (MENA-Land) region is less prominent (i.e., -0.95 (0.18) °C for summer and -1.64 (-0.61) °C for winter).

The statistical downscaling significantly reduces the mean bias on the local and regional scale (Fig. 2e–f). The mean summer and winter biases reduce to -0.03 (0.01) °C and -0.07 (-0.02) °C, respectively, when spatially averaged over the entire MENA (MENA-Land) region. Compared to the CMIP-Unadjusted dataset, the range of local scale mean bias (-1.36 to 0.77 °C) reduces nine times that of the C3S-CMIP-Adjusted dataset.

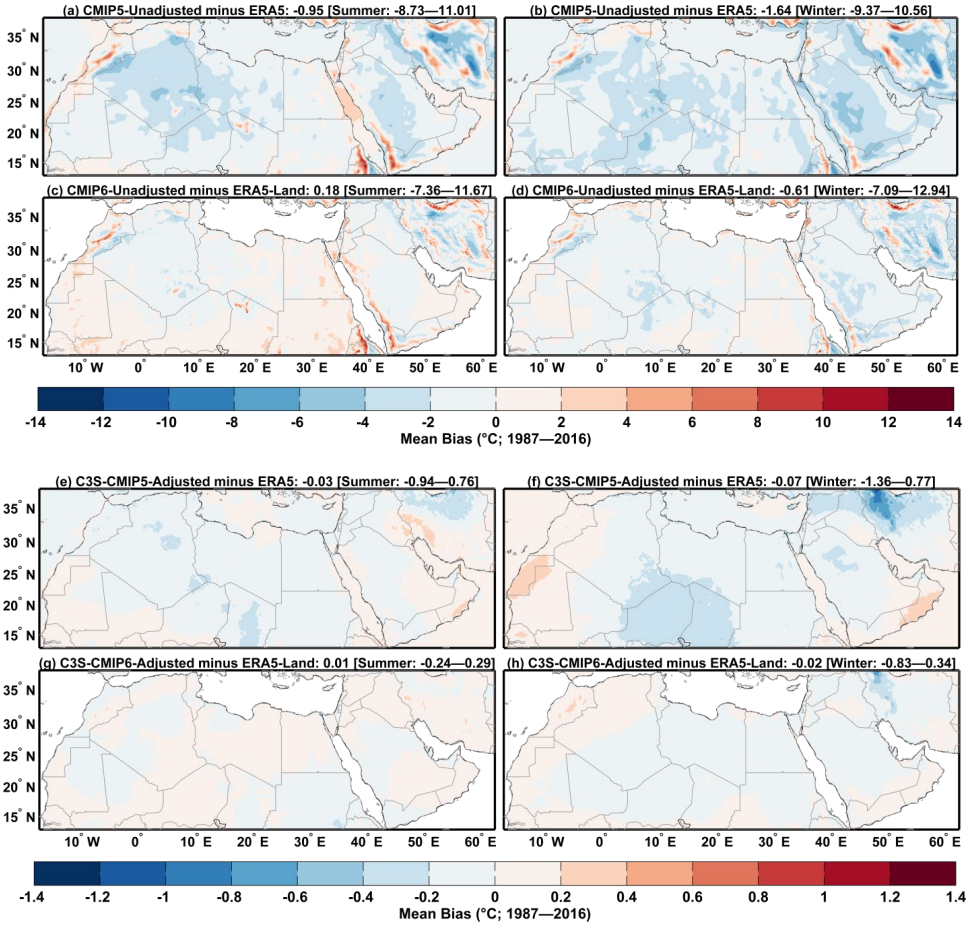

Figure 2. Evaluation of climate models. Mean bias between (a) CMIP5-Unadjusted and ERA5 datasets for summer and (b) for winter. Mean bias between (c) CMIP6-Unadjusted and ERA5-Land datasets for summer and (d) winter. Mean bias between (e) CMIP5-Adjusted and ERA5 dataset for summer and (f) winter. Mean bias between (g) CMIP6-Adjusted and ERA5-Land datasets for summer and (h) winter. The values in the braces indicate the mean bias range over the corresponding spatial domain.

The historical (1987–2016) mean warming of most of the C3S-CMIP5-Adjusted (C3S-CMIP6-Adjusted) models lies within the uncertainty range of ERA5 (WFDE5) calculated from its 10 (10,000 bootstraps) ensemble members; however, models seem to diverge from each other in the

366 future (Figs. S2–S5). Two models, inmcm4 (Fig. S2a) and UKESM1-0-LL (Figs. S4–S5),
367 significantly diverge from other models over the historical and future periods.

368 **3.2. Historical Mean Warming (1987–2016)**

369 The climate change signal is coherent and statistically robust throughout the MENA region
370 (Fig. 3a–f). Significant summer and winter warming hotspots with varying intensities appear
371 across the MENA region. The most prominent summer hotspot emerges over Algeria (AHR),
372 extending toward the southeast and covering a large part of the Sahara Desert. In the Arabian
373 Peninsula, a summer warming hotspot (APHR) dominates its central parts over the Al-Jawf,
374 Hail, Al-Qassim, and Riyadh provinces of Saudi Arabia. In winter, two significant warming
375 hotspots appear over West Africa (WAHR) and the Elburz Mountains, the glacier region in Iran.
376 We identified a third winter warming hotspot of relatively less intensity over Chad and Sudan
377 (NAHR). A strong winter warming over the Elburz Mountains (> 2 °C; Fig. 3d) may have
378 regional effects and require further attention. Most of the eight observational datasets indicate the
379 presence of summer and winter warming hotspots with varying magnitudes (Fig. S6).

380 The coastal zones of the Arabian Peninsula (the west, south, and east coasts) warm less rapidly
381 compared to the central parts in summer and winter. This less-rapid warming could be due to the
382 proximity to the relatively slowly warming regional seas, land-sea breezes, and topographical
383 and land cover differences between coastal and central regions.

384 The Red Sea experiences a contrasting summer and winter warming pattern, a temperature
385 anomaly dipole between the north and south Red Sea, with stronger (weaker) summer (winter)
386 warming in the north than in the south. This temperature anomaly dipole requires further
387 attention regarding its effects on the regional climate at various timescales.

388 We further confirmed the results with high-resolution ERA5-Land and the C3S-CMIP6-Adjusted
389 dataset (9 km grid spacing) and bias-corrected ERA5 (WFDE5; 61 km grid spacing) datasets
390 available over land regions only (Fig. 4). We identified similar warming patterns and hotspots as
391 in Fig. 3. However, a distinct winter warming pattern appears over the Arabian Peninsula,
392 extending across parts of the Riyadh Province, Empty Quarter, Eastern Yemen, and Western
393 Oman.

394 The observations reveal a summer mean warming of 1.12 ± 0.08 °C over MENA (land and
395 ocean; Fig. 3a and Table S8). The ERA5 (Fig. 3c) and C3S-CMIP5-Adjusted (Fig. 3e) models
396 agree with the observations (Fig. 3a) in spatial patterns but display slightly higher summer mean
397 warming (1.14 ± 0.07 and 1.15 ± 0.08 °C, respectively). The C3S-CMIP5-Adjusted winter mean
398 warming (1.13 ± 0.09 °C; Fig. 3f) agrees with the observed warming (1.13 ± 0.09 °C; Fig. 3b). In
399 addition, ERA5 indicates higher winter warming (1.19 ± 0.1 °C; Fig. 3d) than other datasets. The
400 summer (winter) mean warming averaged across all datasets over land and ocean (Figs. 3 and S7
401 and Table S8) is 1.13 ± 0.08 (1.15 ± 0.09 °C), whereas over just land (Figs. 4 and S7 and
402 Table S8), it is 1.22 ± 0.08 (1.25 ± 0.1 °C), with warming ranging from 0.54 °C to 1.74 °C (0.30
403 °C to 2.20 °C) and 0.54 °C to 1.79 °C (0.41 °C to 2.05 °C), respectively.

404

405

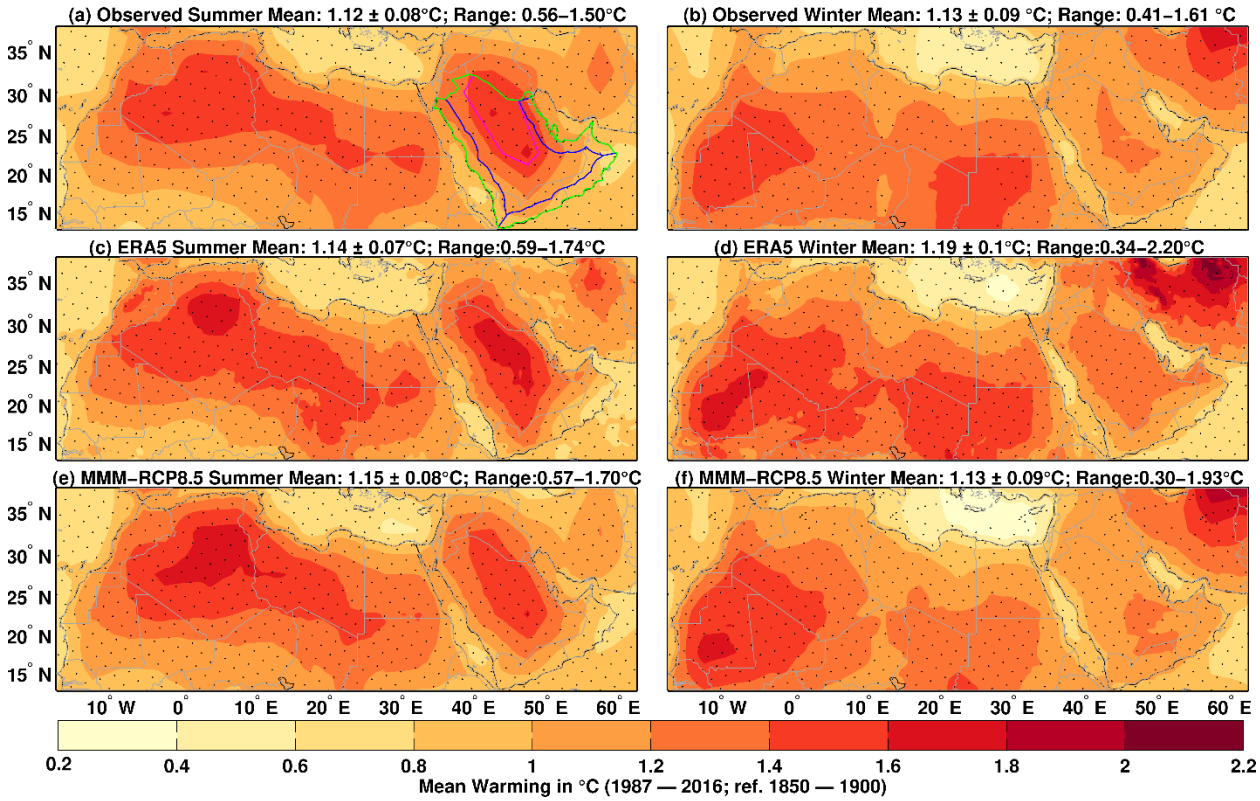

Figure 3. Spatial pattern of historical summer (May–October; left panel) and winter (November–April; right panel) mean climatological warming (1987–2016) relative to the preindustrial climate (1850–1900) over the Middle East and North African region (land and ocean) for multiple datasets. (**a**, **b**) Mean of eight observational datasets; (**c**, **d**) ERA5 reanalysis; (**e**, **f**) multimodel model mean of 21 C3S-CMIP5-Adjusted climate model outputs (historical+RCP8.5). Stippling indicates statistical significance with 2 SDs of internal climate variability and where all corresponding data members agree for a change in sign. Numbers above each subfigure indicate the climatological mean warming with ±1 SD and temperature range (min to max). Green and magenta polygons mark the boundaries of the Arabian Peninsula and Arabian Peninsula Hotspot Region. Blue lines are coastal zones up to 160 km from the coast.

Observations, reanalyses, and the C3S-CMIP-Adjusted dataset reveal consistent and spatially coherent warming patterns over the MENA region, although the intensities of the hotspots vary among them. Further, ERA5/ERA5-Land exhibits slightly higher warming for the summer (0.59 °C to 1.74 °C/0.54 °C to 1.62 °C) and winter (0.34 °C to 2.20 °C /0.41 °C to 2.05 °C) than other datasets. We conclude that the reanalyses (ERA5, ERA5-Land, and WFDE5) and C3S-CMIP-Adjusted datasets agree overall with the observations.

Figure 5 (Fig. S8) provides estimates of historical summer (winter) mean warming with uncertainty due to differences in the datasets, model spread, and internal climate variability over the Arabian Peninsula, APHR, and coastal zones. Mean warming of 1.23 ± 0.08 °C (averaged across all datasets; Fig. 5a and Table S8) has occurred over the Arabian Peninsula with uncertainty ranging from 1.11 °C to 1.35 °C due to internal climate variability. The APHR has already surpassed the mean warming of 1.5 °C, with uncertainty due to internal variability

ranging from 1.35 °C to 1.68 °C. All datasets display comparable warming except ERA5, which has a slightly higher warming and uncertainty range for the Arabian Peninsula and APHR.

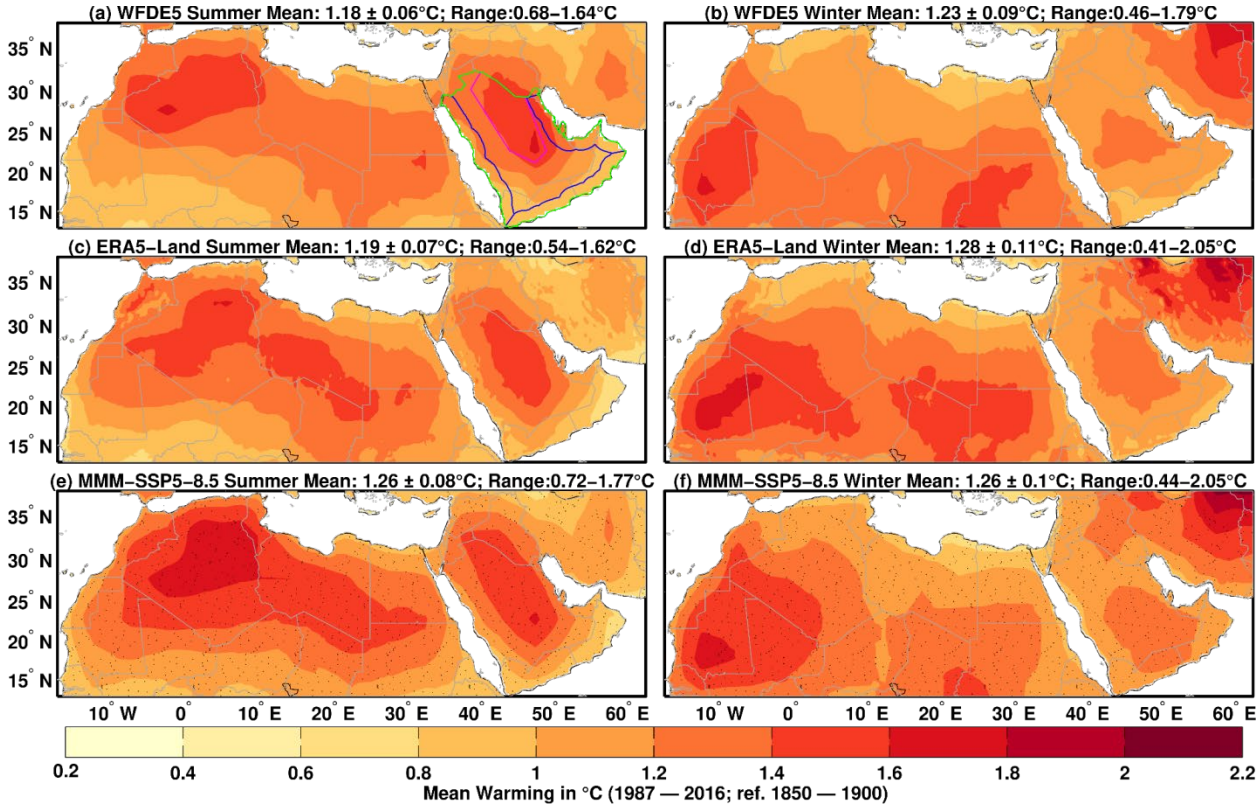

Figure 4. Spatial pattern of historical summer (May–October; left panel) and winter (November–April; right panel) mean climatological warming (1987–2016) relative to the preindustrial climate (1850–1900) over the Middle East and North African region (land only) for multiple datasets. (**a**, **b**) ERA5 bias-corrected with CRUTS4.03, employing the watch forcing data methodology (WFDE5); (**c**, **d**) ERA5-Land; and (**e**, **f**) the multimodel mean of five C3S-CMIP6-adjusted climate model outputs for SSP5–8.5. The rest is the same as in Fig. 3.

The east and west coasts have surpassed the mean warming threshold of 1 °C, whereas the south coast is relatively cooler and remains below 1 °C (Fig. 5b and Table S8). Warming over the east coast (1.17 ± 0.08 °C) is higher than over the west (1.09 ± 0.08 °C) and south coasts (0.9 ± 0.08 °C). Warmer regions seem associated with a slightly higher mean uncertainty range due to internal climate variability. For instance, the uncertainty range of the Arabian Peninsula (0.24 °C) is smaller than that of the APHR (0.33 °C). Similarly, the west and east coasts (0.26 °C and 0.28 °C, respectively) have considerably more uncertainty than the south coast (0.22 °C). All datasets produced comparable warming and uncertainty ranges, except ERA5 and WFDE5, which differ from the other datasets.

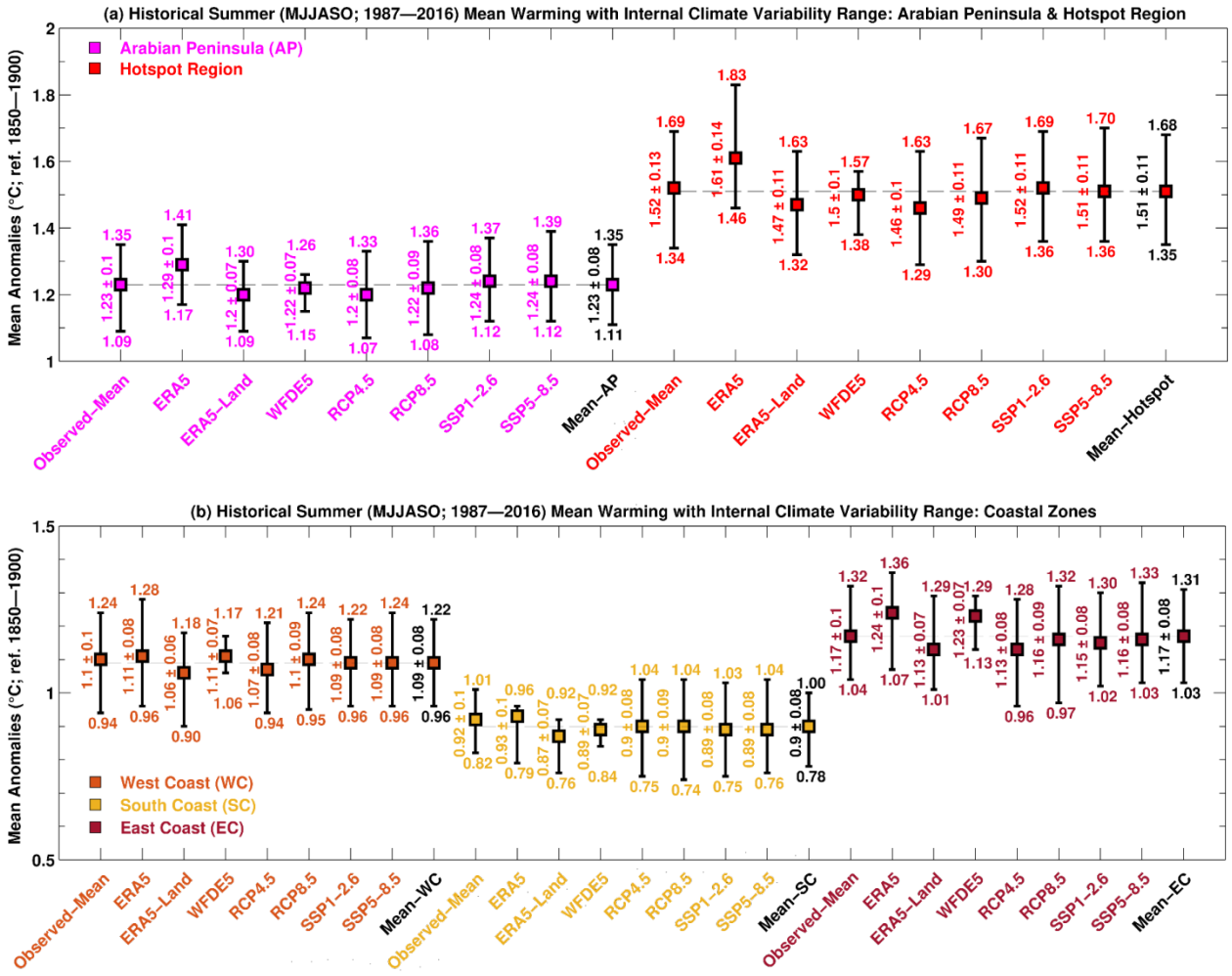

Figure 5. Historical summer (May–October; 1987–2016) mean climatological warming with internal climate variability range (99% confidence interval). (**a**) the Arabian Peninsula and Arabian Peninsula hotspot region, and (**b**) coastal zones.

3.3. Current (2020) Global and Regional Warming

The observations indicate that the world warmed by 1.15 °C over land and ocean overall and by 1.71 °C over land only in 2020 (Fig. 6a and Table S9). The year 2020 experienced summer warming (1.68 ± 0.11 °C) over the MENA region more strongly than in winter (1.49 ± 0.11 °C; Fig. 6a–b and Table S9), and the same is the case for the Arabian Peninsula, APHR, and coastal zones (Fig. 6c–d and Table S9). The most substantial summer warming in 2020 occurred over the APHR (2.29 ± 0.09 °C), revealing that the population in this region is vulnerable to heat stress, and climate change adaptation measures should be considered. The 2020 west coast observed weaker winter warming than summer warming, although the historical summer and winter trends are roughly the same, which could be due to a substantial multidecadal natural variability over the west coast in winter compared to summer (cf. blue curves in Fig. 6c–d). All mean temperature anomalies in the observational datasets over MENA and its subregions are within the uncertainty range measured by the 200 ensemble members of the HadCRUT5 analysis (Figs. 6 and S9–S10), indicating high confidence in the current warming estimates.

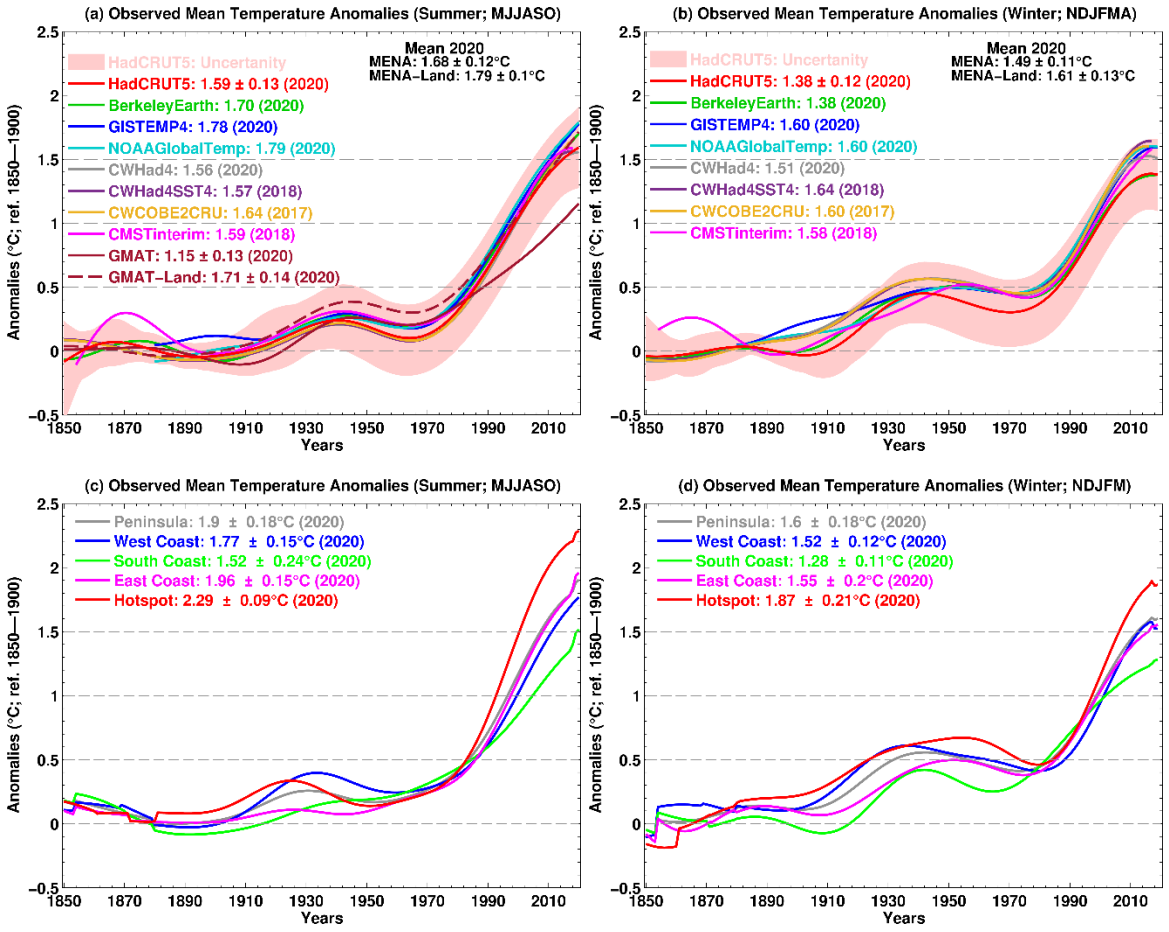

Figure 6. Historical (1850–2020) summer (left panel) and winter (right panel) temperature change relative to the preindustrial climate (1850–1900). (**a**, **b**) over the Middle East and North African region, and (**c**, **d**) the Arabian Peninsula and its coastal zones. The pink shading in **a** and **b** indicates a 99% confidence interval calculated from 200 ensemble members of the HadCRUT5 analysis. In **c** and **d**, temperature anomalies are the mean of eight observational datasets (presented in **a** and **b**).

The magnitude of the current warming among datasets (reanalyses, RCPs, and SSPs) differs for the same region (Table S9). Generally, the C3S-CMP6-Adjusted dataset simulates relatively more substantial warming than the C3S-CMP5-Adjusted dataset. Similarly, ERA5 displays higher warming than ERA5-Land for the same area. Further, ERA5 indicates more substantial warming compared to the observations.

Considering all datasets, the current GSAT (GSAT-Land) median warming is 1.27 ± 0.14 °C (1.83 ± 0.24 °C). The recent median summer warming over the MENA-Land region (1.9 ± 0.25 °C), Arabian Peninsula (1.98 ± 0.31 °C), and east coast (1.92 ± 0.29 °C) are at the brink of exceeding 2 °C, whereas the APHR (2.38 ± 0.29 °C) has already surpassed 2 °C. The west (1.77 ± 0.28 °C) and south coasts (1.36 ± 0.24 °C) are relatively less warm, although the current summer and winter warming over the west coast is more than 1.5 °C (Table S9). The recent warming over MENA and its subregions is much stronger than that of GSAT.

The temperature increase is not spatially homogeneous across the MENA region (Figs. 3–6). For example, the recent warming in the APHR is more profound than the MENA average. Overall, summers (Fig. 6a and c) exhibit stronger current warming than winters (Fig. 6b and d) over the region (except the south coast), particularly in the last four decades. Substantial multidecadal natural variability is also evident before 1970. However, it is masked afterward, possibly due to potent external GHG forcing.

3.4. Future Mean Warming (2021–2050 and 2069–2098)

The warming over MENA is projected to intensify in the near (2021–2050) and far future (2069–2098) under all considered emission scenarios (Figs. 7–8 and Tables S10–S11). The observed hotspots will continue to warm at an accelerating pace, causing further extreme thermal stress for the local populations and ecosystems.

Under the moderate emission scenario (RCP4.5; Fig. 7a–d) in the C3S-CMIP5-Adjusted MMM in summer (winter), the MENA (land and ocean) mean warming would likely reach 2.26 ± 0.07 °C (2.06 ± 0.08 °C) in the near future and up to 3.35 ± 0.09 °C (3.02 ± 0.1 °C) in the far future (relative to the preindustrial era). The high-end GHG emission pathway (RCP8.5; Fig. 7e–h) displays more severe warming over the region, with a mean summer (winter) warming of 2.62 ± 0.05 °C (2.38 ± 0.07 °C) and 5.7 ± 0.11 °C (5.11 ± 0.12 °C) in the near and far future, respectively. In the far future (2069–2098), the mean warming over the summer hotspots would likely exceed 4 °C and 7 °C under the moderate and high-end emission scenarios, respectively.

The wintertime temperature anomaly dipole over the Red Sea observed in the historical period (1987–2016) seems absent in the future. However, like in the historical period, the northern part of the Red Sea warms faster than the southern part in summer.

In the C3S-CMIP6-Adjusted MMM, even under a sustainable pathway (SSP1–2.6), which assumes that the GSAT does not surpass the 2 °C warming limit defined in the Paris Agreement, the mean warming over the MENA-Land region would exceed 2.5 °C (Fig. 8a–d and Tables S10–S11). The MENA-Land region in SSP1–2.6 would warm to 2.54 ± 0.06 °C (2.82 ± 0.04 °C) in summer and up to 2.4 ± 0.09 °C (2.53 ± 0.08 °C) in winter in the near (far) future. In the near (far) future, under this scenario, a maximum winter warming of ~3.5 °C (~3.6 °C) would occur over parts of the Elburz Mountains.

Under the SSP5–8.5 in the C3S-CMIP6-Adjusted MMM (Fig. 8e–h), a mean summer (winter) warming of 2.85 ± 0.11 °C (2.61 ± 0.1 °C) and 6.43 ± 0.14 °C (5.74 ± 0.16 °C) is projected for the near and far future, respectively. In the far future, a maximum summer (winter) warming of ~8 °C (~7 °C) is projected over parts of the Arabian Peninsula and AHR.

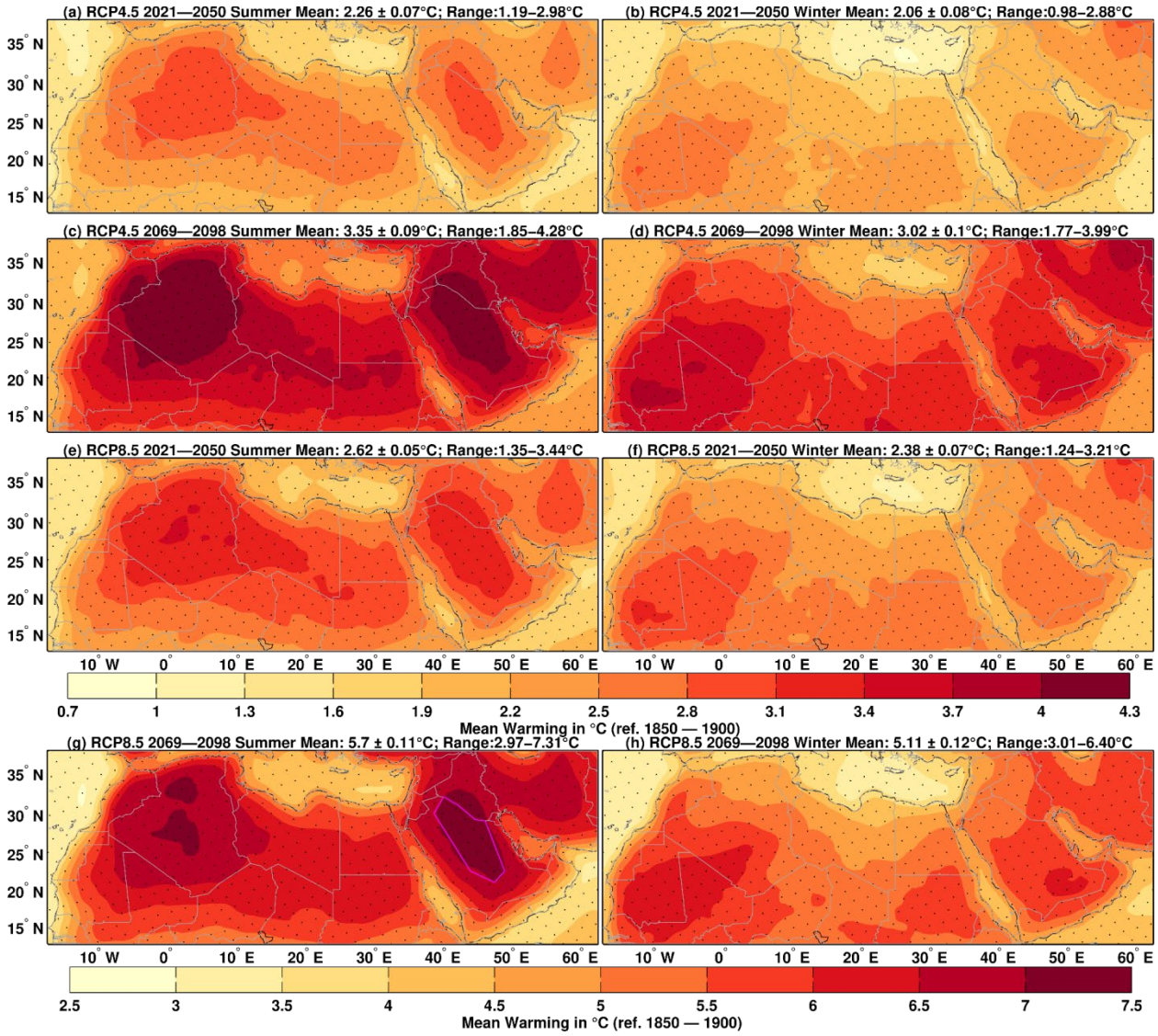

Figure 7. Spatial patterns of near-term (2021–2050; **a**–**b** and **e**–**f**) and long-term (2069–2098; **c**–**d** and **g**–**h**) future summer (May–October; left panel) and winter (November–April; right panel) mean climatological warming relative to the preindustrial climate (1850–1900) using 21 C3S-CMIP5-Adjusted climate model outputs. (**a**–**d**) RCP4.5 and (**e**–**h**) RCP8.5. The magenta polygon marks the hotspot region. Stippling indicates statistical significance with 2 SDs of internal climate variability, where all corresponding data members agree for a change in sign. Numbers above each subfigure indicate the climatological mean warming with ±1 SD and temperature range (min to max).

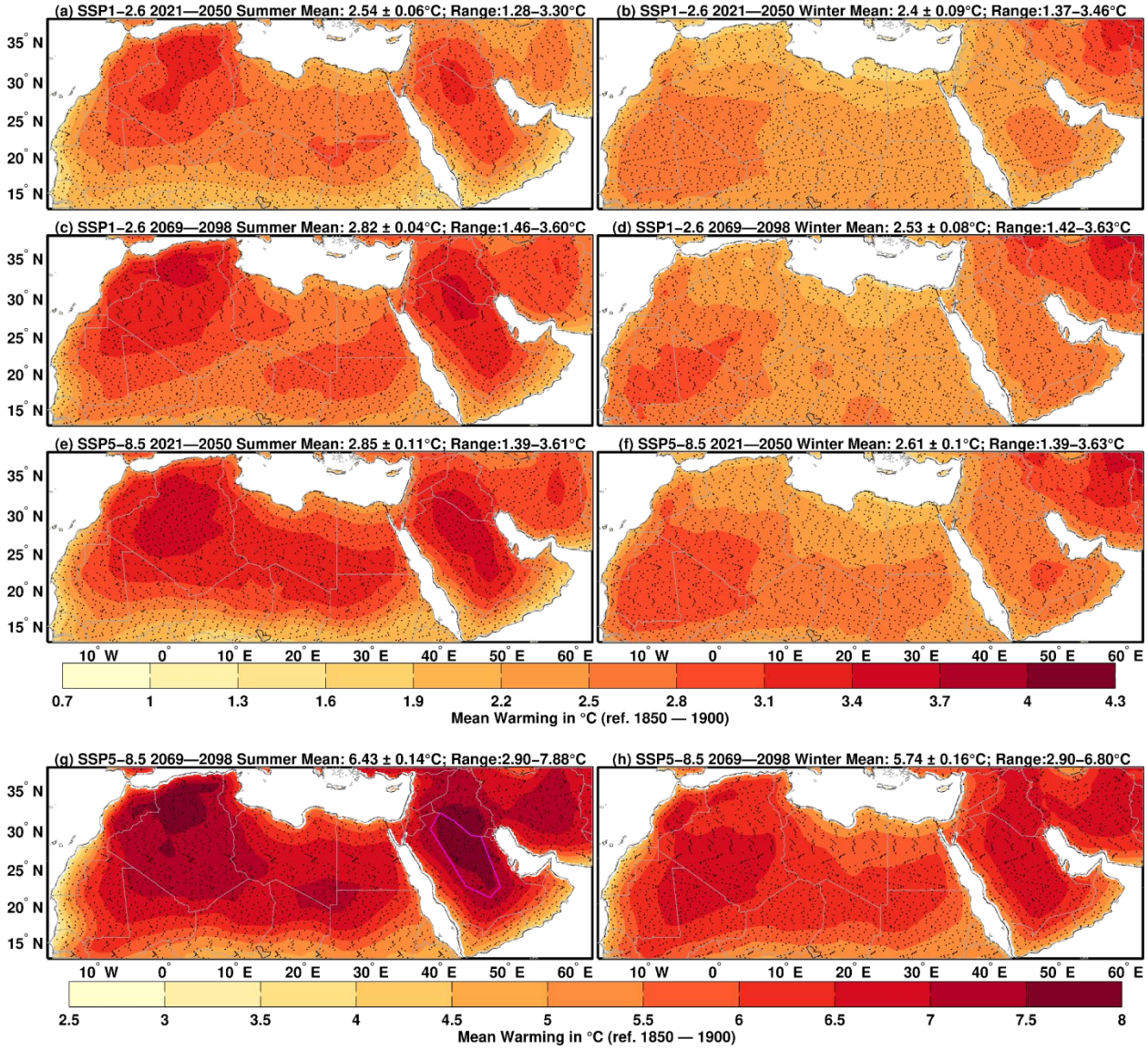

Figure 8. Same as in Fig. 7 but using five C3S-CMIP6-adjusted climate model outputs for the SSP1–2.6 and SSP5–8.5 scenarios.

Figure 9 presents the mean summer warming spatially averaged over the Arabian Peninsula, APHR, and coastal zones under various pathways for the near (2021–2050; Fig. 9a) and far future (2069–2098; Fig. 9b) with uncertainty due to the model spread and internal climate variability. The results for winter are depicted in Fig. S11. In the near (far) future, the mean summer warming over the Arabian Peninsula would range from 2.4 ± 0.08 °C (2.84 ± 0.05 °C) to 2.86 ± 0.11 °C (6.41 ± 0.15 °C), with the lowest warming occurring under RCP4.5 (SSP1–2.6) and highest under RCP8.5 (SSP5–8.5), respectively. The most strongly increased warming projected over the APHR ranges from 2.86 ± 0.1 °C (3.35 ± 0.06 °C) to 3.48 ± 0.13 °C (7.59 ± 0.17 °C) in the near (far) future, with the lowest warming under RCP4.5 (SSP1–2.6) and the highest under SSP5–8.5.

Among the coastal zones, the east (south) coast would warm faster (slower) in the future (Fig. 9a–b and Tables S10–S11), as also observed during the historical period. The warming over the west coast is projected to range from 2.18 ± 0.08 °C (2.56 ± 0.05 °C) to 2.60 ± 0.1 °C (5.73 ± 0.12 °C) in the near (far) future, where the lowest warming occurs under RCP4.5 (SSP1–2.6) and the highest under the RCP8.5 scenario, respectively. In the near (far) future, the south coast would warm from 1.74 ± 0.08 °C (2.1 ± 0.05 °C) to 2.0 ± 0.1 °C (4.67 ± 0.15 °C), whereas the east coast would warm from 2.47 ± 0.07 °C (2.75 ± 0.05 °C) to 2.77 ± 0.11 °C (6.32 ± 0.15 °C) under the considered emission scenarios.

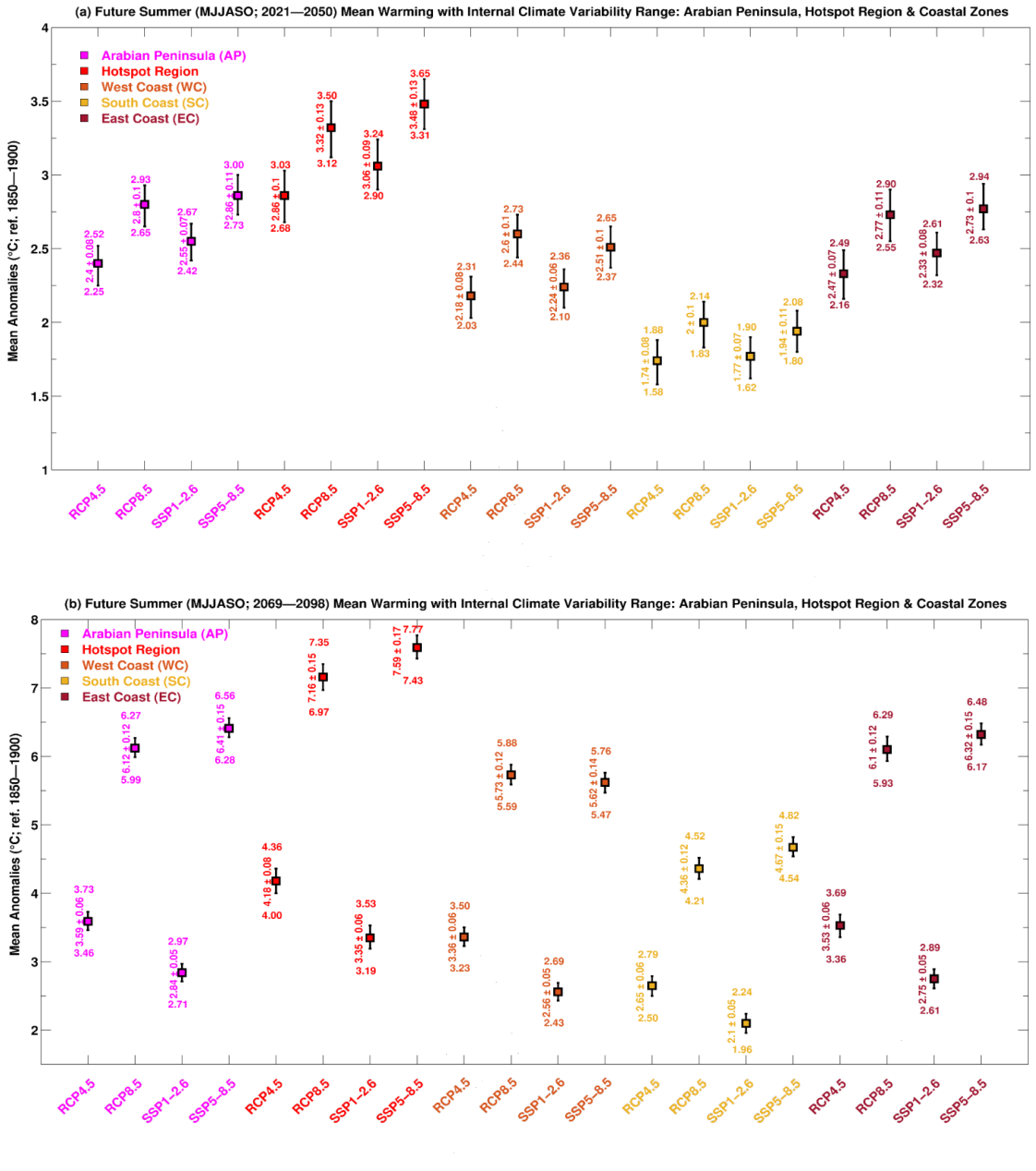

Figure 9. Future summer (May–October) mean climatological warming with internal climate variability range (99% confidence interval) over the Arabian Peninsula, hotspot region, and coastal zones. (**a**) For the near-term (2021–2050) and (**b**) long-term future.

559 ### 3.5. Temperature Trends

560 We compared the historical (1987–2016) and future (2021–2098) global and regional linear
561 temperature trends in degrees Celsius per decade (Table 1). We smoothed the temperature
562 anomaly time series over the whole available period of the dataset using Mann's (2008) adaptive
563 smoothing approach at a cutoff frequency of 40 years. Then, we selected the historical (1987–
564 2016) and future periods (2021–2098) to fit a linear trend and calculated the warming rate in
565 degrees Celsius per decade. We assumed that smoothing the time series before calculating the
566 trend minimizes the influence of internal variability.

567 The GMAT and MENA temperature seem to warm nearly at the same pace until 1980; however,
568 both significantly diverge from each other afterward, where MENA starts to warm at a faster rate
569 compared to the GMAT (Fig. 6a). The GMAT (GMAT-Land) is warming at 0.2 ±
570 0.02 °C/decade (0.33 ± 0.02 °C/decade) (Table 1). In contrast, the observed summer warming
571 trend over MENA is 0.37 ± 0.02 °C/decade (i.e., 1.85 (1.12) times faster than that of GMAT
572 (GMAT-Land)). The observed winter warming trend over MENA (0.35 ± 0.03 °C/decade; Table
573 S12) is 10% slower than in summer and 1.75 times faster than the GMAT trend. The MENA and
574 GMAT-Land are warming roughly at the same pace.

575 Over the historical period, the Arabian Peninsula, APHR, and coastal zones (except the south
576 coast) are warming faster than the GMAT and MENA in summer and winter. The Arabian
577 Peninsula is warming at 0.43 ± 0.03 °C/decade in summer, i.e., 2.15 (1.3) times faster than the
578 GMAT (GMAT-Land)). The climatic conditions over the APHR deteriorate even quicker,
579 warming at 0.55 ± 0.04 °C/decade (i.e., 2.5 times faster than the GMAT). The summer (winter)
580 warming trend over the east (west) coast is higher than other coasts, whereas the south coast
581 warms slower than other coasts throughout the year. The MENA region, Arabian Peninsula,
582 APHR, and coastal zones (except the west coast) are warming faster in summer than winter.
583 Furthermore, all observational datasets display harmonized increasing temperature trends within
584 the uncertainty range of the HadCRUT5 analysis calculated from its 200 ensemble members
585 (Figs. 6a–b and S9–S10).

586 In the models under the intermediate (high-end) GHG emission scenario, RCP4.5 (RCP8.5), the
587 historical GSAT trend equals 0.25 (0.27) ± 0.07 °C/decade (Table 1). The historical ERA5
588 GSAT trend of 0.22 ± 0.003 °C/decade is comparable to the observations (0.2 ± 0.02 °C/decade);
589 however, both intermediate and high-end emission scenarios reveal comparatively larger trend
590 estimates. In the future (2021–2098), under the high-end emission scenario, the GSAT is
591 projected to warm at 0.46 ± 0.08 °C/decade (i.e., 1.7 times faster than in the historical period).

592 The historical summer warming trends over the MENA region under RCP4.5 (0.36 ± 0.1 °C) and
593 RCP8.5 (0.39 ± 0.09 °C) compare well with the observed trend (0.37 ± 0.01 °C). The ERA5
594 trend (0.41 ± 0.004 °C) is overestimated compared to the observations. Under RCP8.5, the
595 warming over the MENA region further accelerates (0.64 ± 0.11 °C/decade) compared to the
596 historical period (0.39 ± 0.09 °C/decade).

597

598

599 **Table 1.** *Historical (1987–2016) and future (2021–2098) linear global (annual) and regional*
600 *(summer) warming trends (*°C/decade*)*

	Global (land and ocean)	Global-Land	MENA (land and ocean)	MENA-Land	Arabian Peninsula	APHR	West coast	South coast	East coast
1987–2016									
Obs8	0.2 ± 0.02	0.33 ± 0.02	0.37 ± 0.01	0.38 ± 0.01	0.43 ± 0.05	0.55 ± 0.04	0.41 ± 0.08	0.28 ± 0.07	0.45 ± 0.07
WFDE5	–	0.27 ± 0.001*	–	0.33 ± 0.01*	0.36 ± 0.01	0.49 ± 0.02	0.34 ± 0.01	0.19 ± 0.003	0.47 ± 0.01
ERA5	0.22 ± 0.003	0.37 ± 0.001	0.41 ± 0.004	0.43 ± 0.004	0.51 ± 0.001	0.72 ± 0.001	0.43 ± 0.01	0.22 ± 0.01	0.57 ± 0.003
ERA5-Land	–	0.34 ± 0.003	–	0.35 ± 0.005	0.41 ± 0.10	0.49 ± 0.01	0.34 ± 0.01	0.16 ± 0.003	0.40 ± 0.01
RCP4.5	0.25 ± 0.07	0.37 ± 0.09	0.36 ± 0.1	0.39 ± 0.11	0.36 ± 0.14	0.41 ± 0.15	0.34 ± 0.14	0.26 ± 0.11	0.36 ± 0.14
RCP8.5	0.27 ± 0.07	0.39 ± 0.09	0.39 ± 0.09	0.42 ± 0.10	0.40 ± 0.13	0.47 ± 0.14	0.37 ± 0.14	0.28 ± 0.10	0.40 ± 0.14
SSP1–2.6	0.26 ± 0.06	0.40 ± 0.1	–	0.43 ± 0.09	0.41 ± 0.10	0.50 ± 0.10	0.36 ± 0.11	0.24 ± 0.08	0.40 ± 0.09
SSP5–8.5	0.26 ± 0.05	0.39 ± 0.1	–	0.43 ± 0.10	0.42 ± 0.10	0.51 ± 0.10	0.37 ± 0.08	0.25 ± 0.09	0.42 ± 0.08
Mean	**0.24 ± 0.05**	**0.36 ± 0.05**	**0.38 ± 0.05**	**0.40 ± 0.05**	**0.41 ± 0.08**	**0.52 ± 0.07**	**0.37 ± 0.07**	**0.24 ± 0.06**	**0.43 ± 0.08**
Median	**0.26 ± 0.06**	**0.37 ± 0.06**	**0.38 ± 0.05**	**0.41 ± 0.05**	**0.41 ± 0.10**	**0.50 ± 0.07**	**0.37 ± 0.06**	**0.25 ± 0.08**	**0.41 ± 0.08**
2021–2050									
	Global (land and ocean)	Global-Land	MENA (land and ocean)	MENA-Land	Arabian Peninsula	APHR	West coast	South coast	East coast
RCP4.5	0.17 ± 0.05	0.30 ± 0.07	0.22 ± 0.06	0.24 ± 0.07	0.25 ± 0.07	0.27 ± 0.07	0.24 ± 0.06	0.19 ± 0.06	0.24 ± 0.07
RCP8.5	0.46 ± 0.08	0.65 ± 0.11	0.64 ± 0.11	0.69 ± 0.12	0.69 ± 0.13	0.79 ± 0.14	0.65 ± 0.12	0.49 ± 0.11	0.70 ± 0.13
SSP1–2.6	0.06 ± 0.04	0.09 ± 0.07	–	0.06 ± 0.06	0.07 ± 0.06	0.07 ± 0.07	0.07 ± 0.04	0.07 ± 0.04	0.06 ± 0.05
SSP5–8.5	0.50 ±0.13	0.73 ± 0.24	–	0.74 ± 0.18	0.74 ± 0.16	0.85 ± 0.19	0.64 ± 0.16	0.57 ± 0.15	0.73 ± 0.15

601 Obs8: Mean of eight observational datasets mentioned in Table S2.
602 * With an asterisk is the standard error, and without an asterisk is ± 1 SD calculated
603 from different datasets or corresponding ensemble members.
604
605 The historical warming trend over the Arabian Peninsula is 0.36 ± 0.14 °C/decade (0.40 ±
606 0.14 °C/decade) under RCP4.5 (RCP8.5). However, under RCP8.5, the future warming trend
607 (0.69 ± 0.13 °C/decade) would be much faster than in the historical period. In addition, ERA5
608 displays a stronger warming trend (0.51 ± 0.001 °C/decade) over the Arabian Peninsula than
609 climate models and observations.

610 Similar to the observations, the coastal zones of the Arabian Peninsula are not warming at the
611 same pace in the reanalyses and RCP scenarios (Table 1). The east coast warms faster than the
612 west and south coasts, and this tendency is expected to continue. The historical heating trends
613 over the coastal zones for ERA5 and the considered RCPs are lower than in the observations.

The historical global warming trends in the C3S-CMIP6-Adjusted dataset are similar to those in the C3S-CMIP5-Adjusted dataset and are overestimated compared to the observations (Table 1). The historical warming trends over the MENA-Land region in SSP1–2.6 (0.43 ± 0.09 °C) and SSP5–8.5 (0.43 ± 0.1 °C) are comparable with RCP4.5 (0.39 ± 0.11 °C) and RCP8.5 (0.42 ± 0.1 °C), respectively. However, the ERA5 (0.43 ± 0.004 °C) and ERA5-Land (0.35 ± 0.005 °C) datasets display considerable trend differences over the MENA-Land region.

Over the Arabian Peninsula, SSP1–2.6 (0.41 ± 0.1 °C) and SSP5–8.5 (0.42 ± 0.1 °C) estimate the historical temperature trends close to the observations (0.43 ± 0.05 °C). In contrast to the temperature trend in ERA5 (0.51 ± 0.001 °C), the temperature trend in ERA5-Land (0.37 ± 0.005 °C) is more realistic when compared with the observed trend.

The historical warming trends over the APHR for ERA5-Land (0.49 ± 0.01 °C) for SSP1–2.6 (0.5 ± 0.1 °C), and SSP5–8.5 (0.51 ± 0.1 °C) are reasonably close to the observed trend (0.55 ± 0.04 °C). Depending on the dataset, APHR is warming two to three times faster than the global warming rate.

Over the coastal zones, the C3S-CMIP5-Adjusted and C3S-CMIP6-Adjusted datasets produced similar historical warming trends and were close to the observed trends. The C3S-CMIP6 warming trends under SSP1–2.6 and SSP5–8.5 are comparable with the ERA5-Land dataset for the west and the east coasts; however, they are primarily underestimated over the south coast. The C3S-CMIP6-Adjusted dataset displays a faster future warming trend over the south coast than the C3S-CMIP5-Adjusted dataset.

3.6. Comparison of Regional Warming with Global Warming Thresholds

Determining when the annual GSAT will surpass certain warming thresholds (1.5, 2, 3, and 4 °C; Figs. 10–11 and Tables S13–14) and the consequences for MENA and its subregions is crucial to support policymakers in planning effective and timely climate change adaptation and mitigation measures, including energy demand and water resource management. The main text only reveals the summer warming response for MENA and its subregions; please see the Supporting Information for the winter (Figs. S12–S13 and Tables S15–S21).

Figures 10–11 depict when GSAT anomalies surpass certain warming thresholds and the warming response of MENA and its subregions. Under RCP4.5 (RCP8.5), the GSAT warming would reach 1.5 °C by about 2031 ± 11 years (2027 ± 7 years) and 2 °C by 2053 ± 12 years (2041 ± 8 years), respectively. The 3 °C and 4 °C warming thresholds would likely be reached under RCP8.5 by about 2062 ± 10 years and 2082 ± 10 years, respectively.

As MENA warms faster than the globe, when the GSAT anomaly reaches 1.5 (2 °C) under RCP4.5, the MENA region would be 2.18 ± 0.09 °C (2.90 ± 0.12 °C) warmer than in the preindustrial climate. Under RCP8.5, the MENA region would warm by 2.21, 2.91, 4.29, and 5.62 °C at global warming thresholds of 1.5, 2, 3, and 4 °C, respectively. The MENA-Land region would warm by approximately 6 °C at the 4 °C GSAT anomaly.

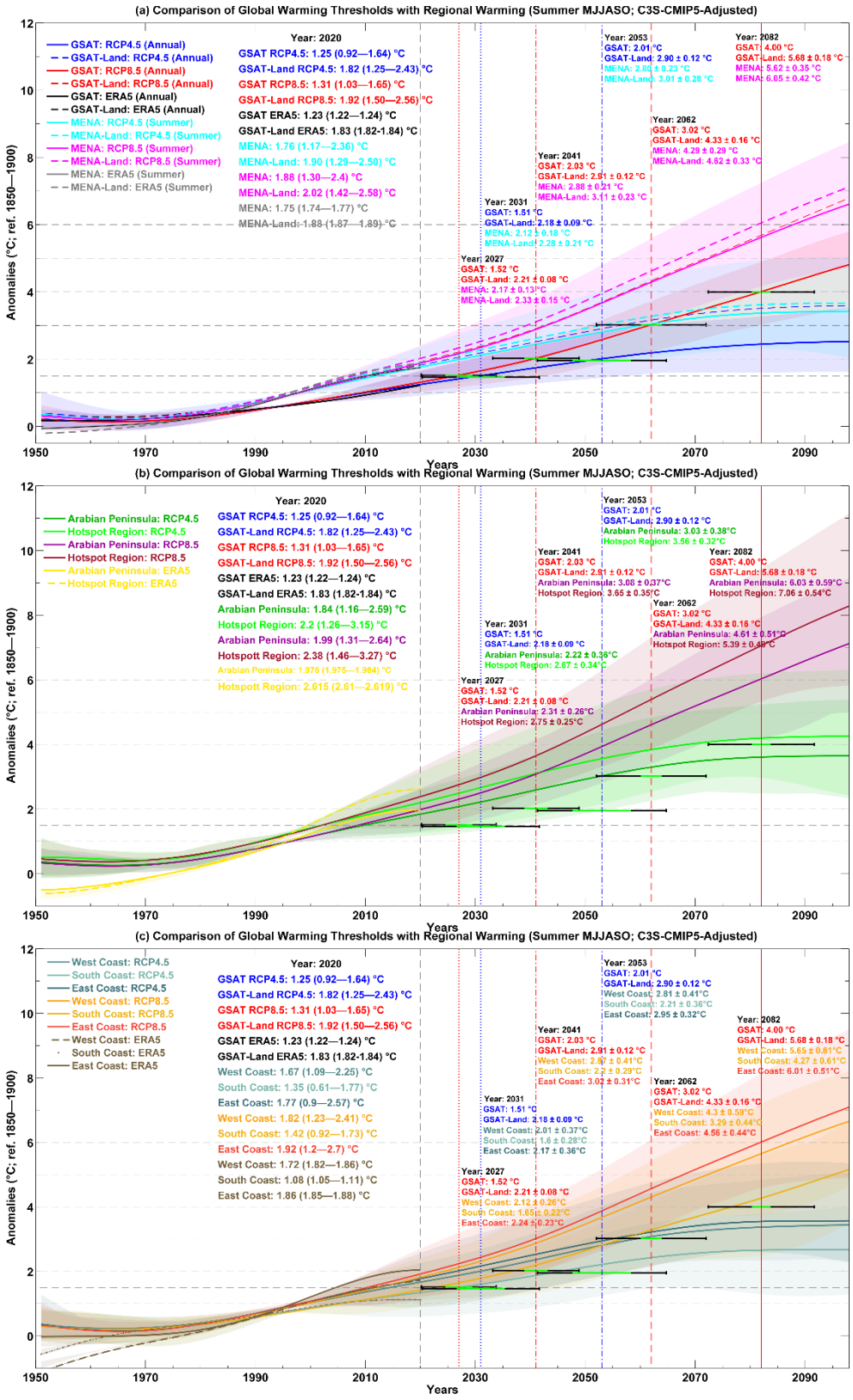

Figure 10. Comparison of summer temperatures over the Middle East and North Africa (MENA) and its subregions with an annual global surface air temperature (GSAT: global land plus ocean; GSAT-land: global land only) at various global temperature thresholds (1.5, 2, 3, and 4 °C).

(**a**) Comparison of MENA, (**b**) the Arabian Peninsula and hotspot region, and (**c**) coastal zones. The C3S-CMIP5-Adjusted curves indicate the multimodel mean of 21 climate models for two emission scenarios (RCP4.5 and RCP8.5) with uncertainty estimates at the 99% confidence interval. The uncertainty for ERA5 is calculated from its 10 ensemble members. The text colors correspond to each dataset, and colored vertical lines mark the year surpassing a particular global temperature threshold for each emission scenario. The horizontal black lines indicate model uncertainty (±1 SD of a year crossing a certain global temperature threshold), whereas green lines indicate uncertainty in a year due to internal climate variability.

Under RCP4.5 (RCP8.5), the Arabian Peninsula would warm to 2.22 ± 0.36 °C (2.31 ± 0.26 °C) and 3.03 ± 0.38 °C (3.08 ± 0.37) °C at the 1.5 and 2 °C GSAT anomalies, respectively. At the 3 °C and 4 °C GSAT anomalies, it would warm to 4.61 ± 0.51 °C and 6.03 ± 0.59 °C, respectively. Under RCP4.5 (RCP8.5), the APHR is projected to warm to 2.67 ± 0.34 °C (2.75 ± 0.25 °C) and 3.56 ± 0.32 °C (3.65 ± 0.35 °C) at 1.5 °C and 2 °C of GSAT warming. At the 3 °C and 4 °C GSAT warming, it would reach 5.39 ± 0.48 °C and 7.06 ± 0.54 °C, respectively.

In the future, the south coast would warm the least compared to the east and west coasts, and under RCP4.5 (RCP8.5), the east coast would heat to 2.17 ± 0.36 °C (2.24 ± 0.23 °C) and 2.95 ± 0.32 °C (3.02 ± 0.31 °C) at 1.5 °C and 2 °C of GSAT warming, respectively. The 3 °C and 4 °C of GSAT warming would result in 4.56 ± 0.44 °C and 6.01 ± 0.51 °C of east coast warming.

Using the C3S-CMIP6-Adjusted data, we found that the GSAT warming would surpass the 1.5 °C threshold in about 2028 ± 8 years under the SSP1–2.6 pathway. Under the SSP5–8.5, the GSAT warming would exceed 1.5, 2, 3, and 4 °C in 2027 ± 6 years, 2040 ± 8 years, 2062 ± 11 years, and 2080 ± 14 years, respectively.

The GSAT warming in the low emission pathway with sustainable development (SSP1–2.6) reaches 1.5 °C. In SSP5–8.5, the GSAT warming is expected to exceed the thresholds (1.5, 2, 3, 4 °C) at more or less the same years as under the RCP8.5.

There is considerably more multimodel uncertainty in reaching certain global temperature thresholds in the CMIP5 and CMIP6 (black horizontal bars in Fig. 10–11). However, the uncertainties due to internal variability (green horizontal bars in Fig. 10–11) are minor compared to the inter-model variability.

The RCP4.5 (2.28 ± 0.21 °C) and SSP1–2.6 (2.35 ± 0.16 °C) simulate comparable MENA-Land regional warming at the 1.5 °C global warming threshold. Similarly, RCP8.5 (2.33, 3.11, 4.62, 6.05 °C) and SSP5–8.5 (2.36, 3.08, 4.66, 6.14 °C) simulate similar warming levels at 1.5, 2, 3, and 4 °C of GSAT warming.

The Arabian Peninsula would warm to 2.33 ± 0.15 °C (2.35 ± 0.2 °C) under SSP1–2.6 (SSP5–8.5) at the 1.5 °C GSAT warming threshold. Under SSP5–8.5 and at 2, 3, and 4 °C global warming levels, the warming over the Arabian Peninsula would be 3.11 ± 0.17 °C, 4.71 ± 0.15 °C, and 6.12 ± 0.17 °C, respectively.

The APHR would warm to 2.84 ± 0.18 °C (2.87 ± 0.28) °C under SSP1–2.6 (SSP5–8.5) at 1.5 °C GSAT warming. Under SSP5–8.5 and at 2, 3, and 4 °C GSAT, the warming over the APHR would be 3.77 ± 0.26 °C, 5.66 ± 0.19 °C, and 7.26 ± 0.13 °C, respectively.

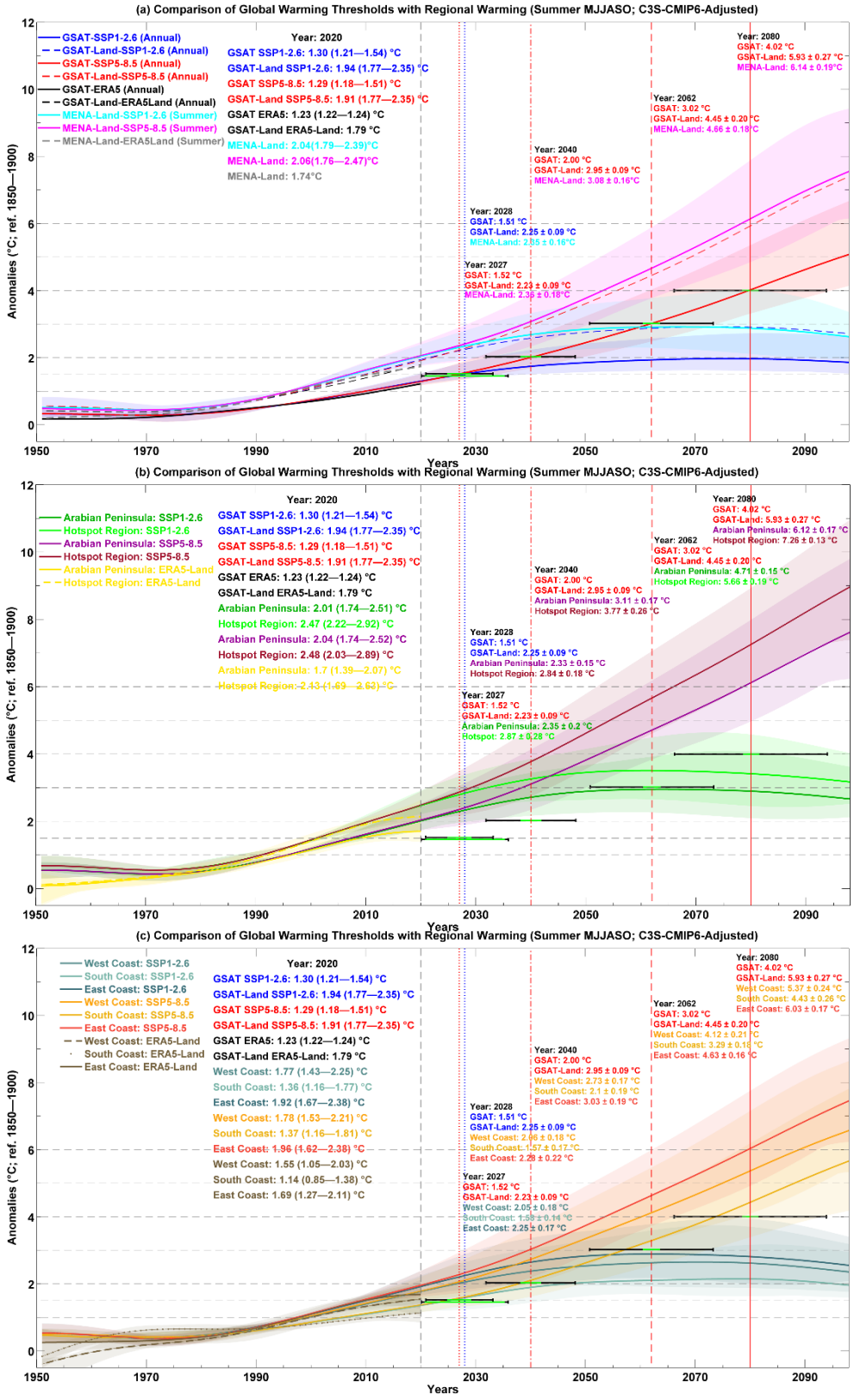

Figure 11. Same as in Fig. 10 but for the C3S-CMIP6-Adjusted dataset with two scenarios (SSP1–2.6 and SSP5–8.5).

The west (south) coast would warm ~2 (~1.5) °C at 1.5 °C of GSAT warming under SSP1–2.6 and SSP5–8.5. At 2, 3, and 4 °C global warming levels under SSP5–8.5, the west (south) coast would warm up to 2.73 ± 0.17 °C (2.10 ± 0.19 °C), 4.12 ± 0.21 °C (3.29 ± 0.18 °C), and 5.37 ± 0.24 °C (4.43 ± 0.26 °C), respectively. At 1.5 °C of GSAT warming, the east coast would warm to 2.25 ± 0.17 °C (2.28 ± 0.22 °C) under SSP51–2.6 (SSP5–8.5). At 2, 3, and 4 °C global warming levels, under SSP5–8.5, the east coast would warm to 3.03 ± 0.19 °C, 4.63 ± 0.16 °C, and 6.03 ± 0.17 °C.

3.7. Warming by the End of the Twenty-first Century (2099)

Since MENA and its subregions are warming at different rates, incoherent warming patterns will persist over the region by the end of the century (2099). Depending upon the emission pathway, the temperature contrast would range from 1 °C to 3.5 °C in the MENA, Arabian Peninsula, APHR, and coastal zones (Table S22).

For the low (SSP1–2.6) and high-end (RCP8.5 and SSP5–8.5) emission pathways, the MENA-Land region would warm from 2.6 ± 0.49 °C to 7.58 ± 1.52 °C and warming over the Arabian Peninsula would be nearly the same. Extreme warming would occur over the APHR ranging from 3.16 ± 0.59 °C to 8.97 ± 1.79 °C between the low and high-end emission pathways. The east (south) coast would be the warmest (coldest) among the coastal zones, ranging from 2.54 ± 0.53 °C (1.95 ± 0.54 °C) to 7.46 ± 1.39 °C (5.65 ± 1.45 °C) between the low and high-end emission pathways. By the end of the century, under the high-end emission pathways, the west coast would be more than 2 °C and about 1 °C cooler than APHR and the east coast, respectively.

3.8. Comparison of CMIP5 and CMIP6

We only compared the CMIP5 and CMIP6 projections for the RCP8.5 and SSP5–8.5 pathways because both have a comparable radiative forcing of 8.5 W/m^2. The historical CMIP5 and CMIP6 simulations reproduce similar spatial warming patterns over the MENA-Land region and are comparable with the observations and reanalysis products (Figs. 3–4). The CMIP5 and CMIP6 ensembles can simulate summer and winter warming hotspots with minor differences in spatial extent and magnitude (cf. Figs. 3e–f, 4e–f, and S7). The historical warming differences between RCP8.5 and SSP5–8.5 are negligible over the Arabian Peninsula, APHR, and coastal zones and compare well to the observations (Fig. 5).

The radiative forcing of SSP5–8.5 is slightly higher than RCP8.5 (see Figure SM1.1 of Abram et al., 2019). Thus, some warming differences exist between RCP8.5 and SSP5–8.5, especially over the hotspot regions in future. In the near (2021–2050) and far (2069–2098) future, compared to RCP8.5, the SSP5–8.5 would substantially warm the APHR, AHR, and WAHR. In the far future (2069–2098), WAHR would shift toward the north and become more pronounced in SSP5–8.5 compared to RCP8.5 (cf. Figs. 7h and 8h). The central parts of the Arabian Peninsula would also warm more in SSP5–8.5 than in RCP8.5.

The difference between RCP8.5 and SSP 5–8.5 warming increases from the historical period to the future over the Arabian Peninsula and APHR. In the far future (2069–2098), the Arabian Peninsula (APHR) mean temperature is projected to be 0.29 °C (0.43 °C) warmer in SSP 5–8.5 than in RCP8.5. The south and west coasts would likely be 0.31 °C and 0.22 °C warmer in

CMIP6/SSP5–8.5 than CMIP5/RCP8.5; however, the west coast would be 0.11 °C colder for the same future period.

Global warming trends in CMIP5 (0.27 ± 0.07 °C/decade) and CMIP6 (0.26 ± 0.05 °C/decade) are similar in the historical period and are the same over land (Table 1). However, in the future, the world would warm 0.04 °C/decade faster in CMIP6 than in CMIP5, and the difference in warming rate doubles (0.08 °C/decade) when considered only over land.

The future warming differences between CMIP5 and CMIP6 could be due to the higher climate sensitivity of some CMIP6 models and the stronger total radiative forcing of SSP5–8.5. The negative aerosol radiative forcing in CMIP6 is more robust than in CMIP5 over the historical period, compensating for the high climate sensitivity with more negative aerosol forcing (Ribes et al., 2021). Further, the CMIP6 models have improved model physics compared to the CMIP5 models; thus, these models could respond differently to a change in climate forcing (Ribes et al., 2021).

4. Discussion and Conclusions

This work provides robust estimates and a comprehensive analysis of the past, present, and future warming over MENA and its subregions using recent and updated observational datasets, high-resolution reanalyses, and statistically downscaled AOGCM outputs from the CMIP5 and CMIP6 ensembles. Here we summarize results based on average from all employed datasets.

Concerning the preindustrial era, the observed warming (1987–2016) over the MENA (MENA-Land) region is 1.13 ± 0.08 °C (1.22 ± 0.08 °C). With the present (2020) warming of 1.77 ± 0.08 °C (1.92 ± 0.13 °C) and a warming rate of 0.38 ± 0.05 °C/decade (0.40 ± 0.05 °C/decade), it follows that the 2 °C regional warming threshold would be reached soon. In the near (2021–2050) and far (2069–2098) futures, a climatological mean warming of 2.62 ± 0.05 °C (2.26 ± 0.07 °C) and 5.7 ± 0.11 °C (3.35 ± 0.09 °C), respectively, is projected under the high (moderate) emission scenario, RCP8.5 (RCP4.5). The MENA-Land-only regional warming would be even stronger. In the near and far future, the MENA-Land region would climatologically warm to 2.85 ± 0.11 °C (2.54 ± 0.06 °C) and 6.43 ± 0.14 °C (2.82 ± 0.09 °C) under the high-end (low) emission scenario, SSP5–8.5 (SSP1–2.6). By the end of the century (2099), the MENA-Land region would warm to 2.6 ± 0.49 °C (SSP1–2.6), 3.66 ± 0.77 °C (RCP4.5), 7.13 ± 1.07 °C (RCP8.5), and 7.58 ± 1.52 °C (SSP5–8.5).

The mean historical warming over the Arabian Peninsula is 1.23 ± 0.08 °C (Table S8). The warming rate (0.41 ± 0.1 °C/decade) exceeds the average for the MENA region (0.38 ± 0.05 °C/decade). It warmed to 1.98 ± 0.31 °C in 2020. The current warming rate has probably surpassed 2 °C of warming. In the near (far) future, climatological mean warming of 2.55 ± 0.07 °C (2.84 ± 0.05 °C), 2.4 ± 0.08 °C (3.59 ± 0.06 °C), 2.80 ± 0.1 °C (6.12 ± 0.12 °C), and 2.86 ± 0.11 °C (6.41 ± 0.15 °C) would likely occur under SSP1.26, RCP4.5, RCP8.5, and SSP585 emission scenarios, respectively. By the end of the century, the Arabian Peninsula would be scorching at 2.66 ± 0.57 °C (SSP1–2.6), 3.64 ± 0.80° C (RCP4.5), 7.12 ± 1.24° C (RCP8.5), and 7.61 ± 1.53 °C (SSP5–8.5) under low, moderate, and high-end emission scenarios.

The central parts of the Arabian Peninsula, referred to as APHR, have already exceeded a 2 °C mean climatological warming with a current (2020) warming of 2.38 ± 0.29 °C. The APHR is

784 warming at a rate of 0.50 ± 0.07 °C/decade (i.e., faster than most parts of the MENA region).
785 The living conditions in the APHR would be significantly harsher, as the mean climatological
786 warming in the far (near) future would reach 4.18 ± 0.08 °C (2.86 ± 0.1 °C), 3.35 ± 0.06 °C (3.06
787 ± 0.09 °C), 7.16 ± 0.15 °C (3.32 ± 0.13 °C), and 7.59 ± 0.17 °C (3.48 ± 0.13 °C) under RCP4.5,
788 SSP1–2.6, RCP8.5, and SSP5–8.5, respectively. By the end of the century, even the low (SSP1–
789 2.6: 3.16 ± 0.59 °C) and moderate (RCP4.5: 3.64 ± 0.80 °C) emission scenarios would cause
790 significant warming. Under high-end emission scenarios, the warming would be extreme
791 (RCP8.5: 8.28 ± 1.36 °C; SSP58.5: 8.97 ± 1.79 °C).

792 The densely populated coastal zones of the Arabian Peninsula would face a severe temperature
793 rise, especially on the east and west coasts. In contrast, the south coast would warm relatively
794 less rapidly. In 2020, at the rate of 0.41 ± 0.08 °C/decade, 0.37 ± 0.06 °C/decade, and 0.25 ±
795 0.08 °C/decade, the east, west, and south coasts had warmed by 1.92 ± 0.29 °C, 1.77 ± 0.28 °C,
796 and 1.36 ± 0.24 °C, respectively. The present mean climatological warming (1987–2016) over
797 the east, west, and south coasts is 1.17 ± 0.08 °C, 1.09 ± 0.08 °C, and 0.9 ± 0.08 °C, respectively.
798 In the near future, the east (west) coast would warm by 2.33 ± 0.08 °C (2.24 ± 0.06 °C), 2.47 ±
799 0.07 °C (2.18 ± 0.08 °C), 2.77 ± 0.11 °C (2.6 ± 0.1 °C), and 2.73 ± 0.1 °C (2.5 ± 0.1 °C),
800 whereas, in the far future, much more significant warming of 2.75 ± 0.05 °C (2.59 ± 0.05), 3.53
801 ± 0.06 °C (3.36 ± 0.06 °C), 6.1 ± 0.12 °C (5.73 ± 0.12 °C), and 6.32 ± 0.15 °C (5.62 ± 0.14 °C)
802 is expected under low (SSP1–2.6), moderate (RCP4.5), and high-end (RCP8.5 and SSP5–8.5)
803 emission scenarios, respectively. By the end of the century, the east (west) coast is projected to
804 warm by 2.54 ± 0.53 °C (2.36 ± 0.51 °C), 3.55 ± 0.84 °C (3.44 ± 0.73 °C), 7.07 ± 1.23 °C (6.65
805 ± 1.11 °C), and 7.46 ± 1.39 °C (6.67 ± 1.40 °C) under SSP1–2.6, RCP4.5, RCP8.5, and SSP5–
806 8.5, respectively. Compared to the east and west coasts, in the near and far future, the south coast
807 would warm slower, warming by 1.95 ± 0.54 °C, 2.66 ± 0.65 °C, 5.15 ± 1.0 °C, and 5.65 ± 1.42
808 °C under SSP1–2.6, RCP4.5, RCP8.5, and SSP5–8.5, respectively.

809 With the contemporary (1987–2016) warming trend of 0.26 ± 0.06 °C/decade, the world warmed
810 by 1.27 ± 0.14 °C in 2020, indicating that the present warming rate would surpass the Paris
811 Accord temperature limit of 1.5 °C by 2029 with uncertainty from 2023 to 2039. However, based
812 on the multimodel and multiscenario analysis, it would cross the 1.5, 2, 3, and 4 °C critical limits
813 by 2028 ± 8 years, 2041 ± 8 years, 2062 ± 11 years, and 2081 ± 12 years, respectively.

814 The mentioned global warming thresholds are associated with significant regional warming over
815 various parts of the MENA region. At the 1.5 ° C global warming threshold, warming in MENA
816 and all its subregions, except the south coast of the Arabian Peninsula, would exceed 2 °C. At
817 1.5 °C of global warming, the temperature over global land would rise by 2.22 ± 0.09 °C. In
818 contrast, the APHR, MENA-Land (MENA), Arabian Peninsula, and east, west, and south coasts
819 would warm by 2.80 ±0.27 °C, 2.34 ± 0.17 °C (2.15 ± 0.16 °C), 2.32 ± 0.23 °C, 2.25 ± 0.23 °C,
820 2.06 ± 0.22 °C, and 1.59 ± 0.20 °C, respectively.

821 At 2 °C of global warming, the global land would heat up by 2.91 ± 0.12 °C. The APHR,
822 MENA-Land (MENA), Arabian Peninsula, and east, west, and south coasts would warm faster
823 than the globe, reaching 3.65 ± 0.32 °C, 3.08 ± 0.23 °C (2.84 ± 0.22 °C), 3.08 ± 0.37 °C, 3.03 ±
824 0.31 °C, 2.81 ± 0.41 °C, and 2.20 ± 0.29 °C, respectively.

825 Based on the observations, the MENA, Arabian Peninsula, APHR, and east, west, and south
826 coasts are warming nearly 1.85, 2.2, 2.8, 2.3, 2.1, and 1.4 times faster than the GMAT. However,
827 based on median values from all datasets, the warming is pacing 1.5, 1.6, 1.9, 1.6, 1.4, and 0.96
828 times faster, respectively.

829 The observational datasets indicate little difference between MENA's warming rates in summer
830 (0.37 ± 0.01 °C/decade) and winter (0.35 ± 0.03 °C/decade). The ERA5 also displays no
831 difference between summer and winter warming rates; however, the MENA-Land-only region is
832 warming faster in winter than in summer. In contrast to observations, all median values in the
833 datasets indicate a faster summer (0.38 ± 0.05 °C/decade) warming than winter (0.34 ±
834 0.06 °C/decade) for MENA and its land-only regions (summer: 0.41 ± 0.05 °C/decade; winter:
835 0.38 ± 0.06 °C/decade). Based on the median value from all datasets, we conclude that the
836 MENA and its subregions, except the west and south coasts, are warming faster in summer than
837 the winter.

838 All the analyzed datasets in this study exhibit consistent regional warming patterns over the
839 MENA region in the past, present, and future. Although previous studies (e.g., Lelieveld et al.,
840 2016) found more rapid warming in summer, the current results in this paper reveal that the
841 magnitude of warming in the MENA region is comparable in summer and winter in
842 observations, which could be due to a different definition of summer and winter seasons in this
843 analysis. However, the locations of warming hotspots are different in summer and winter in the
844 region. For example, in summer, the major hotspots are located over Northwest Africa in Algeria
845 and the north-central parts of the Arabian Peninsula. In contrast, in winter, they are in Iran
846 (Elburz Mountains), Mauritania (West Africa), and Sudan (North Africa). Similarly, although
847 previous studies (e.g., Chaidez et al., 2017) have indicated generally higher warming in the
848 southern Red Sea, the current results reveal that this is valid only in winter and that the higher
849 warming is located in the northern Red Sea in summer, further identifying the seasonal features
850 of warming.

851 The Arabian Peninsula is warming faster than the MENA region, but the warming is not
852 uniformly distributed. In particular, the eastern Arabian Peninsula is warming faster than the
853 southern and western coasts, which is attributable to the proximity to regional water bodies,
854 which is due to the shallowness of the gulf, which adjusts much more rapidly (seasonally and
855 climatologically) to atmospheric warming than the Red Sea, particularly the Arabian Sea. The
856 results demonstrate that warming over the Arabian Peninsula is already well above 1.5 °C and is
857 estimated to exceed 3.8 °C and 7 °C by the end of the twenty-first century under the intermediate
858 (RCP4.5) and extreme scenarios (RCP8.5), respectively. The climate change signal is robust, as
859 the magnitude of warming exceeds the internal climate variability throughout the MENA region,
860 both in observations and climate model outputs. The warming in the C3S-CMIP6-Adjusted
861 dataset, which has a higher resolution than the C3S-CMIP5-Adjusted dataset, is consistent with
862 that from CMIP5 data, both in historical and future periods. Compared with the global warming
863 in the CMIP5 21 model ensemble, the entire MENA region is warming at a rate similar to that of
864 the global land.

865 Extreme regional warming would affect the habitability of the area, and economic activities,
866 increasing the energy demand for cooling and limiting outdoor activities. In a warmer world,
867 heat waves in MENA would be more frequent and intense (Zittis et al., 2021), causing

widespread heat strokes and cardiovascular disease and eventually increasing heat-related mortalities (Hajat et al., 2023). These estimates of regional warming are meant to inform policy decisions on a wide range of topics, including city planning, climate adaptation, energy use, and water resource management in the region. The high-resolution (9 km) CMIP6 datasets could be beneficial for estimating regional and local environmental conditions and calculating the spatially distributed influence of warming on the health and mortality rate of the population. The temperature change during the historic period reveals a significant contribution of the natural variability consistent between the datasets. The future climate projections, evaluated using multimodel ensembles, are consistent between the CMIP5 and CMIP6 models.

Acknowledgements

The study reported in this publication was supported by funding from the King Abdullah University of Science and Technology (KAUST) through Grant BAS/1/1309-01-01. The authors thank the KAUST Supercomputing Laboratory for providing computer resources. We thank the Climatic Research Unit (University of East Anglia) and Met Office for providing the HadCRUT5 analysis data. We thank Harilaos Loukos from the Climate Data Factory for providing the high-resolution statistically downscaled climate model outputs. We thank the Climate Data Store (C3S), Copernicus Climate Change Service, for providing the reanalysis products.

Open Research

All observational, reanalysis products, and climate model outputs used in this study are available online. To download the data, please refer to the following link:
https://repository.kaust.edu.sa/handle/10754/691762

References

Abram, N., Gattuso, J.-P., Prakash, A., Cheng, L., Chidichimo, M. P., Crate, S. et al. (2019). Framing and Context of the Report: Supplementary Material. In H.-O. Pörtner, D.C. Roberts, V. Masson-Delmotte, P. Zhai, M. Tignor, E. Poloczanska, et al. (eds.), *IPCC Special Report on the Ocean and Cryosphere in a Changing Climate* (pp. 1–11). Retrieved from https://www.ipcc.ch/srocc/

Allen, M.R., Dube, O.P., Solecki, W., Aragón-Durand, F., Cramer, W., Humphreys, S. et al. (2018) Framing and Context. In V. Masson-Delmotte, P. Zhai, H.-O. Pörtner, D. Roberts, J. Skea, P.R. Shukla, et al. (eds.), *Global Warming of 1.5°C.* An IPCC Special Report on the impacts of global warming of 1.5°C above pre-industrial levels and related global greenhouse gas emission pathways, in the context of strengthening the global response to the threat of climate change, sustainable development, and efforts to eradicate poverty (pp. 49-92). Cambridge, UK and New York, NY: Cambridge University Press. https://doi.org/10.1017/9781009157940.003

Almazroui, M., (2006). The relationships between atmospheric circulation patterns and surface climatic elements in Saudi Arabia, Ph.D., Climatic Research Unit, University of East Anglia, Norwich, UK. http://www.secheresse.info/spip.php?article9431

Almazroui, M. (2011). Calibration of TRMM rainfall climatology over Saudi Arabia during 1998-2009. *Atmospheric Research*, *99*(3–4), 400–414. https://doi.org/10.1016/j.atmosres.2010.11.006

Almazroui, M., Alowaibdi, T., & Hasanean, H. (2022). Dynamical downscaled CMIP5 scenario–based future climate changes over the Arabian Peninsula. *Arabian Journal of Geosciences*, *15*(10), 1–13. https://doi.org/10.1007/s12517-022-10247-7

Andrews, O., Le Quéré, C., Kjellstrom, T., Lemke, B., & Haines, A. (2018). Implications for workability and survivability in populations exposed to extreme heat under climate change: A modelling study. *The Lancet Planetary Health*, *2*(12), e540–e547. https://doi.org/10.1016/S2542-5196(18)30240-7

Arnell, N. W., Lowe, J. A., Bernie, D., Nicholls, R. J., Brown, S., Challinor, A. J., & Osborn, T. J. (2019). The global and regional impacts of climate change under representative concentration pathway forcings and shared socioeconomic pathway socioeconomic scenarios. *Environmental Research Letters*, *14*(8). https://doi.org/10.1088/1748-9326/ab35a6

Ribes, A., Qasmi, S., & Gillett N. P. (2021). Making climate projections conditional on historical observations. *Science Advances*, *7*(4), https://doi.org/10.1126/sciadv.abc0671

Bathiany, S., Dakos, V., Scheffer, M., & Lenton, T. M. (2018). Climate models predict increasing temperature variability in poor countries. *Science Advances*, *4*(5), 1–11. https://doi.org/10.1126/sciadv.aar5809

Battisti, D.S., & Naylor, R.L. (2009). Historical warnings of future food insecurity with unprecedented seasonal heat. *Science*, *323*(5911), 240-244. https://doi.org/10.1126/science.1164363

Bazza, M., Kay, M., & Knutson, C. (2018). *Drought characteristics and management in North Africa and the Near East* (Rep. FAO Water Reports 45, ISSN 1020-1203). Rome: Food and Agriculture Organization of the United Nations. Retrieved from http://www.fao.org/3/CA0034EN/ca0034en.pdf

Bindoff, N.L., Stott, P.A., AchutaRao, K.M., Allen, M.R., Gillett, N., Gutzler, D. et al. (2013). Detection and Attribution of Climate Change: from Global to Regional. In T.F. Stocker, D. Qin, G.-K. Plattner, M. Tignor, S.K. Allen, J. Boschung, et al. (eds.), *Climate Change 2013: The Physical Science Basis.* Contribution of Working Group I to the Fifth Assessment Report of the Intergovernmental Panel on Climate Change (pp. 867–952). Cambridge, United Kingdom and New York, NY: Cambridge University Press

Botkin, D. B., Saxe, H., Araújo, M. B., Betts, R., Bradshaw, R. H. W., Cedhagen, T. et al. (2007). Forecasting the effects of global warming on biodiversity. *BioScience*, *57*(3), 227–236. https://doi.org/10.1641/B570306

British Antarctic Survey (2022). Natural Environment Research Council, Science Briefing. Retrieved from https://www.bas.ac.uk/wp-content/uploads/2015/04/ice_shelf_science_briefing.pdf

Chaidez, V., Dreano, D., Agusti, S. Duarte, C.M., & Hoteit I. (2017). Decadal trends in Red Sea maximum surface temperature. *Scientific Reports*, *7*, 8144. https://doi.org/10.1038/s41598-017-08146-z

Coffel, E. D., Horton, R. M., & De Sherbinin, A. (2018). Temperature and humidity based projections of a rapid rise in global heat stress exposure during the 21st century. *Environmental Research Letters*, *13*(1). https://doi.org/10.1088/1748-9326/aaa00e

Cohen, J., Zhang, X., Francis, J., Jung, T., Kwok, R., Overland, J. et al. (2020). Divergent consensuses on Arctic amplification influence on midlatitude severe winter weather. *Nature Climate Change*, *10*(1), 20–29. https://doi.org/10.1038/s41558-019-0662-y

Collins, M., Knutti, R., Arblaster, J., Dufresne, J.-L., Fichefet, T., Friedlingstein, P. et al. (2013). Long-term Climate Change: Projections, Commitments and Irreversibility. In T. F. Stocker, D. Qin, G.-K. Plattner, M. Tignor, S.K. Allen, J. Boschung et al. (eds.), *Climate Change 2013: The Physical Science Basis. Contribution of Working Group I to the Fifth Assessment Report of the Intergovernmental Panel on Climate Change* (pp. 1029–1136). Cambridge, United Kingdom and New York, NY: Cambridge University Press

Copernicus Climate Change Service (2022a). ERA5-Land monthly averaged data from 1950 to present. Copernicus Climate Change Service (C3S) Climate Data Store (CDS). https://doi.org/10.24381/cds.68d2bb30 (Accessed on 23-NOV-2021)

Copernicus Climate Change Service (2022b): Near surface meteorological variables from 1979 to 2019 derived from bias-corrected reanalysis, version 2.1. Copernicus Climate Change Service (C3S) Climate Data Store (CDS), https://doi.org/10.24381/cds.20d54e34 (Accessed on 09-MAR-2022)

Copernicus Climate Change Service (2023). ERA5 monthly averaged data on single levels from 1940 to present. Copernicus Climate Change Service (C3S) Climate Data Store (CDS). https://doi.org/10.24381/cds.f17050d7 (Accessed on 04-APR-2021)

Cowtan, K., & Way, R. G. (2014). Coverage bias in the HadCRUT4 temperature series and its impact on recent temperature trends. *Quarterly Journal of the Royal Meteorological Society*, *140*(683), 1935–1944. https://doi.org/10.1002/qj.2297

Cucchi, M., Weedon, G. P., Amici, A., Bellouin, N., Lange, S., Schmied, H.M. et al. (2020). WFDE5: Bias-adjusted ERA5 reanalysis data for impact studies. *Earth System Science Data*, *12*(3), 2097–2120. https://doi.org/10.5194/essd-12-2097-2020

Cucchi M., Weedon G. P., Amici A., Bellouin N., Lange S., Schmied H.M. et al. (2021). Near surface meteorological variables from 1979 to 2019 derived from bias-corrected reanalysis, version 2.0. Copernicus Climate Change Service (C3S) Climate Data Store (CDS), (Accessed on 09-MAR-2022), https://doi.org/10.24381/cds.20d54e34

Dai, A. (2013). Increasing drought under global warming in observations and models. *Nature Climate Change*, *3*(1), 52–58. https://doi.org/10.1038/nclimate1633

Dasari, H. P., Desamsetti, S., Langodan, S., Viswanadhapalli, Y., & Hoteit, I. (2021). Analysis of outdoor thermal discomfort over the Kingdom of Saudi Arabia. *GeoHealth*, *5*(6). https://doi.org/10.1029/2020GH000370

De Pauw, E. (2002). An agroecological exploration of the Arabian Peninsula. ICARDA, Aleppo, Syria, 77pp. ISBN 92-9127-119-5. http://www.icarda.cgiaro.org

Diffenbaugh, N. S., & Giorgi, F. (2012). Climate change hotspots in the CMIP5 global climate model ensemble. *Climatic Change*, *114*(3–4), 813–822. https://doi.org/10.1007/s10584-012-0570-x

Doney, S. C., Ruckelshaus, M., Emmett Duffy, J., Barry, J. P., Chan, F., English, C. A. et al. (2012). Climate change impacts on marine ecosystems. *Annual Review of Marine Science*, *4*, 11–37. https://doi.org/10.1146/annurev-marine-041911-111611

995 Eyring, V., Bony, S., Meehl, G. A., Senior, C. A., Stevens, B., Stouffer, R. J., & Taylor, K. E.
996 (2016). Overview of the Coupled Model Intercomparison Project Phase 6 (CMIP6)
997 experimental design and organization. *Geoscientific Model Development*, *9*(5), 1937–1958.
998 https://doi.org/10.5194/gmd-9-1937-2016
999 Fischer, E. M., & Knutti, R. (2013). Robust projections of combined humidity and temperature
1000 extremes. *Nature Climate Change*, *3*(2), 126–130. https://doi.org/10.1038/nclimate1682
1001 Fonseca, R., Francis, D., Nelli, N., & Thota, M. (2022). Climatology of the heat low and the
1002 intertropical discontinuity in the Arabian Peninsula. *International Journal of Climatology*,
1003 *42*(2), 1092–1117. https://doi.org/10.1002/joc.7291
1004 Fowler, H. J., & Ali, H. (2022). Analysis of extreme rainfall events under the climatic change. In
1005 R. Morbidelli (eds.), *Rainfall: Modeling, Measurement and Applications* (pp. 307–326).
1006 Amsterdam, The Netherlands, Elsevier Inc. https://doi.org/10.1016/B978-0-12-822544-
1007 8.00017-2
1008 Freychet, N., Hegerl, G. C., Lord, N. S., Lo, Y. T. E., Mitchell, D., & Collins, M. (2022). Robust
1009 increase in population exposure to heat stress with increasing global warming.
1010 *Environmental Research Letters*, *17*(6). https://doi.org/10.1088/1748-9326/ac71b9
1011 Gao, L., Tao, B., Miao, Y., Zhang, L., Song, X., Ren, W., He, L., & Xu, X. (2019). A global data
1012 set for economic losses of extreme hydrological events during 1960-2014. *Water Resources*
1013 *Research*, *55*(6), 5165–5175. https://doi.org/10.1029/2019WR025135
1014 Giorgi, F. (2006). Climate change hot-spots. *Geophysical Research Letters*, *33*(8), 1–4.
1015 https://doi.org/10.1029/2006GL025734
1016 Hajat, S., Proestos, Y., Araya-Lopez, J. L., Economou, T., & Lelieveld, J. (2023). Current and
1017 future trends in heat-related mortality in the MENA region: a health impact assessment with
1018 bias-adjusted statistically downscaled CMIP6 (SSP-based) data and Bayesian inference. *The*
1019 *Lancet Planetary Health*, *7*(4), e282–e290. https://doi.org/10.1016/S2542-5196(23)00045-1
1020 Handmer, J., Honda, Y., Kundzewicz, Z.W., Arnell, N., Benito, G., Hatfield, J. et al. (2012).
1021 Changes in impacts of climate extremes: Human systems and ecosystems. In C. B. Field, V.
1022 Barros, T.F. Stocker, D. Qin, D. J. Dokken, K. L. Ebi, et al. (eds.), *Managing the risks of*
1023 *extreme events and disasters to advance climate change adaptation (*pp. 231–290). A
1024 Special Report of Working Groups I and II of the Intergovernmental Panel on Climate
1025 Change (IPCC). Cambridge, UK, and New York, NY: Cambridge University Press
1026 Harris, I., Osborn, T. J., Jones, P., & Lister, D. (2020). Version 4 of the CRU TS monthly high-
1027 resolution gridded multivariate climate dataset. *Scientific Data*, *7*(1), 1–18.
1028 https://doi.org/10.1038/s41597-020-0453-3
1029 Hawkins, E., Osborne, T. M., Ho, C. K., & Challinor, A. J. (2013). Calibration and bias
1030 correction of climate projections for crop modelling: An idealized case study over Europe.
1031 *Agricultural and Forest Meteorology*, *170*, 19–31.
1032 https://doi.org/10.1016/j.agrformet.2012.04.007
1033 Hersbach, H., Bell, B., Berrisford, P., Biavati, G., Horányi, A., Muñoz Sabater, J. et al. (2019a):
1034 ERA5 monthly averaged data on single levels from 1959 to present. Copernicus Climate
1035 Change Service (C3S) Climate Data Store (CDS). (Accessed on 04-APR-2021).
1036 https://doi.org/10.24381/cds.f17050d7
1037 Hersbach, H., Bell, B., Berrisford, P., Hirahara, S., Horányi, A., Muñoz-Sabater, J. et al. (2020).
1038 The ERA5 global reanalysis. *Quarterly Journal of Royal Meteorological Society*, *146*(730),
1039 1999-2049. https://doi.org/10.1002/qj.3803

1040 Hersbach, H., Bell, B., Berrisford, P., Horányi, A., Muñoz-Sabater, J., Nicolas, J. et al. (2019b).
1041 Global reanalysis: goodbye ERA-Interim, hello ERA5. *ECMWF Newsletter*, *159*, 17–24.
1042 https://doi.org/10.21957/vf291hehd7
1043 Im, E. S., Pal, J. S., & Eltahir, E. A. B. (2017). Deadly heat waves projected in the densely
1044 populated agricultural regions of South Asia. *Science Advances*, *3*(8), 1–8.
1045 https://doi.org/10.1126/sciadv.1603322
1046 IPCC, (2018). Global warming of 1.5°C. An IPCC special report on the impacts of global
1047 warming of 1.5°C above pre-industrial levels and related global greenhouse gas emission
1048 pathways, in the context of strengthening the global response to the threat of climate
1049 change, sustainable development, and efforts to eradicate poverty (616 pp). In V. Masson-
1050 Delmotte, P. Zhai, H.-O. Pörtner, D. Roberts, J. Skea, P.R. Shukla et al. (eds.), Cambridge,
1051 UK and New York, NY: Cambridge University Press. https://doi.org/
1052 10.1017/9781009157940
1053 IPCC, (2021). Climate Change (2021). The Physical Science Basis. Contribution of working
1054 group I to the Sixth Assessment Report of the Intergovernmental Panel on Climate Change
1055 (2391 pp). In V. Masson-Delmotte, P. Zhai, A. Pirani, S.L. Connors, C. Péan, S. Berger, et
1056 al. (eds.), Cambridge, United Kingdom and New York, NY: Cambridge University Press.
1057 https://doi.org/10.1017/9781009157896
1058 Kang, S. (2019). Future heat stress during muslim pilgrimage (Hajj) projected to exceed
1059 "extreme danger levels. *Geophysical Research Letters*, 94–100.
1060 https://doi.org/10.1029/2019GL083686
1061 Kjellstrom, T., Kovats, R. S., Lloyd, S. J., Holt, T., Tol, R. S. J. (2010). The direct impact of
1062 climate change on regional labor productivity. *Archives of Environmental & Occupational*
1063 *Health, 64*(4), 217–227. https://doi.org/10.1080/19338240903352776
1064 Knutson, T. R., Zhang, R., & Horowitz, L. W. (2016). Prospects for a prolonged slowdown in
1065 global warming in the early 21st century. *Nature Communications*, *7*.
1066 https://doi.org/10.1038/ncomms13676
1067 Kugiumtzis D (2000) Surrogate data test on time series. In A. Soofi, L. Cao (eds.), *Modeling and*
1068 *forecasting financial data* (pp 267–282). New York, Springer
1069 Lamboll, R., Nicholls, Z., Smith, C., & Byers, E. (2022). Assessing the size and uncertainty of
1070 remaining carbon budgets. *Nature Portfolio*, https://doi.org/10.21203/rs.3.rs-1934427/v1
1071 Lange, S., (2021). ISIMIP3b bias adjustment fact sheet. Retrieved from
1072 https://www.isimip.org/gettingstarted/isimip3b-bias-correction/ (Accessed on 10-APR-
1073 2021)
1074 Lelieveld, J., Hadjinicolaou, P., Kostopoulou, E., Chenoweth, J., El Maayar, M.,
1075 Giannakopoulos, C. et al. (2012). Climate change and impacts in the Eastern Mediterranean
1076 and the Middle East. *Climatic Change*, *114*(3–4), 667–687. https://doi.org/10.1007/s10584-
1077 012-0418-4
1078 Lelieveld, J., Proestos, Y., & Hadjinicolaou, P. (2016). Strongly increasing heat extremes in the
1079 Middle East and North Africa (MENA) in the 21st century. *Climatic Change*, 245–260.
1080 https://doi.org/10.1007/s10584-016-1665-6
1081 Lenssen, N. J. L., Schmidt, G. A., Hansen, J. E., Persin, A., Ruedy, R., & Zyss, D. (2019).
1082 Improvements in the GISTEMP uncertainty model. *Journal of Geophysical Research:*
1083 *Atmospheres*, *124*, 6307–6326. https://doi.org/10.1029/2018JD029.
1084 https://doi.org/10.1029/2018JD029522

1085 Majdi, F., Asaad, S., Alireza, H., Maryam, K., & Sara, K. (2022). Future projection of
1086 precipitation and temperature changes in the Middle East and North Africa (MENA) region
1087 based on CMIP6. *Theoretical and Applied Climatology*, *147*, 1249–1262.
1088 https://doi.org/10.1007/s00704-021-03916-2
1089 Malcolm, J. A. Y. R., Liu, C., Neilson, R. P., Hansen, L., & Hannah, L. E. E. (2006). Global
1090 warming and extinctions of endemic species from biodiversity hotspots. *Conservation*
1091 *Biology, 20*(2), 538–542. https://doi.org/10.1111/j.1523-1739.2006.00364.x
1092 Malik, A., Brönnimann, S., & Perona, P. (2018). Statistical link between external climate
1093 forcings and modes of ocean variability. *Climate Dynamics*, *50*(9–10).
1094 https://doi.org/10.1007/s00382-017-3832-5
1095 Mann, M. E. (2008). Smoothing of climate time series revisited. *Geophysical Research Letters*,
1096 35, L16708. https://doi.org/10.1029/2008GL034716
1097 Mengel, M., Levermann, A., Frieler, K., Robinson, A., & Marzeion, B. (2016). Future sea level
1098 rise constrained by observations and long-term commitment. *PNAS*, *113*(10), 2597–2602.
1099 https://doi.org/10.1073/pnas.1500515113
1100 Mora, C., Dousset, B., Caldwell, I. R., Powell, F. E., Geronimo, R. C., Bielecki, C. R. et al.
1101 (2017). Global risk of deadly heat. *Nature Climate Change, 7*, 501–506.
1102 https://doi.org/10.1038/NCLIMATE3322
1103 Morice, C. P., Kennedy, J. J., Rayner, N. A., Winn, J. P., Hogan, E., Killick, R. E. et al. (2021).
1104 An updated assessment of near-surface temperature change from 1850: The HadCRUT5
1105 data set. *Journal of Geophysical Research: Atmospheres, 126*, e2019JD032361.
1106 https://doi.org/10.1029/2019JD032361
1107 Muñoz-sabater, J., Dutra, E., Agustí-panareda, A., Albergel, C., Hersbach, H., Martens, B. et al.
1108 (2021). ERA5-Land: a state-of-the-art global reanalysis dataset for land applications. *Earth*
1109 *System Science Data*, *13*, 4349–4383. https://doi.org/10.5194/essd-13-4349-2021
1110 Moss, R. H., Edmonds, J. A., Hibbard, K. A., Manning, M. R., Rose, S. K., Vuuren, D. P. Van et
1111 al. (2010). The next generation of scenarios for climate change research and assessment.
1112 *Nature*, *463*, 747–756. https://doi.org/10.1038/nature08823
1113 Naumann, G., Al, L., & Wyser, K. (2018). Global changes in drought conditions under different
1114 levels of warming. *Geophysical Research Letters*, *45*(7), 3285–3296.
1115 https://doi.org/10.1002/2017GL076521
1116 Noël, T., Loukos, H., Defrance, D., Vrac, M., & Levavasseur, G. (2021). A high-resolution
1117 downscaled CMIP5 projections dataset of essential surface climate variables over the globe
1118 coherent with the ERA5 reanalysis for climate change impact assessments. *Data in Brief,*
1119 *35*, 106900. https://doi.org/10.1016/j.dib.2021.106900
1120 Noël, T., Loukos, H., Defrance, D., Vrac, M., & Levavasseur, G. (2022). Extending the global
1121 high-resolution downscaled projections dataset to include CMIP6 projections at increased
1122 resolution coherent with the ERA5-Land reanalysis. *Data in Brief, 45*, 108669.
1123 https://doi.org/10.1016/j.dib.2022.108669
1124 Ntoumos, A., Hadjinicolaou, P., Zittis, G., Proestos, Y., & Lelieveld, J. (2022). Projected air
1125 temperature extremes and maximum heat conditions over the Middle-East-North Africa
1126 (MENA) Region. *Earth Systems and Environment*, *6*(2), 343–359.
1127 https://doi.org/10.1007/s41748-022-00297-y
1128 Odnoletkova, N., & Patzek, T. W. (2021). Data-driven analysis of climate change in Saudi
1129 Arabia: Trends in temperature extremes and human comfort indicators. *Journal of Applied*

Meteorology and Climatology, *60*(8), 1055–1070. https://doi.org/10.1175/JAMC-D-20-0273.1

Olonscheck, D., Schurer, A. P., Lücke, L., & Hegerl, G. C. (2021). Large-scale emergence of regional changes in year-to-year temperature variability by the end of the 21st century. *Nature Communications*, *12*, 7237. https://doi.org/10.1038/s41467-021-27515-x

Park, T., Hashimoto, H., Wang, W., Thrasher, B., Michaelis, A.R., Lee, T. et al. (2022). What does global land climate look like at 2 degrees warming? *Earth's Future*, e2022EF003330, https://doi.org/10.1029/2022EF003330

Pal, J. S., & Eltahir, E. A. B. (2016). Future temperature in southwest Asia projected to exceed a threshold for human adaptability. *Nature Climate Change*, *6*, 197–200. https://doi.org/10.1038/NCLIMATE2833

Power, S. B., & Delage, F. P. D. (f2019). Setting and smashing extreme temperature records over the coming century. *Nature Climate Change*, *9*(7), 529–534. https://doi.org/10.1038/s41558-019-0498-5

Raymond, C., Matthews, T., & Horton, R. M. (2020). The emergence of heat and humidity too severe for human tolerance. *Science Advances*, *6*(19). https://doi.org/10.1126/sciadv.aaw1838

Riahi, K., Rao, S., Krey, V., Cho, C., Chirkov, V., & Fischer, G. (2011). RCP 8 .5 — A scenario of comparatively high greenhouse gas emissions. *Climatic Change*, *109*(33), 33–57. https://doi.org/10.1007/s10584-011-0149-y

Riahi, K., van Vuuren, D. P., Kriegler, E., Edmonds, J., Neill, B. C. O., Fujimori, S. et al. (2017). The Shared Socioeconomic Pathways and their energy, land use, and greenhouse gas emissions implications: An overview. *Global Environmental Change*, *42*, 153–168. https://doi.org/10.1016/j.gloenvcha.2016.05.009

Rogelj, J., Elzen, M. Den, Höhne, N., Fransen, T., Fekete, H., Winkler, H., Schaeffer, R., & Sha, F. (2016). Paris Agreement climate proposals need a boost to keep warming well below 2 °C. *Nature*, 534, 631–639. https://doi.org/10.1038/nature18307

Rogelj, J., Schleussner, C.-F., & Hare, W. (2017). Getting it right matters: Temperature goal interpretations in geoscience research. *Geophysical Research Letters*, *44*(20), 10662–10665. https://doi.org/10.1002/2017GL075612

Rohde, R. A., & Hausfather, Z. (2020). The Berkeley Earth land / ocean temperature record. *Earth System Science Data, 12,* 3469–3479. https://doi.org/10.5194/essd-12-3469-2020

Safieddine, S., Clerbaux, C., Clarisse, L., Whitburn, S., & Eltahir, E. A. B. (2022). Present and future land surface and wet bulb temperatures in the Arabian Peninsula. *Environmental Research Letters*, *17*, 044029. https://doi.org/10.1088/1748-9326/ac507c

Seneviratne, S. I., Zhang, X., Adnan, M., Badi, W., Dereczynski, C., Luca, A. D. (2021) Weather and climate extreme events in a changing climate. In V. Masson-Delmotte, P. Zhai, A. Pirani, S. L. Connors, C. Péan, S. Berger et al. (eds.), *Climate Change 2021: The Physical Science Basis* (pp. 1513–1766). Contribution of working group I to the Sixth Assessment Report of the Intergovernmental Panel on Climate Change. Cambridge, United Kingdom and New York, NY: Cambridge University Press. https://doi.org/10.1017/9781009157896.013

Smith, C. J., & Forster, P. M. (2021). Suppressed late-20th century warming in CMIP6 models explained by forcing and feedbacks. *Geophysical Research Letters*, *48*(19). https://doi.org/10.1029/2021GL094948

1175 Suarez-Gutierrez, L., Wolfgang, G., Chao, A. M., & Jochem, L. (2020). Hotspots of extreme
1176 heat under global warming. *Climate Dynamics*, *55*(3), 429–447.
1177 https://doi.org/10.1007/s00382-020-05263-w
1178 Sun, W., Li, Q., Huang, B., Cheng, J., Song, Z., Li, H. et al. (2021). The assessment of global
1179 surface temperature change from 1850s: The C-LSAT2.0 ensemble and the CMST-Interim
1180 datasets. Advances in Atmospheric Sciences, *38*, 875–888. https://doi.org/10.1007/s00376-
1181 021-1012-3
1182 Tabari, H. (2020). Climate change impact on flood and extreme precipitation increases with
1183 water availability. *Scientific Reports*, 1–10. https://doi.org/10.1038/s41598-020-70816-2
1184 Taylor, K. E., Stouffer, R. J., & Meehl, G. A. (2012). An overview of CMIP5 and the experiment
1185 design. Bulletin of the American Meteorological Society, 485–498.
1186 https://doi.org/10.1175/BAMS-D-11-00094.1
1187 Tebaldi, C., Ranasinghe, R., Vousdoukas, M., Rasmussen, D. J., Vega-westhoff, B., Kirezci, E.
1188 et al. (2021). Extreme sea levels at different global warming levels. *Nature Climate Change*,
1189 *11,* 746–751. https://doi.org/10.1038/s41558-021-01127-1
1190 Thomson, A. M., Calvin, K. V, Smith, S. J., Kyle, G. P., Volke, A., Patel, P. et al. (2011).
1191 RCP4.5: A pathway for stabilization of radiative forcing by 2100. *Climatic Change*, *109*,
1192 77–94. https://doi.org/10.1007/s10584-011-0151-4
1193 Tollefson, J. (2021). Earth is warmer than it's been in 125,000 years, says landmark climate
1194 report. *Nature*, *596*, 171-172. https://doi.org/10.1038/d41586-021-02179-1
1195 Vargas Zeppetello, L. R., Raftery, A. E., & Battisti, D. S. (2022). Probabilistic projections of
1196 increased heat stress driven by climate change. *Communications Earth and Environment*,
1197 *3*(1), 1–7. https://doi.org/10.1038/s43247-022-00524-4
1198 Waha, K., Krummenauer, L., Adams, S., Aich, V., Baarsch, F., Coumou, D. et al. (2017).
1199 Climate change impacts in the Middle East and Northern Africa (MENA) region and their
1200 implications for vulnerable population groups. *Regional Environmental Change*, *17*(6),
1201 1623–1638. https://doi.org/10.1007/s10113-017-1144-2
1202 Weedon, G. P., Gomes, S., Viterbo, P., Shuttleworth, W. J., Blyth, E., Osterle, H. et al.
1203 (2011). Creation of the WATCH forcing data and its use to assess global and regional
1204 reference crop evaporation over land during the twentieth century. *Journal of*
1205 *Hydrometeorology*, *12* (5), 823–848. https://doi.org/10.1175/2011JHM1369.1
1206 Willett, K. M., & Sherwood, S. (2012). Exceedance of heat index thresholds for 15 regions under
1207 a warming climate using the wet-bulb globe temperature. *International Journal of*
1208 *Climatology*, *32*(2), 161–177. https://doi.org/10.1002/joc.2257
1209 World Bank (2018). Beyond scarcity: Water security in the Middle East and North Africa.
1210 *MENA Development Report Series* (License: CC BY 3.0 IGO). Washington, DC, World
1211 Bank. https://doi.org/10.1596/978-1-4648-1144-9
1212 Wouters, H., Keune, J., Petrova, I. Y., van Heerwaarden, C. C., Teuling, A. J., Pal, J. S. et al.
1213 (2022). Soil drought can mitigate deadly heat stress thanks to a reduction of air humidity.
1214 *Science Advances*, *8*(1), 1–12. https://doi.org/10.1126/sciadv.abe6653
1215 Yan, Y. Y. (2005). Land and sea breezes. In J. E. Oliver (eds.), *Encyclopedia of World*
1216 *Climatology. Encyclopedia of Earth Sciences Series*. Dordrecht, Springer.
1217 https://doi.org/10.1007/1-4020-3266-8_121
1218 Yun, X., Huang, B., Cheng, J., Xu, W., Qiao, S., & Li, Q. (2019). A new merge of global surface
1219 temperature datasets since the start of the 20th century. *Earth System Science Data*, *11*,
1220 1629–1643, https://doi.org/10.5194/essd-11-1629-2019

1221 Zhang, H.-M., Huang, B., Lawrimore, J. H., Menne, M. J., & Smith, T. M. (2021) NOAA global
1222 surface temperature dataset (NOAAGlobalTemp), version 4.0 [1880–2020]. NOAA
1223 National Centers for Environmental Information. https://doi.org/10.7289/V5FN144H
1224 (Accessed on 23-FEB-2021)
1225 Zhang, H.-M., Lawrimore, J. H., Huang, B., Menne, M. J., Yin, X., Sánchez-Lugo, A. et al.
1226 (2019). Updated temperature data give a sharper view of climate trends. *Eos, 100*,
1227 https://doi.org/10.1029/2019EO128229
1228 Zhao, L., Oleson, K., Bou-zeid, E., Krayenhoff, E. S., Bray, A., Zhu, Q. et al. (2021). Global
1229 multi-model projections of local urban climates. *Nature Climate Change*, *11*, 152–157
1230 https://doi.org/10.1038/s41558-020-00958-8
1231 Zittis, G., Almazroui, M., Alpert, P., Ciais, P., Cramer, W., Dahdal, Y. et al. (2022). Climate
1232 change and weather extremes in the Eastern Mediterranean and Middle East. *Reviews of*
1233 *Geophysics*, *60*(3), e2021RG000762. https://doi.org/10.1029/2021RG000762
1234 Zittis, G., Hadjinicolaou, P., Almazroui, M., Bucchignani, E., Driouech, F., & Rhaz, K. El.
1235 (2021). Business-as-usual will lead to super and ultra-extreme heatwaves in the Middle East
1236 and North Africa. *npj|Climate and Atmospheric Science*, *4*(20),
1237 https://doi.org/10.1038/s41612-021-00178-7

Earth's Future

Supporting Information for

Accelerated Historical and Future Warming over the Middle East and North Africa in Response to the Global Temperature Change

Abdul Malik[1], Georgiy Stenchikov[1], Suleiman Mostamandi[1], Sagar Parajuli[2], Jos Lelieveld[3,4], George Zittis[4], Muhammad Sheraz Ahsan[5], Luqman Atique[6,7], Muhammad Usman[8]

[1]Physical Science and Engineering Division, King Abdullah University of Science and Technology, 23955 Thuwal, Jeddah, Saudi Arabia
[2]Scripps Institution of Oceanography, University of California, San Diego, CA, USA California
[3]Max Planck Institute for Chemistry, Mainz, Germany
[4]Climate and Atmospheric Research Center (CARE-C), The Cyprus Institute, Nicosia, Cyprus
[5]Institute of Geographical Information Systems, School of Civil and Environmental Engineering, National University of Sciences and Technology, Islamabad, Pakistan
[6]School of Earth Sciences, Zhejiang University, Hangzhou, China
[7]Department of Meteorology, COMSATS University, Islamabad, Pakistan
[8]Department of Life and Environmental Sciences, Zayed University, Abu Dhabi, United Arab Emirates

Contents of this file

Introduction

This document provides supplementary details about eight observational datasets, reanalysis products, and climate models from Coupled Model Intercomparison Project (CMIP) Phases 5 and 6 employed in this research work. Further, here we also show some additional figures and tables supporting the text in the main document. The figures related to winter warming are included in this document. How the temperature anomalies evolved from 1850 to 2020 for each observational data and related uncertainty are also depicted in supplementary figures. The download links for all the datasets are given under supplement section S5. The main document reference list provides all the references cited in the supplement document.

Text S1. Details of observational datasets

All observational datasets are detailed in the text below and summarized in Table S2.

Text S1.1. HadCRUT5 analysis

The recent version of the Met Office Hadley Centre/Climate Research Unit surface temperature data set, HadCRUT5-Analysis (Morice et al., 2021), merges CRUTEMP5 surface air temperature and HadSST4 Sea Surface Temperature (SST) at a coarse resolution (5° x 5°). HadCRUT5-Analysis provides coverage in data-sparse regions with spatial gaps filled using a Gaussian process-based statistical method. It offers significant spatial coverage over the MENA region after 1880 and almost complete spatial coverage onward 1886. It is available with a 200-member ensemble providing uncertainties arising from methods for measuring SSTs, homogenization, measurement errors, presence of data-sparse regions, and statistical data reconstruction methods for filling the gaps.

Text S1.2. Berkeley Earth

The Berkeley Earth (1° x 1°) global land and ocean monthly temperature record use land air temperature where the sea is covered with ice; elsewhere, it uses sea surface temperature as a proxy for air temperature. In Berkeley Earth land temperature data is combined with spatially kriged HadSST3 (Rohde et al., 2020), providing complete spatial coverage over the MENA region after 1880.

Text S1.3. GISTEMPv4

The Goddard Institute for Space Studies Surface Temperature Product v4 (GISTEMPv4; 2° x 2°) is based on version 4 of the monthly Global Historical Climatological Network (GHCNv4) land surface air temperature from the NOAA NCEI (National Oceanic and Atmospheric Administration / National Centers for Environmental Information). GISTEMPv4 merges GHCNv4 and Extended Reconstructed Sea Surface Temperature v5 (ERSSTv5) with 1200 km smoothing (Lenssen et al., 2020). It provides complete spatial coverage over the MENA region after 1911 and partially before 1911.

Text S1.4. NOAAGlobalTemp

The NOAA global surface temperature (NOAAGlobalTemp; 5° x 5°) combines ERSSTv4 with land surface air temperature GHCN monthly version 3.3 (GHCNm v3.3) (Zhang et al., 2019; Zhang et al., 2021). It provides almost complete spatial coverage over the MENA region after 1907 and partially before.

Text S1.5. CMST-Interim

The China Global Merged Surface Temperature (CMST-Interim) dataset (5° x 5°) combines China-Land Surface Air Temperature v2 (C-LSAT2.0) and ERSSTv5. C-LSAT2.0 is based on high- and low-frequency components reconstruction methods combined with observation constraint masking (Yun et al., 2019; Sun et al., 2021). It provides complete spatial coverage over the MENA region after 1940 and partially before.

Text S1.6. Cowtan & Way v2

Cowton & Way v2 (5° x 5°) (Cowtan and Robert 2014) has three variants viz. i) HadCRUT4 ensemble medians infilled by kriging, ii) HadCRUT4+HadSST4 infilled by kriging and iii) COBE2CRU based on HadCRUT4 land ensemble median and COBE-SST2. All these three variants provide partial spatial coverage over the MENA region.

Text S2. Details of Reanalysis Products

All reanalysis products are detailed in the text below and summarized in Table S3.

Text S2.1. European ReAnalysis (ERA5)

ERA5 is ECMWF's fifth-generation reanalysis product that combines model output with several observational data sets using a data assimilation technique. It is available at 31 km spatial resolution (0.25° × 0.25°) with a 10-member ensemble at 63 km (0.5° × 0.5°) for uncertainty estimates (Hersbach et al., 2019a; Hersbach et al., 2019b, Hersbach et al., 2020).

Text S2.2. ERA5-Land

ERA5-Land is produced using ECMWF's land surface model. The Model was forced by downscaled meteorological data from ERA5, with elevation correction for the thermodynamic near-surface state (Muñoz-Sabater et al., 2021). It has a high native spatial resolution of 9 km and thus can provide a relatively good estimate of temperature changes over coastal zones. We use 2m air temperature (T2m) from the ERA5-Land, available at an hourly timescale, and we calculate monthly means from the hourly data set.

Text S2.3. WFDE5

ERA5 was bias corrected by applying the Water and Global Change (WATCH) Forcing Data (WFD) methodology (Weedon et al., 2011), thus referred to as WFDE5 (Cucchi et al., 2020; Cucchi et al., 2021). For producing WFDE5, ERA5 data were re-gridded at 0.5° spatial resolution and then adjusted using elevation and monthly-scale bias corrections based on Climatic Research Unit (CRU) data (Cucchi et al., 2020; Cucchi et al., 2021). We

use this data set to evaluate the quality of ERA5 reanalysis and other climate model outputs over the MENA region.

S3 Supplementary tables

Table S1. Geographic coordinates of the Arabian Peninsula Hotspot Region (APHR).

No.	Latitude	Longitude
1	32.007	40.07
2	32.006	40.075
3	31.948	40.413
4	31.373	41.440
5	31.112	42.085
6	30.516	42.925
7	30.417	43.065
8	29.869	43.810
9	29.198	44.722
10	29.200	44.720
11	29.090	46.120
12	22.500	49.000
13	21.000	47.500
14	22.500	44.000
15	30.000	38.700
16	32.007	40.070

Table S2. Observational datasets

Sr. No.	Data	Period	Spatial Resolution	Temporal Resolution	Ensemble Members	Original Baseline	Remarks
1	HadCRUT5-Analysis	1850-2020	5º x 5º	Monthly	200	1961-1990	Land and ocean (Accessed on 23/02/2021)
2	Berkeley Earth	1850-2020	1º x 1º	Monthly	No	1951-1980	Land and ocean (Accessed on 27/04/2021)
3	GISTEMPv4	1880-2020	2º x 2º	Monthly	No	1951-1980	Land and ocean (Accessed on 23/02/2021)
4	NOAA-Global-Temp	1880-2020	5º x 5º	Monthly	No	1971-2000	Land and ocean (Accessed on 23/02/2021)
5	CMST-Interim	1854-2018	5º x 5º	Monthly	No	1961-1990	Land and ocean (Accessed on 16/03/2021)
	Cowtan and Way v2						Available as following three reconstructions (Accessed on 24/02/2021)
6	HadCRUT4	1850-2020	5º x 5º	Monthly	No	1961-1990	Land and ocean
7	HadCRUT4+HadSST 4	1850-2018	5º x 5º	Monthly	No	1961-1990	Land and ocean
8	COBE2CRU	1850-2017	5º x 5º	Monthly	No	1961-1990	Land and ocean

Table S3. Reanalysis products

Sr. No.	Data	Period	Spatial Resolution	Temporal Resolution	Ensemble Members Used	Remarks
1	ERA5	1951-2020	0.25° x 0.25° (31 km)	Monthly	10	Land and ocean (Accessed on 04/04/2021)
2	ERA5-Land	1951-2020	0.1° x 0.1° (9 km)	Monthly	No	Land only (Accessed on 23/11/2021)
3	WFDE5	1979-2019	0.5° x 0.5°	Hourly	No	Bias-corrected over land with CRUTSv4.06 (Harris et al., 2020) (Accessed on 09/03/2022)

Table S4. C3S-CMIP5-Adjusted 2-meter air temperature (T2m; 0.25° x 0.25°, 31 km, monthly, 1951-2099)

Sr. No.	Model	Institute	Forcing Scenario	Ensemble Number
1	ACCESS1–0	BoM-CSIRO, Australia	RCP4.5, RCP8.5	r1i1p1
2	ACCESS1–3	BoM-CSIRO, Australia	〃	〃
3	bcc-csm1–1	BCC, China	〃	〃
4	bcc-csm1–1-m	BCC, China	〃	〃
5	BNU-ESM	BNU, China	〃	〃
6	CMCC–CM	CMCC, Italy	〃	〃
7	CMCC–CMS	CMCC. Italy	RCP8.5	〃
8	CNRM-CM5	CNRM-CERFACS, France	RCP4.5	〃
9	GFDL-CM3	NOAA, USA	RCP4.5, RCP8.5	〃
10	GFDL-ESM2G	NOAA, USA	〃	〃
11	GFDL-ESM2M	NOAA, USA	〃	〃
12	HadGEM2-CC	UK Met Office, UK	〃	〃
13	HadGEM2-ES	UK Met Office, UK	〃	〃
14	inmcm4	INM, Russia	〃	〃
15	IPSL-CM5A-LR	IPSL, France	〃	〃
16	IPSL-CM5A-MR	IPSL, France	〃	〃
17	IPSL-CM5B-LR	IPSL, France	〃	〃
18	MIROC5	UTCCSR, Japan	〃	〃
19	MPI-ESM-LR	MPI, Germany	〃	〃
20	MPI-ESM-MR	MPI, Germany	〃	〃
21	NorESM1-M	NCC, Norway	〃	〃

Table S5. C3S-CMIP6-Adjusted 2-meter air temperature (T2m; 0.1° x 0.1°, 9 km, monthly, 1951-2099)

Sr. No.	Model	Institute	Forcing Scenario	Ensemble Number	Remarks
1	GFDL-ESM4	Geophysical Fluid Dynamics Laboratory / USA	SSP1-2.6, SSP5-8.5	r1i1p1f1	Low climate sensitivity and good process representation
2	MPI-ESM1-2-HR	L'Institut Pierre–Simon Laplace/Franc	〃	〃	Low climate sensitivity and fair process representation
3	MRI-ESM2-0	Max Planck Institute for Meteorology/Germany	〃	〃	Low climate sensitivity and good process representation
4	IPSL-CM6A-LR	Meteorological Research Institute /Japan	〃	〃	High climate sensitivity and fair process representation
5	UKESM1-0-LL	Met Office Hadley Centre/	〃	r1i1p1f2	High climate sensitivity and good process representation

Table S6. Annual global warming offsets (1986-2005) calculated from 8 observational data sets.

Sr. No.	Data Set	Offset °C (Land and Ocean)	Offset °C (Land Only)
1	HadCRUT5-Analysis	0.71	0.99
2	Berkeley Earth	0.69	0.98
3	GISTEMPv4	0.69	1.03
4	NOAA-Global-Temp	0.43	0.71
5	CMST-Interim	0.56	0.84
6	HadCRUT4	0.66	0.97
7	HadCRUT4+HadSST4	0.71	0.99
8	COBE2CRU	0.62	0.97
Mean Offset		**0.63**	**0.94**

Table S7. MENA and its sub-regions warming offsets (1986-2005). Offsets shown here are the mean of 8 observation data sets over the corresponding region.

Sr. No.	Region	Offset °C (Annual, Jan-Dec)	Offset °C (Summer, MJJASO)	Offset °C (Winter, NDJFMA)
1	MENA	0.90	0.92	0.93
2	MENA-Land	0.98	0.99	1.02
3	Arabian Peninsula	0.95	1.00	0.92
4	Arabian Peninsula Hotspot Region	1.08	1.23	0.96
5	West Coast	0.84	0.89	0.79
6	South Coast	0.81	0.75	0.89
7	East Coast	0.88	0.93	0.90

Table S8. Mean climatological warming (°C; 1987—2016).

Summer (MJJASO)							
	MENA (Land and Ocean)	MENA-Land	Arabian Peninsula	APHR	West Coast	South Coast	East Coast
Obs8	1.12 ± 0.08	1.21 ± 0.08	1.23 ± 0.10	1.52 ± 0.13	1.10 ± 0.10	0.92 ± 0.10	1.17 ± 0.10
ERA5	1.14 ± 0.07	1.24 ± 0.08	1.29 ± 0.10	1.61 ± 0.14	1.11 ± 0.08	0.93 ± 0.10	1.24 ± 0.10
ERA5-Land	–	1.19 ± 0.07	1.20 ± 0.07	1.47 ± 0.11	1.06 ± 0.06	0.87 ± 0.07	1.13 ± 0.07
WFDE5	–	1.18 ± 0.06	1.22 ± 0.07	1.50 ± 0.1	1.11 ± 0.07	0.89 ± 0.07	1.23 ± 0.07
RCP4.5	1.12 ± 0.07	1.21 ± 0.07	1.20 ± 0.08	1.46 ± 0.1	1.07 ± 0.08	0.90 ± 0.08	1.13 ± 0.08
RCP8.5	1.15 ± 0.08	1.24 ± 0.08	1.22 ± 0.09	1.49 ± 0.11	1.10 ± 0.09	0.90 ± 0.09	1.16 ± 0.09
SSP1-2.6	–	1.24 ± 0.08	1.24 ± 0.08	1.52 ± 0.11	1.09 ± 0.08	0.89 ± 0.08	1.15 ± 0.08
SSP5-8.5	–	1.26 ± 0.08	1.24 ± 0.08	1.51 ± 0.11	1.09 ± 0.08	0.89 ± 0.08	1.16 ± 0.08
Mean	**1.13 ± 0.08**	**1.22 ± 0.08**	**1.23 ± 0.08**	**1.51 ± 0.11**	**1.09 ± 0.08**	**0.90 ± 0.08**	**1.17 ± 0.08**
Median	**1.13 ± 0.08**	**1.23 ± 0.08**	**1.23 ± 0.08**	**1.51 ± 0.11**	**1.10 ± 0.08**	**0.90 ± 0.08**	**1.16 ± 0.08**
Winter (NDJFMA)							
	MENA (Land and Ocean)	MENA-Land	Arabian Peninsula	APHR	West Coast	South Coast	East Coast
Obs8	1.13 ± 0.09	1.23 ± 0.12	1.09 ± 0.12	1.20 ± 0.16	1.02 ± 0.12	0.98 ± 0.12	1.05 ± 0.12
ERA5	1.19 ± 0.1	1.32 ± 0.12	1.17 ± 0.13	1.31 ± 0.17	1.09 ± 0.12	0.94 ± 0.13	1.20 ± 0.13
ERA5-Land	–	1.28 ± 0.11	1.14 ± 0.12	1.25 ± 0.15	1.06 ± 0.12	0.98 ± 0.12	1.14 ± 0.12
WFDE5	–	1.23 ± 0.09	1.12 ± 0.1	1.20 ± 0.13	1.08 ± 0.12	0.97 ± 0.10	1.13 ± 0.10
RCP4.5	1.13 ± 0.08	1.23 ± 0.08	1.12 ± 0.1	1.16 ± 0.13	1.00 ± 0.09	1.07 ± 0.1	1.09 ± 0.10
RCP8.5	1.13 ± 0.09	1.24 ± 0.09	1.11 ± 0.10	1.16 ± 0.13	0.99 ± 0.09	1.07 ± 0.1	1.09 ± 0.10
SSP1-2.6	–	1.23 ± 0.10	1.14 ± 0.10	1.18 ± 0.13	1.00 ± 0.1	1.10 ± 0.1	1.11 ± 0.10
SSP5-8.5	–	1.26 ± 0.10	1.17 ± 0.11	1.21 ± 0.14	1.02 ± 0.1	1.12 ± 0.11	1.14 ± 0.11
Mean	**1.15 ± 0.09**	**1.25 ± 0.10**	**1.13 ± 0.11**	**1.21 ± 0.14**	**1.03 ± 0.11**	**1.03 ± 0.11**	**1.12 ± 0.11**
Median	**1.13 ± 0.09**	**1.24 ± 0.10**	**1.13 ± 0.11**	**1.20 ± 0.14**	**1.04 ± 0.10**	**1.03 ± 0.11**	**1.13 ± 0.11**

Note: Obs8 is the mean of eight observational datasets described in Table S2.

Table S9. Current global (annual) and regional warming (°C; 2020)

Summer (MJJASO)									
	Global (Land and Ocean)	Global-Land	MENA (Land and Ocean)	MENA-Land	Arabian Peninsula	APHR	West Coast	South Coast	East Coast
Obs8	1.15 ± 0.13	1.71 ± 0.14	1.68 ± 0.11	1.79 ± 0.10	1.9 ± 0.18	2.29 ± 0.09	1.77 ± 0.15	1.52 ± 0.24	1.96 ± 0.15
ERA5	1.23 ± 0.01	1.83 ± 0.004	1.75 ± 0.01	1.88 ± 0.01	1.976 ± 0.003	2.615 ± 0.003	1.72 ± 0.01	1.08 ± 0.02	1.86 ± 0.01
ERA5-Land	–	1.79 ± 0.004*	–	1.74 ± 0.01*	1.70 ± 0.003*	2.13 ± 0.003*	1.55 ± 0.01*	1.14 ± 0.02*	1.69 ± 0.01*
RCP4.5	1.25 ± 0.18	1.82 ± 0.24	1.76 ± 0.25	1.90 ± 0.27	1.84 ± 0.35	2.20 ± 0.37	1.67 ± 0.33	1.35 ± 0.26	1.77 ± 0.38
RCP8.5	1.31 ± 0.18	1.92 ± 0.24	1.88 ± 0.24	2.02 ± 0.26	1.99 ± 0.34	2.38 ± 0.38	1.82 ± 0.31	1.42 ± 0.23	1.92 ± 0.35
SSP1-2.6	1.30 ± 0.14	1.94 ± 0.24	–	2.04 ± 0.25	2.01 ± 0.31	2.47 ± 0.29	1.77 ± 0.33	1.36 ± 0.25	1.92 ± 0.29
SSP5-8.5	1.29 ± 0.14	1.91 ± 0.24	–	2.06 ± 0.28	2.04 ± 0.32	2.48 ± 0.33	1.78 ± 0.28	1.37 ± 0.26	1.96 ± 0.31
Mean	**1.26 ± 0.13**	**1.85 ± 0.16**	**1.77 ± 0.15**	**1.92 ± 0.17**	**1.92 ± 0.22**	**2.37 ± 0.21**	**1.73 ± 0.21**	**1.32 ± 0.18**	**1.87 ± 0.21**
Median	**1.27 ± 0.14**	**1.83 ± 0.24**	**1.76 ± 0.18**	**1.90 ± 0.25**	**1.98 ± 0.31**	**2.38 ± 0.29**	**1.77 ± 0.28**	**1.36 ± 0.24**	**1.92 ± 0.29**
Winter (NDJFMA)									
	Global (Land and Ocean)	Global-Land	MENA (Land and Ocean)	MENA-Land	Arabian Peninsula	APHR	West Coast	South Coast	East Coast
Obs8	1.15 ± 0.13	1.71 ± 0.14	1.49 ± 0.11	1.61 ± 0.13	1.60 ± 0.18	1.87 ± 0.21	1.52 ± 0.12	1.28 ± 0.11	1.55 ± 0.20
ERA5	1.23 ± 0.01	1.83 ± 0.004	1.61 ± 0.01	1.80 ± 0.01	1.82 ± 0.01	2.39 ± 0.01	1.63 ± 0.01	1.25 ± 0.02	1.92 ± 0.01
ERA5-Land	–	1.79 ± 0.004*	–	1.76 ± 0.01*	1.65 ± 0.01*	1.93 ± 0.01*	1.5 ± 0.01	1.24 ± 0.02*	1.72 ± 0.01*
RCP4.5	1.25 ± 0.18	1.82 ± 0.24	1.67 ± 0.21	1.80 ± 0.21	1.67 ± 0.23	1.70 ± 0.26	1.54 ± 0.20	1.59 ± 0.21	1.61 ± 0.30
RCP8.5	1.31 ± 0.18	1.92 ± 0.24	1.73 ± 0.22	1.87 ± 0.24	1.72 ± 0.24	1.79 ± 0.27	1.58 ± 0.23	1.63 ± 0.19	1.68 ± 0.28
SSP1-2.6	1.30 ± 0.14	1.94 ± 0.24	–	1.97 ± 0.50	1.80 ± 0.47	1.90 ± 0.65	1.69 ± 0.49	1.63 ± 0.29	1.76 ± 0.45
SSP5-8.5	1.29 ± 0.14	1.91 ± 0.24	–	1.99 ± 0.46	1.89 ± 0.38	1.98 ± 0.46	1.71 ± 0.40	1.72 ± 0.32	1.86 ± 0.33
Mean	**1.26 ± 0.13**	**1.85 ± 0.16**	**1.63 ± 0.14**	**1.83 ± 0.22**	**1.74 ± 0.22**	**1.94 ± 0.27**	**1.60 ± 0.21**	**1.48 ± 0.17**	**1.73 ± 0.23**
Median	**1.27 ± 0.14**	**1.83 ± 0.24**	**1.64 ± 0.16**	**1.80 ± 0.21**	**1.72 ± 0.23**	**1.90 ± 0.26**	**1.58 ± 0.20**	**1.59 ± 0.19**	**1.72 ± 0.28**

Table S10. Mean climatological warming (°C; 2021—2050)

Summer (MJJASO)							
	MENA (Land and Ocean)	MENA-Land	Arabian Peninsula	APHR	West Coast	South Coast	East Coast
RCP4.5	2.26 ± 0.07	2.43 ± 0.07	2.40 ± 0.08	2.86 ± 0.10	2.18 ± 0.08	1.74 ± 0.08	2.47 ± 0.07
RCP8.5	2.62 ± 0.05	2.82 ± 0.09	2.80 ± 0.10	3.32 ± 0.13	2.60 ± 0.10	2.00 ± 0.10	2.77 ± 0.11
SSP1-2.6	–	2.54 ± 0.06	2.55 ± 0.07	3.06 ± 0.09	2.24 ± 0.06	1.77 ± 0.07	2.33 ± 0.08
SSP5-8.5	–	2.85 ± 0.11	2.86 ± 0.11	3.48 ± 0.13	2.51 ± 0.10	1.94 ± 0.11	2.73 ± 0.10
Winter (NDJFMA)							
	MENA (Land and Ocean)	MENA-Land	Arabian Peninsula	APHR	West Coast	South Coast	East Coast
RCP4.5	2.06 ± 0.08	2.21 ± 0.08	2.15 ± 0.10	2.18 ± 0.12	1.99 ± 0.09	2.04 ± 0.10	2.38 ± 0.10
RCP8.5	2.38 ± 0.07	2.55 ± 0.10	2.49 ± 0.12	2.56 ± 0.14	2.34 ± 0.11	2.31 ± 0.12	2.58 ± 0.11
SSP1-2.6	–	2.40 ± 0.09	2.38 ± 0.11	2.49 ± 0.12	2.14 ± 0.08	2.15 ± 0.10	2.08 ± 0.10
SSP5-8.5	–	2.61 ± 0.10	2.59 ± 0.11	2.71 ± 0.14	2.34 ± 0.10	2.37 ± 0.11	2.42 ± 0.12

Table S11. Mean climatological warming (°C; 2069—2098)

Summer (MJJASO)							
	MENA (Land and Ocean)	MENA-Land	Arabian Peninsula	APHR	West Coast	South Coast	East Coast
RCP4.5	3.35 ± 0.09	3.60 ± 0.05	3.59 ± 0.06	4.18 ± 0.08	3.36 ± 0.06	2.65 ± 0.06	3.53 ± 0.06
RCP8.5	5.70 ± 0.11	6.14 ± 0.11	6.12 ± 0.12	7.16 ± 0.15	5.73 ± 0.12	4.36 ± 0.12	6.1 ± 0.12
SSP1-2.6	–	2.82 ± 0.04	2.84 ± 0.05	3.35 ± 0.06	2.59 ± 0.05	2.10 ± 0.05	2.75 ± 0.05
SSP5-8.5	–	6.43 ± 0.14	6.41 ± 0.15	7.59 ± 0.17	5.62 ± 0.14	4.67 ± 0.15	6.32 ± 0.15
Winter (NDJFMA)							
	MENA (Land and Ocean)	MENA-Land	Arabian Peninsula	APHR	West Coast	South Coast	East Coast
RCP4.5	3.02 ± 0.1	3.22 ± 0.07	3.24 ± 0.09	3.28 ± 0.11	3.03 ± 0.08	3.06 ± 0.09	3.17 ± 0.09
RCP8.5	5.11 ± 0.12	5.45 ± 0.12	5.55 ± 0.14	5.65 ± 0.16	5.26 ± 0.13	5.09 ± 0.14	5.49 ± 0.14
SSP1-2.6	–	2.53 ± 0.08	2.50 ± 0.08	2.62 ± 0.11	2.33 ± 0.07	2.44 ± 0.08	2.52 ± 0.08
SSP5-8.5	–	5.74 ± 0.16	5.89 ± 0.17	5.98 ± 0.18	5.42 ± 0.15	5.52 ± 0.17	5.72 ± 0.17

Table S12. Global (annual) and regional (winter) warming trends (°C/Decade)

1987-2016									
	Global (Land and Ocean)	Global-Land	MENA (Land and Ocean)	MENA-Land	Arabian Peninsula	APHR	West Coast	South Coast	East Coast
Obs8	0.2 ± 0.02	0.33 ± 0.02	0.35 ± 0.03	0.38 ± 0.03	0.37 ± 0.06	0.49 ± 0.04	0.42 ± 0.03	0.21 ± 0.06	0.35 ± 0.07
WFDE5	–	0.27 ± 0.001*	–	0.34 ± 0.02	0.30 ± 0.02	0.36 ± 0.02	0.34 ± 0.02	0.21 ± 0.01	0.33 ± 0.03
ERA5	0.22 ± 0.003	0.37 ± 0.001	0.41 ± 0.003	0.51 ± 0.001	0.43 ± 0.005	0.59 ± 0.003	0.49 ± 0.002	0.12 ± 0.01	0.50 ± 0.01
ERA5-Land	–	0.34 ± 0.003	–	0.39 ± 0.01	0.37 ± 0.01	0.50 ± 0.01	0.39 ± 0.01	0.18 ± 0.01	0.41 ± 0.01
RCP4.5	0.25 ± 0.07	0.37 ± 0.09	0.31 ± 0.09	0.32 ± 0.09	0.32 ± 0.11	0.31 ± 0.13	0.31 ± 0.10	0.30 ± 0.09	0.31 ± 0.14
RCP8.5	0.27 ± 0.07	0.39 ± 0.09	0.32 ± 0.08	0.34 ± 0.09	0.34 ± 0.11	0.34 ± 0.12	0.32 ± 0.11	0.32 ± 0.07	0.33 ± 0.13
SSP1-2.6	0.26 ± 0.06	0.40 ± 0.1	–	0.38 ± 0.20	0.35 ± 0.19	0.37 ± 0.3	0.36 ± 0.19	0.30 ± 0.12	0.34 ± 0.19
SSP5-8.5	0.26 ± 0.05	0.39 ± 0.1	–	0.41 ± 0.19	0.40 ± 0.16	0.42 ± 0.19	0.38 ± 0.15	0.34 ± 0.13	0.40 ± 0.15
Mean	**0.24 ± 0.05**	**0.36 ± 0.05**	**0.35 ± 0.05**	**0.38 ± 0.08**	**0.36 ± 0.08**	**0.42 ± 0.10**	**0.38 ± 0.08**	**0.25 ± 0.06**	**0.37 ± 0.09**
Median	**0.26 ± 0.06**	**0.37 ± 0.06**	**0.34 ± 0.06**	**0.38 ± 0.06**	**0.36 ± 0.09**	**0.40 ± 0.08**	**0.37 ± 0.07**	**0.26 ± 0.07**	**0.35 ± 0.10**
2021-2098									
	Global (Land and Ocean)	Global-Land	MENA (Land and Ocean)	MENA-Land	Arabian Peninsula	APHR	West Coast	South Coast	East Coast
RCP4.5	0.17 ± 0.05	0.30 ± 0.07	0.19 ± 0.06	0.20 ± 0.06	0.22 ± 0.06	0.22 ± 0.07	0.21 ± 0.06	0.21 ± 0.06	0.22 ± 0.06
RCP8.5	0.46 ± 0.08	0.65 ± 0.11	0.56 ± 0.10	0.59 ± 0.11	0.63 ± 0.11	0.64 ± 0.12	0.60 ± 0.11	0.57 ± 0.10	0.64 ± 0.11
SSP1-2.6	0.06 ± 0.04	0.09 ± 0.07	–	0.04 ± 0.06	0.04 ± 0.05	0.03 ± 0.06	0.04 ± 0.05	0.06 ± 0.04	0.03 ± 0.04
SSP5-8.5	0.50 ±0.13	0.73 ± 0.24	–	0.65 ± 0.18	0.68 ± 0.20	0.68 ± 0.22	0.63 ± 0.18	0.66 ± 0.18	0.65 ± 0.18

Obs8: Mean of eight observational datasets mentioned in Table S2.

* With an asterisk is the standard error, and without an asterisk is ± 1 SD calculated from different datasets or corresponding ensemble members.

Table S13. Years crossing global warming thresholds

	1.5 ºC	2 ºC	3 ºC	4 ºC
RCP4.5	2031 ± 11 (4)	2053 ± 12 (5)	–	–
RCP8.5	2027 ± 7 (3)	2041 ± 8 (2)	2062 ± 10 (2)	2082 ± 10 (2)
SSP1-2.6	2028 ± 8 (7)		–	–
SSP5-8.5	2027 ± 6 (2)	2040 ± 8 (2)	2062 ± 11 (2)	2080 ± 14 (2)
Mean	**2028 ± 8 (4)**	**2044 ± 9 (3)**	**2062 ± 11 2)**	**2081 ± 12 (2)**
Median	**2028 ± 8 (4)**	**2041 ± 8 (2)**	**2062 ± 11 (2)**	**2081 ± 12 (2)**

Table S14. Global land warming at global warming thresholds

	1.5 ºC	2 ºC	3 ºC	4 ºC
RCP4.5	2.18 ± 0.09	2.90 ± 0.12		
RCP8.5	2.21 ± 0.08	2.91 ± 0.12	4.33 ± 0.16	5.68 ± 0.18
SSP1-2.6	2.25 ± 0.09			
SSP5-8.5	2.23 ± 0.09	2.95 ± 0.09	4.45 ± 0.12	5.93 ± 0.27
Mean	**2.22 ± 0.09**	**2.92 ± 0.11**	**4.39 ± 0.18**	**5.81 ± 0.23**
Median	**2.22 ± 0.09**	**2.91 ± 0.12**	**4.39 ± 0.18**	**5.81 ± 0.23**

Table S15. MENA warming at global warming thresholds

(Summer; MJJASO)				
	1.5 ºC	2 ºC	3 ºC	4 ºC
RCP4.5	2.12 ± 0.18	2.80 ± 0.23		
RCP8.5	2.17 ± 0.13	2.88 ± 0.21	4.29 ± 0.29	5.62 ± 0.35
SSP1-2.6				
SSP5-8.5				
Mean	**2.15 ± 0.16**	**2.84 ± 0.22**	**4.29 ± 0.29**	**5.62 ± 0.35**
Median	**2.15 ± 0.16**	**2.84 ± 0.22**		
(Winter; NDJFMA)				
	1.5 ºC	2 ºC	3 ºC	4 ºC
RCP4.5	1.95 ± 0.14	2.51 ± 0.17		
RCP8.5	1.99 ± 0.13	2.62 ± 0.15	3.84 ± 0.20	5.02 ± 0.26
SSP1-2.6				
SSP5-8.5				
Mean	**1.97 ± 0.14**	**2.57 ± 0.16**	**3.84 ± 0.20**	**5.02 ± 0.26**
Median	**1.97 ± 0.14**	**2.57 ± 0.16**	**3.84 ± 0.20**	**5.02 ± 0.26**

Table S16. MENA-Land warming at global warming thresholds

(Summer; MJJASO)				
	1.5 ºC	2 ºC	3 ºC	4 ºC
RCP4.5	2.28 ± 0.21	3.01 ± 0.28		
RCP8.5	2.33 ± 0.15	3.11 ± 0.23	4.62 ± 0.33	6.05 ± 0.42
SSP1-2.6	2.35 ± 0.16			
SSP5-8.5	2.36 ± 0.18	3.08 ± 0.16	4.66 ± 0.18	6.14 ± 0.19
Mean	**2.33 ± 0.18**	**3.07 ± 0.22**	**4.64 ± 0.26**	**6.10 ± 0.31**
Median	**2.34 ± 0.17**	**3.08 ± 0.23**	**4.64 ± 0.26**	**6.10 ± 0.31**
(Winter; NDJFMA)				
	1.5 ºC	2 ºC	3 ºC	4 ºC
RCP4.5	2.11 ± 0.16	2.69 ± 0.21		
RCP8.5	2.14 ± 0.14	2.82 ± 0.12	4.11 ± 0.25	5.35 ± 0.32
SSP1-2.6	2.25 ± 0.34			
SSP5-8.5	2.22 ± 0.34	2.78 ± 0.24	4.18 ± 0.19	5.41 ± 0.25
Mean	**2.18 ± 0.25**	**2.76 ± 0.21**	**4.15 ± 0.22**	**5.38 ± 0.29**
Median	**2.18 ± 0.25**	**2.78 ± 0.21**	**4.15 ± 0.22**	**5.38 ± 0.29**

Table S17. Arabian Peninsula warming at global warming thresholds

(Summer; MJJASO)				
	1.5 ºC	2 ºC	3 ºC	4 ºC
RCP4.5	2.22 ± 0.36	3.03 ± 0.38		
RCP8.5	2.31 ± 0.26	3.08 ± 0.37	4.61 ± 0.51	6.03 ± 0.59
SSP1-2.6	2.33 ± 0.15			
SSP5-8.5	2.35 ± 0.20	3.11 ± 0.17	4.71 ± 0.15	6.12 ± 0.17
Mean	**2.30 ± 0.24**	**3.07 ± 0.31**	**4.66 ± 0.33**	**6.08 ± 0.38**
Median	**2.32 ± 0.23**	**3.08 ± 0.37**	**4.66 ± 0.33**	**6.08 ± 0.38**
(Winter; NDJFMA)				
	1.5 ºC	2 ºC	3 ºC	4 ºC
RCP4.5	2.02 ± 0.16	2.65 ± 0.22		
RCP8.5	2.04 ± 0.16	2.76 ± 0.19	4.14 ± 0.28	5.45 ± 0.3
SSP1-2.6	2.16 ± 0.29			
SSP5-8.5	2.18 ± 0.23	2.78 ± 0.2	4.24 ± 0.22	5.53 ± 0.46
Mean	**2.1 ± 0.21**	**2.73 ± 0.2**	**4.19 ± 0.25**	**4.49 ± 0.38**
Median	**2.1 ± 0.20**	**2.76 ± 0.2**	**4.19 ± 0.25**	**4.49 ± 0.38**

Table S18. Arabian Peninsula Hotspot Region (APHR) warming at global warming thresholds

(Summer; MJJASO)				
	1.5 ºC	2 ºC	3 ºC	4 ºC
RCP4.5	2.67 ± 0.34	3.56 ± 0.32		
RCP8.5	2.75 ± 0.25	3.65 ± 0.35	5.39 ± 0.48	7.06 ± 0.54
SSP1-2.6	2.84 ± 0.18			
SSP5-8.5	2.87 ± 0.28	3.77 ± 0.26	5.66 ± 0.19	7.26 ± 0.13
Mean	**2.78 ± 0.26**	**3.66 ± 0.31**	**5.53 ± 0.34**	**7.16 ± 0.34**
Median	**2.80 ± 0.27**	**3.65 ± 0.32**	**5.53 ± 0.34**	**7.16 ± 0.34**
(Winter; NDJFMA)				
	1.5 ºC	2 ºC	3 ºC	4 ºC
RCP4.5	2.07 ± 0.22	2.71 ± 0.31		
RCP8.5	2.12 ± 0.18	2.84 ± 0.23	4.24 ± 0.33	5.53 ± 0.4
SSP1-2.6	2.29 ± 0.46			
SSP5-8.5	2.29 ± 0.32	2.9 ± 0.28	4.37 ± 0.31	5.6 ± 0.65
Mean	**2.19 ± 0.32**	**2.82 ± 0.27**	**4.31 ± 0.32**	**5.57 ± 0.53**
Median	**2.21 ± 0.32**	**2.84 ± 0.28**	**4.31 ± 0.32**	**5.57 ± 0.53**

Table S19. West coast warming at global warming thresholds

(Summer; MJJASO)				
	1.5 ºC	2 ºC	3 ºC	4 ºC
RCP4.5	2.01 ± 0.37	2.81 ± 0.41		
RCP8.5	2.12 ± 0.26	2.87 ± 0.41	4.3 ± 0.59	5.65 ± 0.61
SSP1-2.6	2.06 ± 0.18			
SSP5-8.5	2.05 ± 0.18	2.73 ± 0.17	4.12 ± 0.21	5.37 ± 0.24
Mean	**2.06 ± 0.25**	**2.80 ± 0.33**	**4.21 ± 0.40**	**5.51 ± 0.43**
Median	**2.06 ± 0.22**	**2.81 ± 0.41**	**4.21 ± 0.40**	**5.51 ± 0.43**
(Winter; NDJFMA)				
	1.5 ºC	2 ºC	3 ºC	4 ºC
RCP4.5	1.88 ± 0.15	2.48 ± 0.17		
RCP8.5	1.9 ± 0.19	2.61 ± 0.21	3.89 ± 0.28	5.18 ± 0.28
SSP1-2.6	1.98 ± 0.28			
SSP5-8.5	1.99 ± 0.35	2.51 ± 0.24	3.9 ± 0.17	5.1 ± 0.31
Mean	**1.94 ± 0.24**	**2.53 ± 0.21**	**3.90 ± 0.23**	**5.14 ± 0.30**
Median	**1.94 ± 0.24**	**2.51 ± 0.21**	**3.90 ± 0.23**	**5.14 ± 0.30**

Table S20. South coast warming at global warming thresholds

(Summer; MJJASO)				
	1.5 ºC	2 ºC	3 ºC	4 ºC
RCP4.5	1.6 ± 0.28	2.21 ± 0.36		
RCP8.5	1.65 ± 0.22	2.20 ± 0.29	3.29 ± 0.44	4.27 ± 0.61
SSP1-2.6	1.57 ± 0.17			
SSP5-8.5	1.58 ± 0.14	2.10 ± 0.19	3.29 ± 0.18	4.43 ± 0.26
Mean	**1.60 ± 0.20**	**2.17 ±**	**3.29 ± 0.31**	**4.35 ± 0.44**
Median	**1.59 ± 0.20**	**2.20 ±**	**3.29 ± 0.31**	**4.35 ± 0.44**
(Winter; NDJFMA)				
	1.5 ºC	2 ºC	3 ºC	4 ºC
RCP4.5	1.92 ± 0.13	2.51 ± 0.19		
RCP8.5	1.91 ± 0.14	2.56 ± 0.19	3.81 ± 0.3	5 ± 0.32
SSP1-2.6	1.99 ± 0.16			
SSP5-8.5	1.94 ± 0.11	2.54 ± 0.13	3.92 ± 0.17	5.21 ± 0.25
Mean	**1.94 ± 0.14**	**2.54 ± 0.17**	**3.87 ± 0.24**	**5.11 ± 0.29**
Median	**1.93 ± 0.14**	**2.54 ± 0.19**	**3.87 ± 0.24**	**5.11 ± 0.29**

Table S21. East coast warming at global warming thresholds

(Summer; MJJASO)				
	1.5 ºC	2 ºC	3 ºC	4 ºC
RCP4.5	2.17 ± 0.36	2.95 ± 0.32		
RCP8.5	2.24 ± 0.23	3.02 ± 0.31	4.56 ± 0.44	6.01 ± 0.51
SSP1-2.6	2.28 ± 0.22			
SSP5-8.5	2.25 ± 0.17	3.03 ± 0.19	4.63 ± 0.16	6.03 ± 0.17
Mean	**2.24 ± 0.25**	**3 ± 0.22**	**4.60 ± 0.30**	**6.02 ± 0.34**
Median	**2.25 ± 0.23**	**3.03 ± 0.31**	**4.60 ± 0.30**	**6.02 ± 0.34**
(Winter; NDJFMA)				
	1.5 ºC	2 ºC	3 ºC	4 ºC
RCP4.5	1.95 ± 0.21	2.59 ± 0.3		
RCP8.5	1.98 ± 0.17	2.68 ± 0.2	4.1 ± 0.29	5.39 ± 0.37
SSP1-2.6	2.15 ± 0.2			
SSP5-8.5	2.15 ± 0.25	2.77 ± 0.16	4.18 ± 0.23	5.35 ± 0.57
Mean	**2.06 ± 0.21**	**2.68 ± 0.22**	**4.14 ± 0.26**	**5.37 ± 0.47**
Median	**2.07 ± 0.21**	**2.68 ± 0.2**	**4.14 ± 0.26**	**5.37 ± 0.47**

Table S22. Warming by the end of the 21st century (°C; 2099)

(MJJASO)							
	MENA (Land and Ocean)	MENA-Land	Arabian Peninsula	APHR	West Coast	South Coast	East Coast
RCP4.5	3.41 ± 0.70	3.66 ± 0.77	3.64 ± 0.80	4.25 ± 0.87	3.44 ± 0.73	3.55 ± 0.84	2.66 ± 0.65
RCP8.5	6.62 ± 0.98	7.13 ± 1.07	7.12 ± 1.24	8.28 ± 1.36	6.65 ± 1.11	7.07 ± 1.23	5.15 ± 1.0
SSP1-2.6	–	2.60 ± 0.49	2.66 ± 0.57	3.16 ± 0.59	2.36 ± 0.51	2.54 ± 0.53	1.95 ± 0.54
SSP5-8.5	–	7.58 ± 1.52	7.61 ± 1.53	8.97 ± 1.79	6.67 ± 1.40	7.46 ± 1.39	5.65 ± 1.45
Winter (NDJFMA)							
	MENA (Land and Ocean)	MENA-Land	Arabian Peninsula	APHR	West Coast	South Coast	East Coast
RCP4.5	3.05 ± 0.55	3.25 ± 0.58	3.26 ± 0.63	3.34 ± 0.67	3.04 ± 0.59	3.11 ± 0.56	3.21 ± 0.67
RCP8.5	5.88 ± 0.90	6.26 ± 0.97	6.41 ± 1.02	6.57 ± 1.09	6.06 ± 0.94	5.86 ± 0.99	6.35 ± 0.99
SSP1-2.6	–	2.42 ± 0.74	2.39 ± 0.68	2.49 ± 0.75	2.25 ± 0.72	2.27 ± 0.58	2.34 ± 0.51
SSP5-8.5	–	6.84 ± 1.55	7.10 ± 1.61	7.23 ± 1.81	6.41 ± 1.65	6.59 ± 1.41	6.98 ± 1.36

S4 Supplementary figures

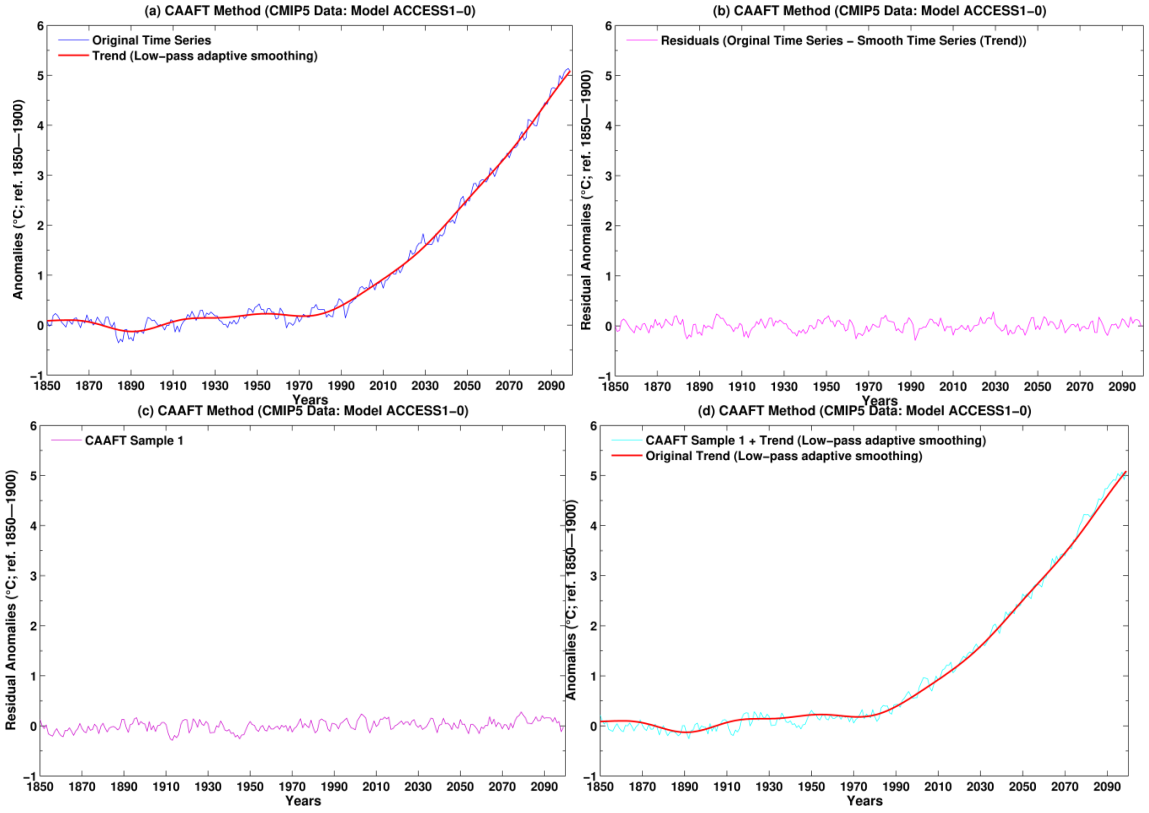

Figure S1. Residual sample generation using corrected Amplitude Fourier Transform (CAAFT) algorithm for measuring uncertainty due to internal climate variability. The climate model data is ACCESS1-0 from CMIP5 (RCP8.5 merged with historical after 2005). Adaptive smoothing was performed using Mann's (2008) approach with a 0.25 (40-year) cut-off frequency.

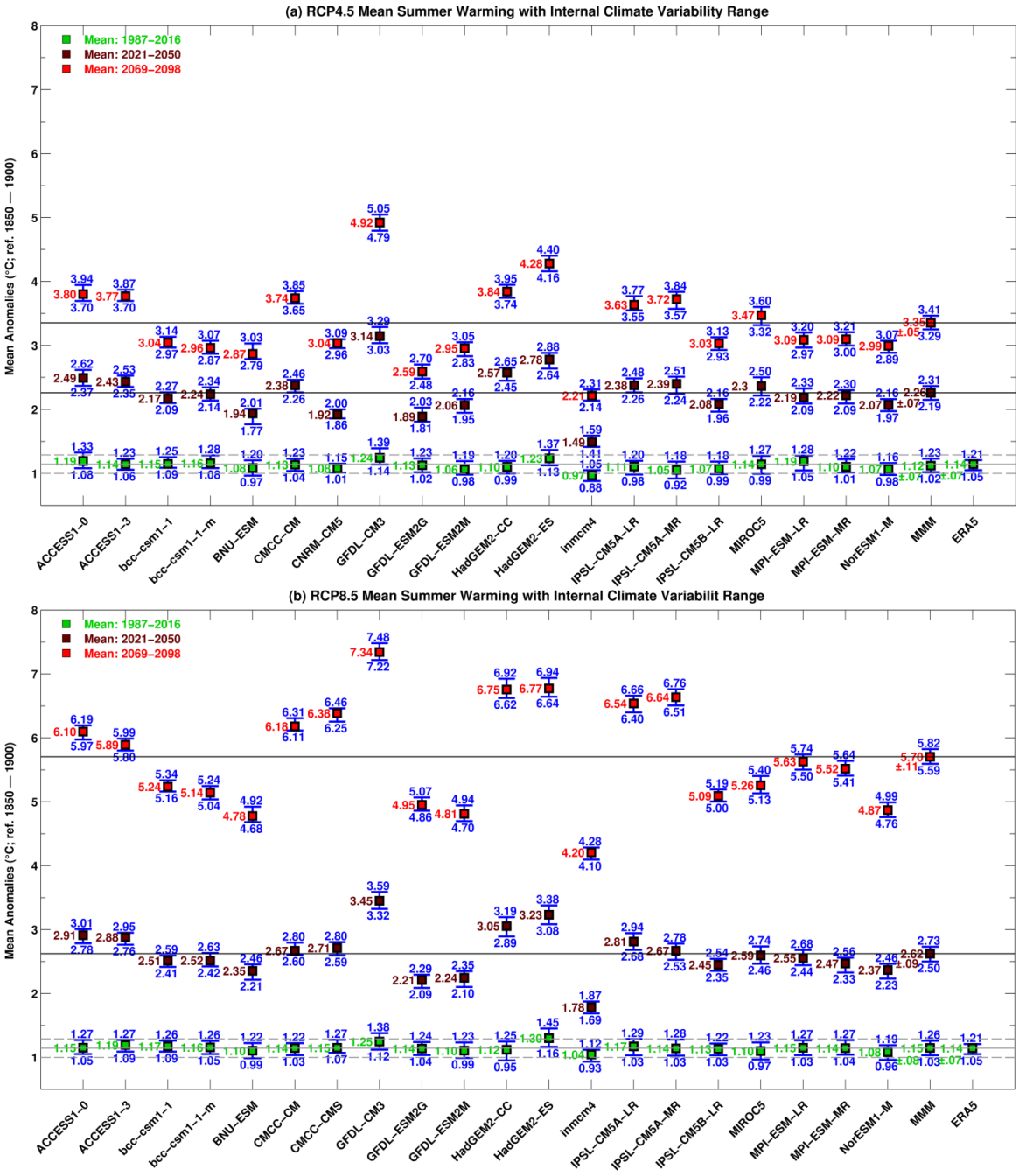

Figure S2. Mean summer warming with internal climate variability range over the MENA region for (a) RCP4.5 and (b) RCP8.5. The solid gray horizontal line indicates mean warming calculated from the ERA5. The dashed gray horizontal lines indicate ±2 standard deviation uncertainty range of the mean warming calculated from 10 ensemble members of ERA5. The solid black lines indicate multimodel means (MMM) for future periods. The blue vertical bars and text tell the uncertainty (at a 99% confidence level) due to internal climate variability.

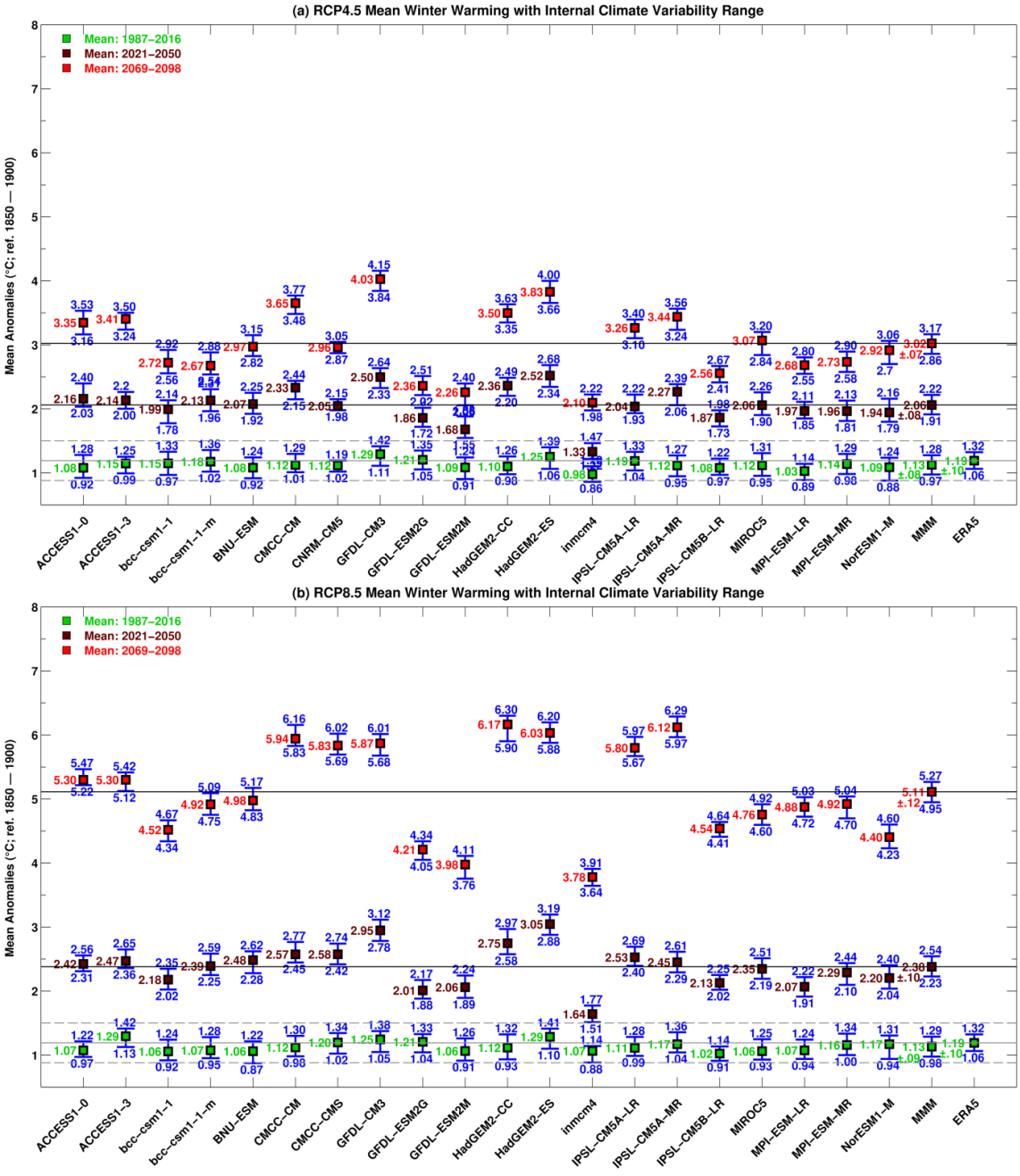

Figure S3. Mean winter warming with internal climate variability range over the MENA region for (a) RCP4.5 and (b) RCP8.5. The solid gray horizontal line indicates mean warming calculated from the ERA5. The dashed gray horizontal lines indicate ±2 standard deviation uncertainty range of the mean warming calculated from 10 ensemble members of ERA5. The solid black lines indicate multimodel means (MMM) for future periods. The blue vertical bars and text tell the uncertainty (at a 99% confidence level) due to internal climate variability.

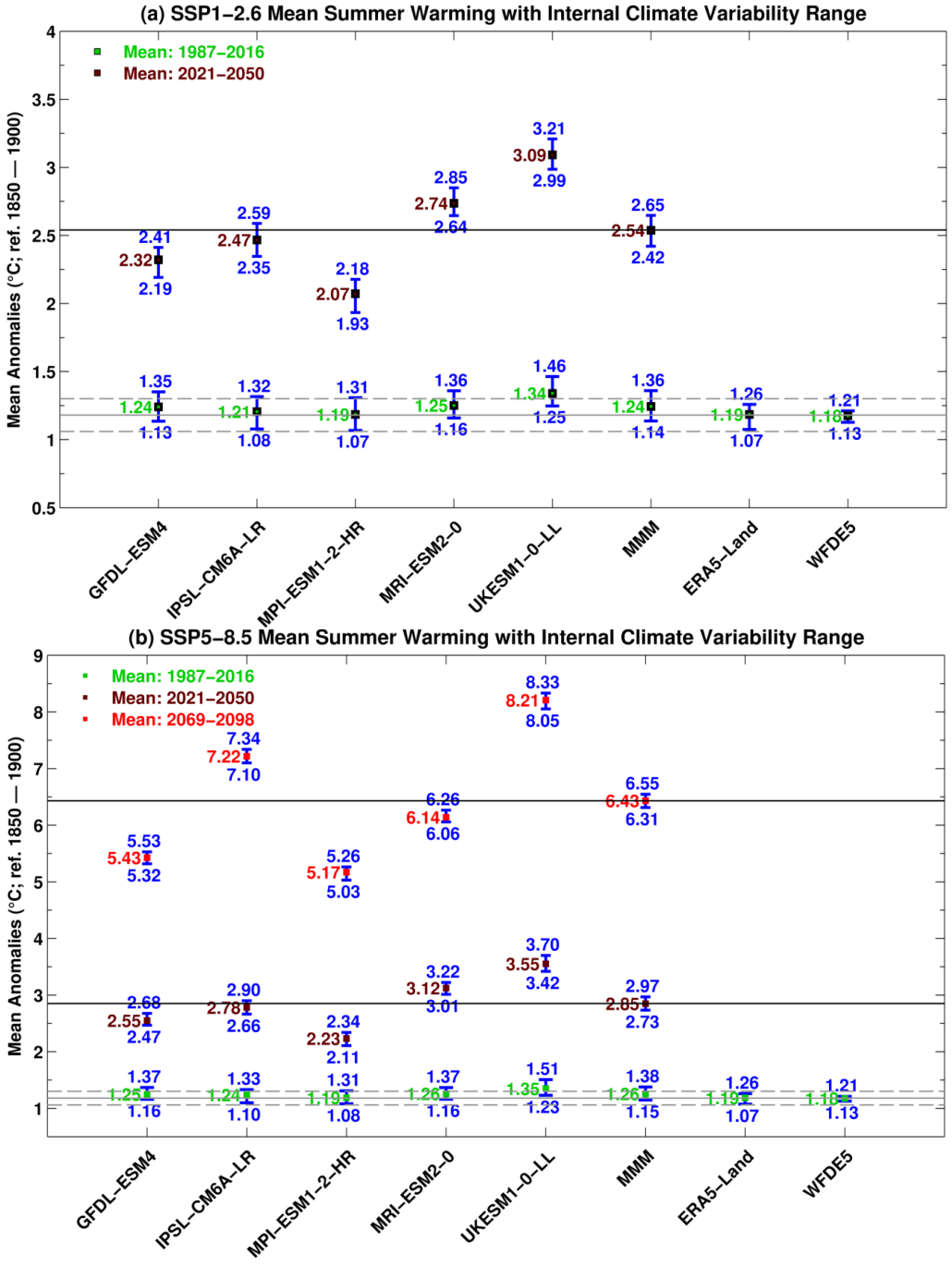

Figure S4. Mean summer warming with internal climate variability range over the MENA-Land region for (a) SSP1-2.6 and (b) SSP5-8.5. The solid gray horizontal line indicates mean warming calculated from WFDE5. The dashed gray horizontal lines indicate ±2 standard deviation uncertainty range of the mean warming calculated from 10,000 bootstrap samples of WFDE5. The solid black lines indicate multimodel means (MMM) for future periods. The blue vertical bars and text tell the uncertainty (at a 99% confidence level) due to internal climate variability.

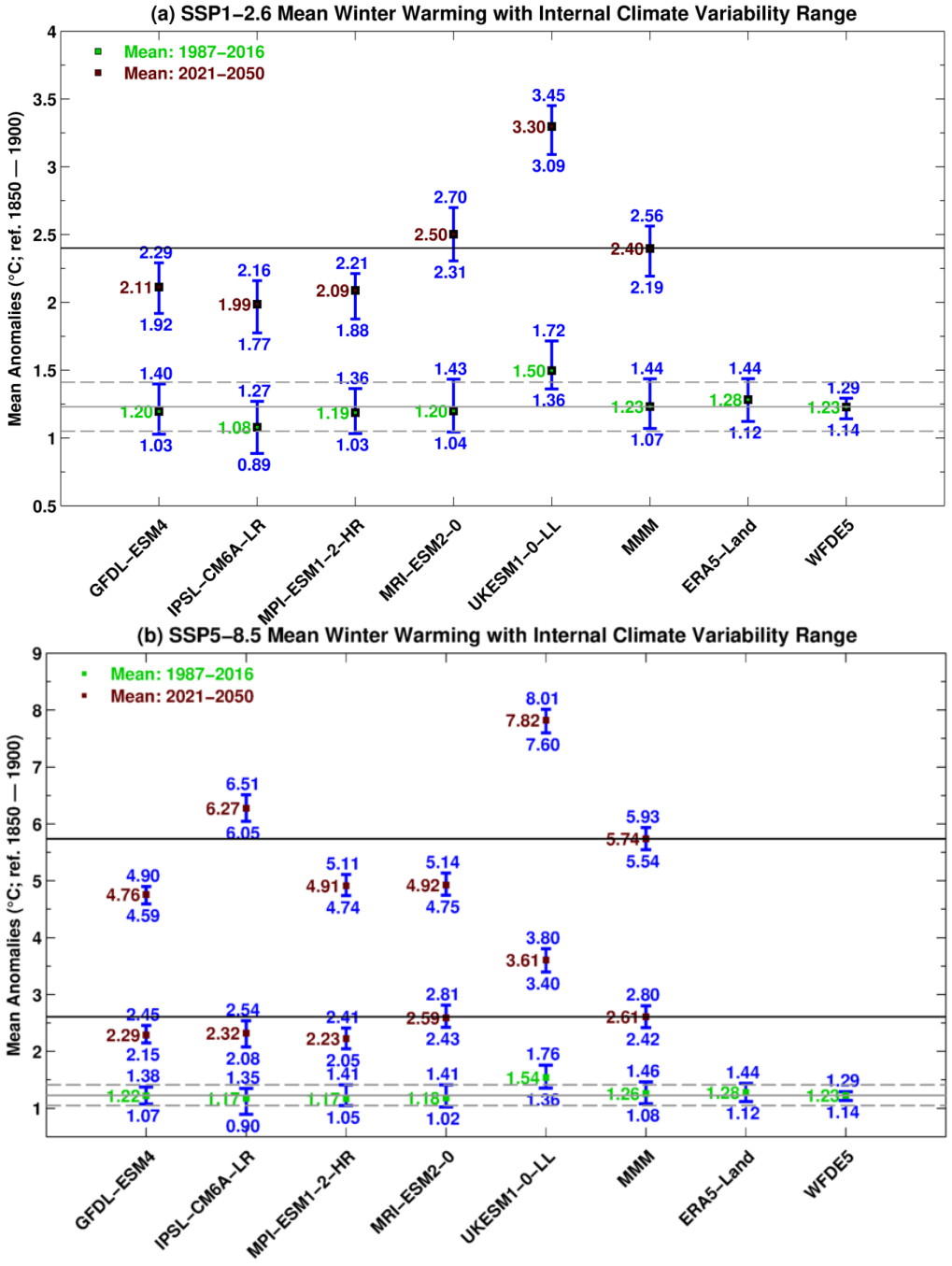

Figure S5. Mean winter warming with internal climate variability range over the MENA-Land region for (a) SSP1-2.6 and (b) SSP5-8.5. The solid gray horizontal line indicates mean warming calculated from WFDE5. The dashed gray horizontal lines indicate ±2 standard deviation uncertainty range of the mean warming calculated from 10,000 bootstrap samples of WFDE5. The solid black lines indicate multimodel means (MMM) for future periods. The blue vertical bars and text tell the uncertainty (at a 99% confidence level) due to internal climate variability.

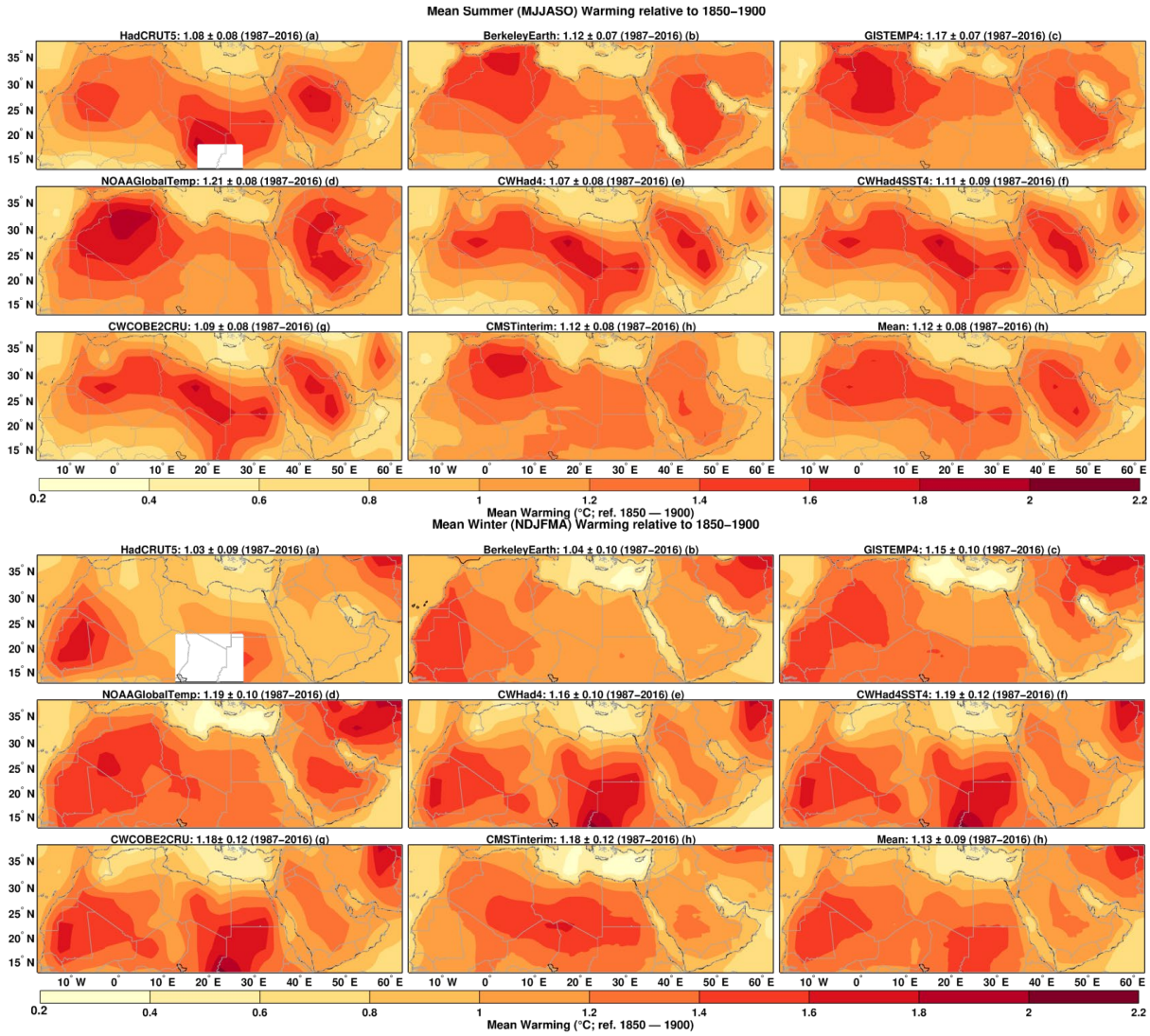

Figure S6. Spatial pattern of observed summer (May-October; upper panel) and winter (November-April; lower panel) mean climatological warming (1987-2016) relative to preindustrial climate (1850-1900) over the MENA region for multiple observational datasets.

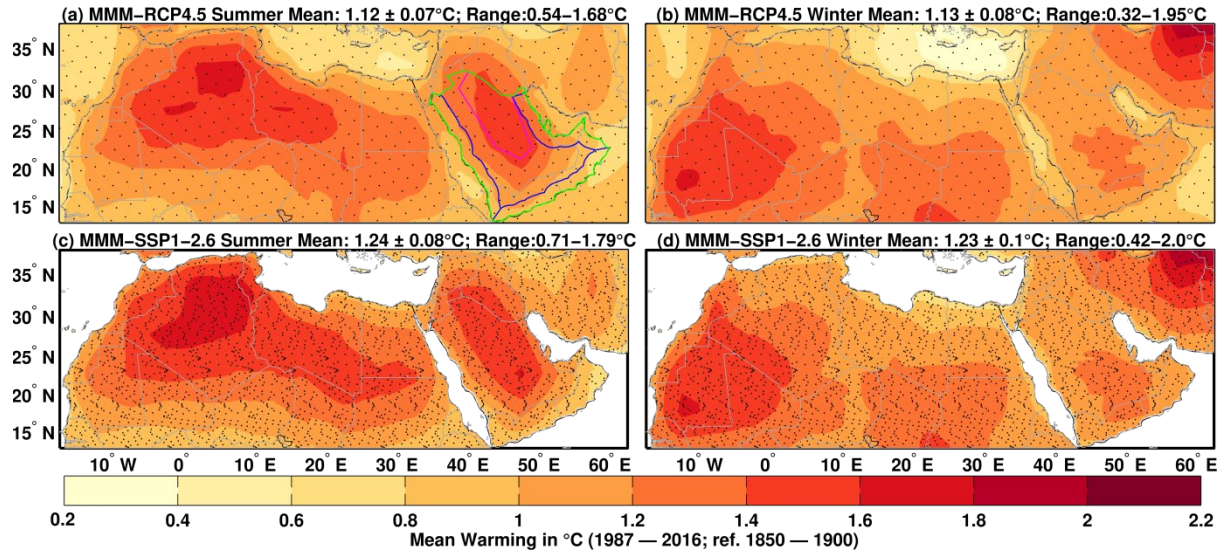

Figure S7. Spatial pattern of historical summer (May-October; left panel) and winter (November-April; right panel) mean climatological warming (1987-2016) relative to preindustrial climate (1850-1900). (a, b) Multimodel Model Mean (MMM) of 21 C3S-CMIP5-Adjusted climate model outputs for RCP4.5; and (c, d) Multimodel Model Mean of 5 C3S-CMIP6-Adjusted climate model outputs for SSP1-2.6. Stipplings indicate statistical significance with 2 SD of internal climate variability and where all corresponding data members agree for change in sign. Numbers above each sub-figure show climatological mean warming with ± 1 std and temperature range (min to max). Green and magenta polygons show the boundaries of the Arabian Peninsula (AP) and Arabian Peninsula Hotspot Region (APHR). Blue lines are coastal zones defined up to 160 km of the coast.

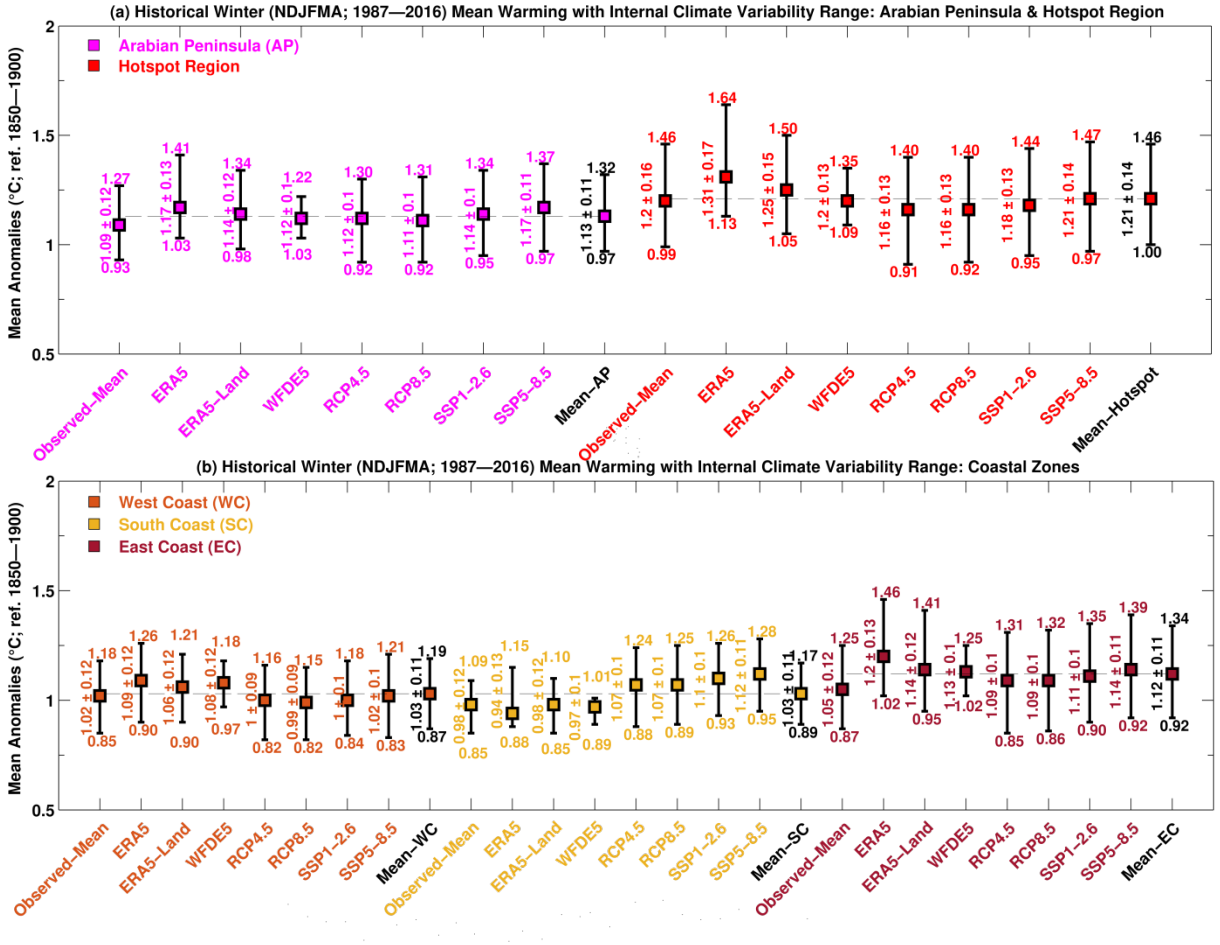

Figure S8. Historical winter (May-October; 1987-2016) mean climatological warming with internal climate variability range (99% confidence level) for (a) Arabian Peninsula and hotspot region, and (b) coastal zones.

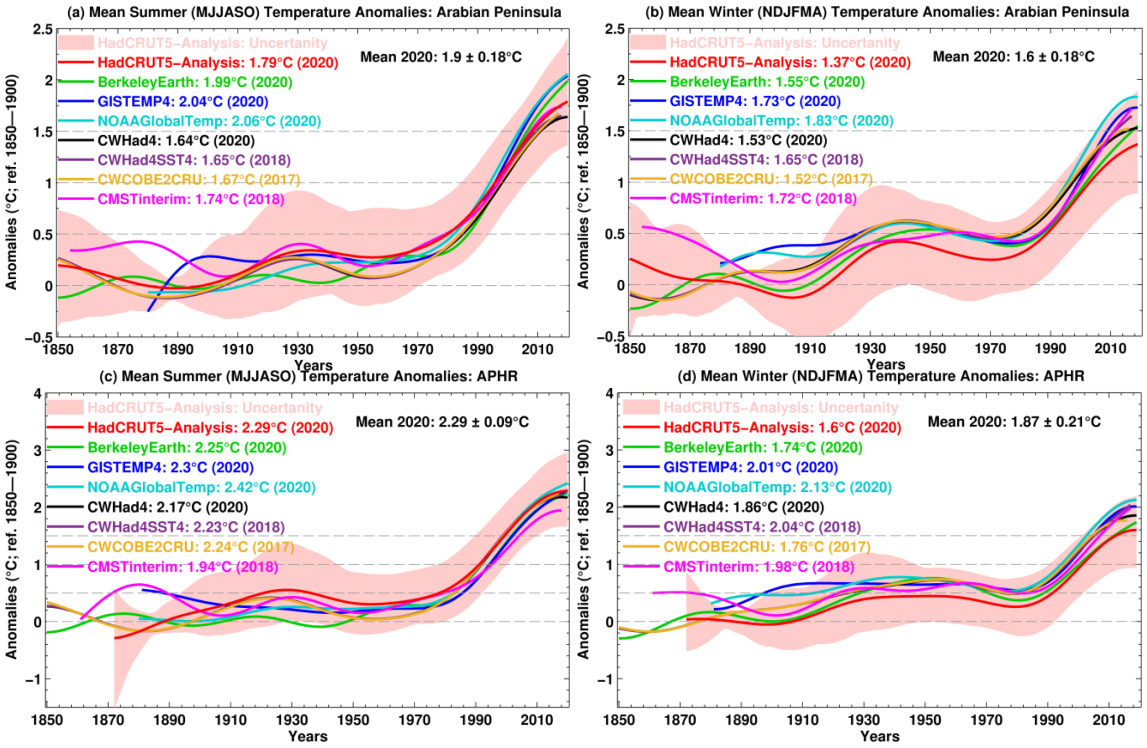

Figure S9. Historical (1850-2020) summer (left panel) and winter (right panel) temperature change relative to preindustrial climate (1850-1900). (a, b) over Arabian Peninsula, and (c, d) APHR. The pink shading shows a 99% confidence interval calculated from 200 ensemble members of HadCRUT5-Analysis.

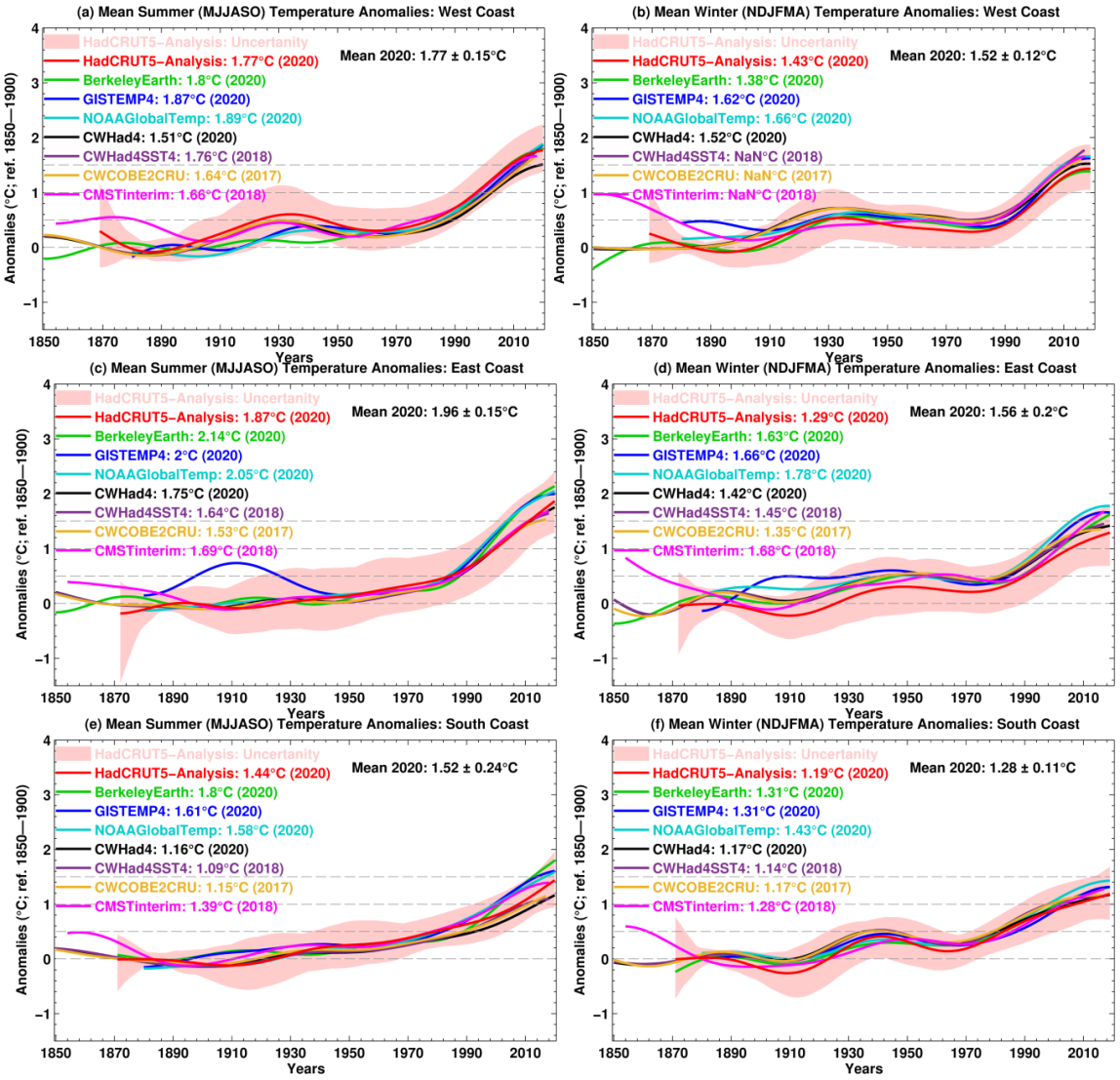

Figure S10. Historical (1850-2020) summer (left panel) and winter (right panel) temperature change relative to preindustrial climate (1850-1900). (a, b) over the west coast, (c, d) the east coast and (e, f) the south coast. The pink shading shows a 99% confidence interval calculated from 200 ensemble members of HadCRUT5-Analysis.

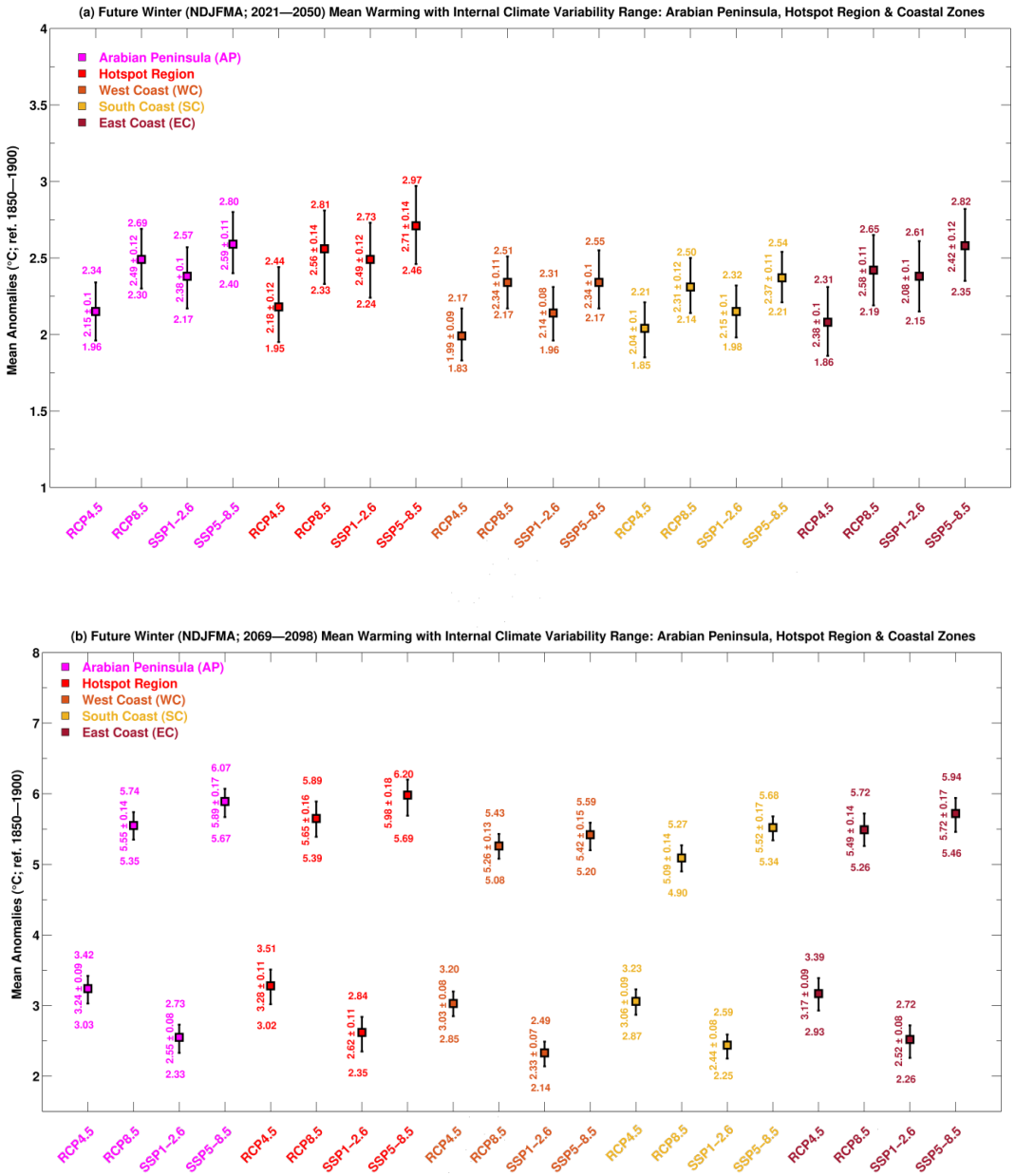

Figure S11. Future winter (May-October) mean climatological warming with internal climate variability range (99% confidence level) over the Arabian Peninsula, hotspot region, and coastal zones for (a) near-(2021-2050) and (b) long-term futures.

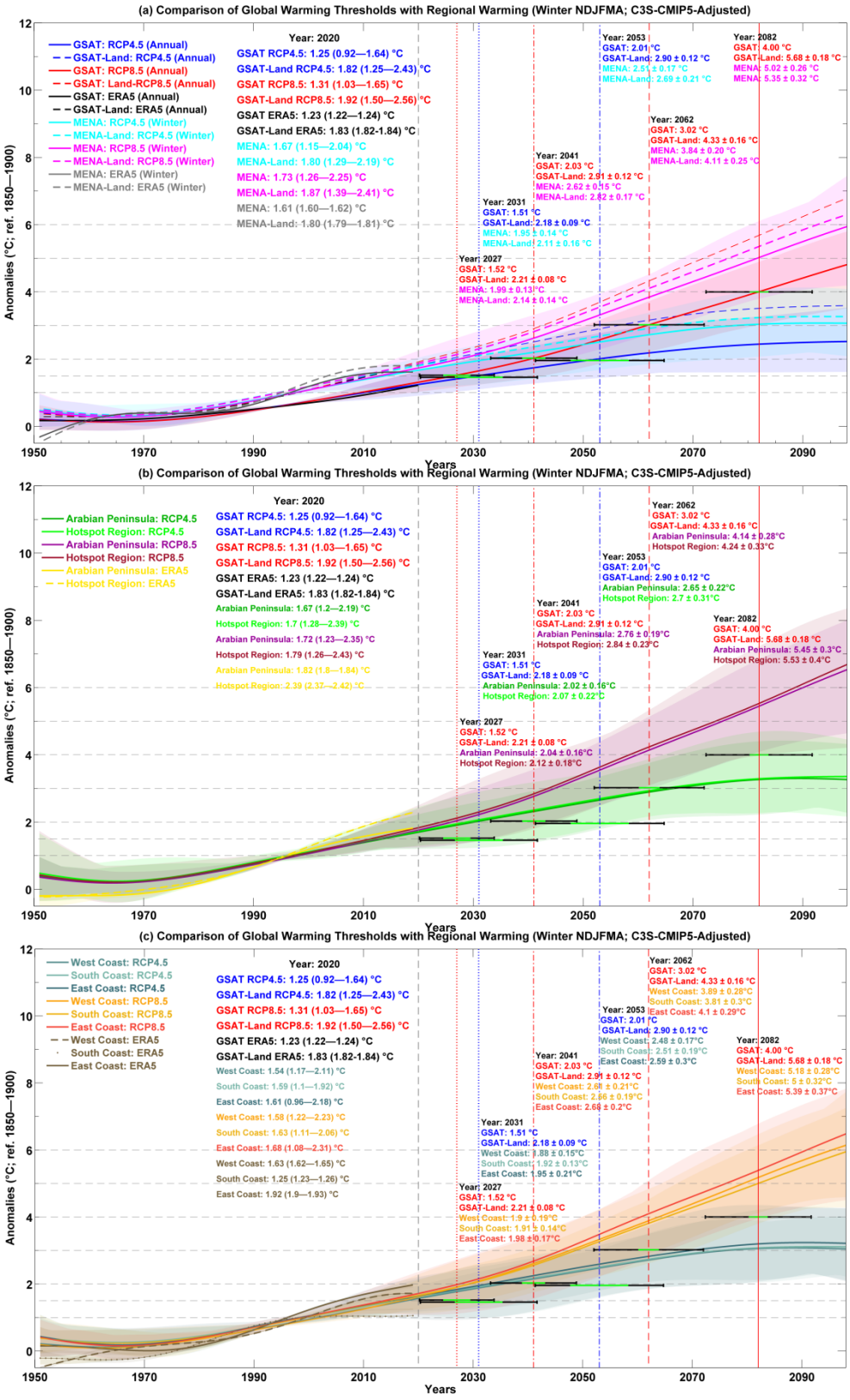

Figure S12. Comparison of winter temperatures over MENA and its subregions with annual Global Surface Air Temperature (GSAT: global land plus ocean; GSAT-Land: global

land only) at different global temperature thresholds (1.5, 2, 3, and 4 0C). (a) Comparison for MENA, (b) for Arabian Peninsula and hotspot region, and (c) for coastal zones. For C3S-CMIP5-Adjusted, the curves are shown as the multimodel mean of 21 climate models for two emission scenarios (RCP4.5 and RCP8.5) with uncertainty estimates at a 99% confidence level. The uncertainty for ER5 is calculated from its ten ensemble members. The text colours correspond to each data set used, and coloured vertical lines show the year surpassing a particular global temperature threshold for each emission scenario. The horizontal black lines indicate model uncertainty (± 1 std of a year crossing a certain global temperature threshold), whereas green lines indicate uncertainty in a year due to internal climate variability.

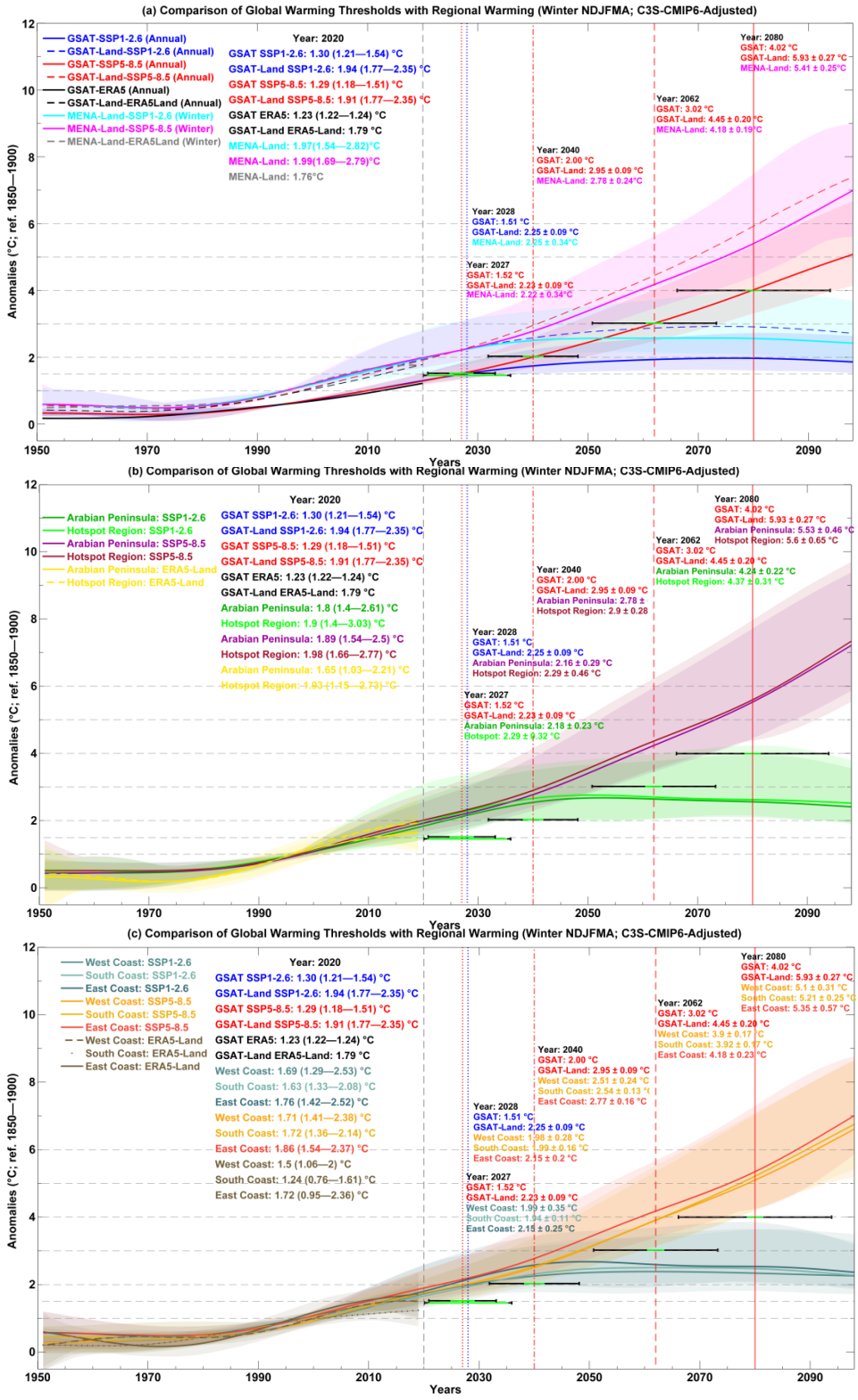

Figure S13. Same as in Fig.S12 but for C3S-CMIP6-Adjusted with two scenarios (SSP1-2.6 and SSP5-8.5).

S5 Open research data availability

The datasets used in this research work can be downloaded from the following links:

1) HadCRUT5 analysis (Morice et al., 2021)
https://crudata.uea.ac.uk/cru/data/temperature/

2) Berkeley Earth (Rohde & Hausfather, 2020)
http://berkeleyearth.org/data/

3) CMST-Interim (Sun et al., 2021; Yun et al., 2019)
https://doi.pangaea.de/10.1594/PANGAEA.929389

4) Cowtan and Way v2 (Cowtan and Way, 2014)
https://www-users.york.ac.uk/~kdc3/papers/coverage2013/series.html

5) GISTEMP v4 (Lenssen et al., 2019)
https://data.giss.nasa.gov/gistemp/

6) NOAAGlobalTemp v5 (Zhang et al., 2019, 2021):
https://psl.noaa.gov/data/gridded/data.noaaglobaltemp.html

7) ERA5 (Copernicus Climate Change Service, 2023; Hersbach et al., 2019a, 2019b, 2020)
https://cds.climate.copernicus.eu/cdsapp#!/dataset/reanalysis-era5-single-levels-monthly-means?tab=overview

8) ERA5-Land (Copernicus Climate Change Service, 2022a; Muñoz-Sabater et al., 2021)
https://cds.climate.copernicus.eu/cdsapp#!/dataset/reanalysis-era5-land-monthly-means?tab=overview

9) WFDE5 (Copernicus Climate Change Service, 2022b; Cucchi et al., 2020, 2021)
https://cds.climate.copernicus.eu/cdsapp#!/dataset/derived-near-surface-meteorological-variables?tab=overview

10) C3S-CMIP5-Adjusted (Noël et al., 2021)
https://esgf-node.ipsl.upmc.fr/search/c3s-cmip5-adjust/

11) C3S-CMIP6-Adjusted (Noël et al., 2022)
https://esgf-node.ipsl.upmc.fr/search/cmip6-adjust/

12) CMIP5 (Taylor et al., 2012)

https://cds.climate.copernicus.eu/cdsapp#!/dataset/projections-cmip5-monthly-single-levels?tab=overview

13) CMIP6 (Eyring et al., 2016)
https://cds.climate.copernicus.eu/cdsapp#!/dataset/projections-cmip6?tab=overview